Change in photochemistry, thylakoid organization and lipid accumulation under iron starvation in *Chlamydomonas reinhardtii*

A thesis submitted to the University of Hyderabad for the award of Doctor of Philosophy in Plant sciences

By

D. Elsinraju

(Reg. No: 14LPPH09)



Department of Plant Sciences School of Life Science University of Hyderabad Hyderabad-500 046 India.

AUGUST, 2020



School of Life Sciences

University of Hyderabad Hyderabad-500046

AUTHORSHIP DECLARATION

I, D. Elsinraju, hereby declare that this thesis entitled "Change in photochemistry, thylakoid organization and lipid accumulation under iron starvation in *Chlamydomonas reinhardtii*" submitted by me under the guidance and supervision of Prof. S Rajagopal is an original and independent research work. I also declare that it has not been submitted previously in part or in full to this University or Institution for the award of any degree or diploma.

Date: 31.08.2020

D. Elsinraju

(Red. No: 14LPPH09)

Prof. S. Rajagopa (Supervisor)

Prof. S. RAJAGOPAL Dept. of Plant Sciences

Dept. of Plant Sciences School of Life Sciences University of Hyderabad Hyderabad-500 046.



School of Life Sciences

University of Hyderabad Hyderabad-500046

CERTIFICATE

This is to certify that this thesis entitled "Change in photochemistry, thylakoid organization and lipid accumulation under iron starvation in *Chlamydomonas reinhardtii*" submitted by D. Elsinraju, for partial fulfilment of the requirements for the award of Doctor of Philosophy in the Department of Plant Sciences, School of Life Sciences, University of Hyderabad is a record of bonafide work carried out by him under my supervision and guidance. This thesis is free from plagiarism and has not been submitted in part or in full to this or any other University or Institution for the award of any degree or diploma.

Parts of the thesis have been:

- A. Published in the following publication:
- 1. Iron deficiency causes the changes in photochemistry, thylakoid organization and accumulation of Photosystem II proteins in Chlamydomonas reinhardtii. (Chapter 3)
- 2. Changes in the photosynthetic apparatus and lipid droplets formation in C.reinhardtii under Iron deficiency. (Chapter 5)
- B. Presented in the following conferences:
 - "Oral presentation in 8th international conference on "Photosynthesis and hydrogen energy research for sustainability-2017" held at University of Hyderabad, Hyderabad, India; from October 30th- November 3rd, 2017.
 - Oral presentation on "Lipid droplet formation and fatty acid changes in *C.reinhardtii* under iron deprivation" Andhra Pradesh Science congress held at Yogi Vemana University, Kadapa during November 9-11, 2018.
 - Oral presentation in international conference on "Solar energy to Biomass" on "Restoration of photosynthetic activity and supercomplexes from severe iron deficiency in *C.reinhardtii*" held at Porto, Portugal, from Feb 11-14, 2020.

Further, the student has been passed the following courses towards the fulfilment of the coursework required for PhD.

S.No.	Course code	Name	Credits	Pass/Fail
1	PL 801	Research methodology	4	Pass
2	PL 802	Research ethics and management	2	Pass
3	PL 801	Biostatistics	2	Pass
4	PL 801	Lab work	4	Pass

1

Head of the Department 08 20 20

Dean

अध्यक्ष / HEAD

Prof. S. RAJAGOPA विनस्पति विज्ञान विभाग / Dept. of Plant Sciences Dept. of Plant Sciences जैविक विज्ञान संक्ष्मा / School of Life Sciences School of Life Sciences हैदराबाद विश्वविद्यालय / University of Hyderabad University of Hyderabad Hyderabad-500 046.

DEAN School of Life Sciences University of Hyderabad Hyderabad - 500 046.



School of Life Sciences

University of Hyderabad Hyderabad-500046

Plagiarism Free Certificate

This is to certify that the similarity index of this thesis as checked by the Library of University of Hyderabad is 42%. Out of this 34% similarity has been found to be identified from the candidate's own publication which forms the major part of the thesis. The details of student's publication are as follows:

- 1. Iron deficiency causes the changes in photochemistry, thylakoid organization and accumulation of Photosystem II proteins in Chlamydomonas reinhardtii (Chapter 3).
- 2. Restoration of photosynthetic activity and apparatus from severe iron starvation in C.reinhardtii (Chapter 4)
- 3. Lipid productivity and droplets formation in C.reinhardtii under Iron deficiency (Chapter 5).

About 8% similarity was identified from external sources in the present thesis which is according to prescribed regulations of the University. All the publications related to this thesis have been appended at the end of the thesis. Hence, the present thesis considered to be plagiarism free.

Prof. S. Rajag (Supervisor)

Prof. S. RAJAGOPAL
Dept. of Plant Sciences
School of Life Sciences
University of Hyderabad
Hyderabad-500 046.



Dedicated to my parents & family

ACKNOWLEDGEMENTS

I would to express my gratitude towards my research supervisor **Prof. S. Rajagopal** for accepting me as his research student and providing me the opportunity to work under his guidance and support throughout my doctoral research, and giving me freedom to select the directions of my work. I gratefully acknowledge his support and guidance during every single problem that I faced during my research. His dedication and persistence towards work, patience and help me to overcome the hurdles in my research, without it is impossible to complete this journey.

I thank the present and former Deans, Prof. S. Dayananda and Prof. K.V.A. Ramaiah, Prof. P. Reddenna, and Prof. M. Ramanadam, School of Life Sciences, for allowing me to school facilities. I thank present and former Heads, Prof. G. Padmaja, Prof. Ch. Venkataramana, and Prof. A.R. Reddy, Dept. of Plant sciences for allowing me to use School and Department facilities. I also thank Heads of Dept. of Plant sciences for allowing me to use their department facilities.

I am gratefully acknowledge my Doctoral committee members Prof. A.R. Reddy, Prof. G. Padmaja, and Dr. J. Madhu Prakash for their valuable suggestions and encouragement.

I express my gratitude to Prof. Aparna Dutta Gupta, Prof. P. Appa Rao, Dr. Bindu Madava Reddy and Prof. G. Ravi kumar for permitting me to use their lab facilities.

My sincere thanks to my host supervisor Prof. Thomus S. Bibby for scientific discussions, Dr. John Gittins, Lab scientific manager and Ms. Nikki for their scientific guidance during my visit (Newton PhD placement programme-2018) to National oceanography centre, University of Southampton, UK.

I would like to thank my lab mates for good company Drs. Mahesh, Tirupathi, Dinesh kumar, Veera Babu, Sai kiran, Daniel, Aparna, Srilatha, Monika, Mrs. Shreya, Nisha, Manisri, Ranay, Jayendra, Kunal, Yusuf, Pavithra, Amy and Jyoti Ranjan for their cooperation and help.

My sincere thanks go to Mr. Ganesh and Mr. Prasanth for their cooperation and assistance in daily in the lab.

I thank my teachers N. D. V. Prasad, Victor Kumar, Kenadi, Lakshimi, and Mani to instigate the interest in me during my schooling.

I specially thank my dear friends and my well-wishers Drs. Venkata Rao, Vinod kumar, Paul, B. Sunil, R. Girish Kumar, Loka Reddy, Ch. Suresh kumar, K. Ravindra, Rameswar Reddy, Sitarami Reddy, A Madhavi, Mr. Ramaraju, Anand, and Trindha Rao, Varma Gajapathi, Sunil Kanth, D. Sanker, Bantu, Yerranna, Gangathar and Vikranth for their moral support and encouragement in the time of need.

I thank my colleges in my previous work place **friend's names** for their suggestions and constant support that enabled me to enter research form teaching profession.

I thank faculty members of school of Life Sciences for their support and encouragement. Sincere thanks to non-teaching staff for their help and support. Special thanks to staff of CIL, HCU for allowing me to use CD spectroscopy and Proteomic facility, SLS.

I thank funding agencies DST, SERB, DBT, CSIR, UGC-ISI for financial support to Prof. S. Rajagopal lab and DST-FIST, DBT CREBB and UGC-SAP for infrastructure and also thank DST-SERB, DST-ITS, CCSTDS-Chennai, DBT and, British council for Newton Bhabha Indo-UK PhD placement programme. My sincere thanks to UGC-RGNF for fellowship and financial support for my PhD and to the lab.

Finally, I thank my parents, brother, sister and my lovely family members, Chinnari, Harsha and Kalyan dharma for their love and moral support.

ELSINRAJU

CONTENTS

Chapter 1. INTRODUCTION	Page Nos 1-27
1.1 Photosynthesis	1
1.2 Light harvesting and energy transfer in photosynthesis	2
1.3 The photosynthetic machinery of the thylakoid membrane	6
1.3.1 Structure and function of PSII-LHCII complex	6
1.3.2 Cytochrome <i>b6/f</i> complex	10
1.3.3 Structure and function of PSI-LHCI complex	10
1.4 Structure and function of thylakoid membrane (polar) lipids	16
1.5 Algal biofuels	20
1.6 Abiotic stress	21
1.6.1 Iron homeostasis in Chlamydomonas	21
1.6.2 Methods for creation of iron deficiency in Chlamydomonas	22
1.6.3 Role of iron (Fe ²⁺) in photosynthesis in Chlamydomonas	24
1.7 strain C. reinhardtii	25
1.8 Objectives of the study	27
Chapter 2. Experimental procedures	28-44
2.1 Description of <i>C. reinhardtii</i>	28
2.2 Culturing and maintenance of <i>C.reinhardtii</i>	28
2.3 Spectrophotometric measurements	29
2.4 The fast OJIP Chlorophyll <i>a</i> fluorescence transient measurements	30
2.5 Chlorophyll <i>a</i> fluorescence induction measurements	31
2.6 Room temperature fluorescence measurements	32
2.7 ROS measurements	33
2.8 Quantification of Neutral Lipids	33
2.9 Fourier-transform infrared spectroscopy	34
2.10 Lyophilisation for dry weight measurements2.11 Quantification of total lipids	35 36
2.12 Extraction of Lipids by Bligh & Dyer method	36
2.13 Isolation of Thylakoid membranes	37
2.14 Quantification of total Chlorophyll	38
2.15 Sucrose density gradient separation method	38
2.16 Circular dichroism studies	39
2.17 Blue Native-BN-PAGE and 2D SDS PAGE	39
2.18 Protein extraction	40
2.19 Immunoblots	40
2.20 Protein aggregation	41
2.21 Thin layer Chromatography	42
2.22 Liquid Chromatography/ Mass spectrometry	42
2.23 Transmission electron microscopy	44

Chapter 3. Photochemistry and biochemical characterization of F	SII-LHCII		
supercomplexes under iron starvation.	45-58		
3.1 INTRODUCTION	45		
3.2 RESULTS & DISCUSSION	47		
3.2.1 Growth analysis and morphological changes	47		
3.2.2 Analysis of fluorescence emission spectra	48		
3.2.3 Analysis of transient Chl <i>a</i> fluorescence	50		
3.2.4 Separation of supercomplexes from thylakoid membranes	52		
3.2.5 Protein profile of PSII reaction centre changes in Fe deficiency	54		
3.2.6 Light harvesting complex (LHCII) protein profile	56		
3.3 CONLUSIONS	58		
Chantar 4 Destaration of photographatic activity and apparatus from severe is	.on		
Chapter 4. Restoration of photosynthetic activity and apparatus from severe in			
deficiency in C.reinhardtii.	59-84		
4.1 RESULTS & DISCUSSION	59		
4.1.1 Growth, total chlorophyll and, cell morphological analysis	59		
4.1.2 Analysis of chlorophyll <i>a</i> fluorescence transients and OJIP-test	61		
4.1.3 Circular dichroism spectra analysis from thylakoid membranes	65		
4.1.4 Thylakoid membranes supercomplexes analysis by BN-PAGE	68		
4.1.5 Characterization of supercomplexes from sucrose density gradient	70		
4.1.6 Immunoblots of PSII Core and LHCII Polypeptides 4.1.7 Protein profile of PSI and LHCI complex	74 78		
4.1.8 Observation of aggregated proteins	82		
4.2 CONCLUSIONS	83		
Chapter 5. Alteration of thylakoid membrane lipids and lipid accumulation	n		
under iron starvation.	85-103		
5.1 INTRODUCTION	85		
5.2 RESULTS AND DISCUSSIONS	86		
5.2.1 Growth and biomass analysis in iron deficient Chlamydomonas			
5.2.2 Confocal microscopy for lipid droplets study	89 91		
5.2.3 Neutral lipid analysis by Nile Red fluorescence and Lipid content			
5.2.4 Lipid and carbohydrate measurements by FTIR 5.2.5 TLC for TAG accumulation			
5.2.6 Identification of lipids through LC/MS mass spectrometry			
5.2.7 Iron starvation induces the DGAT2A expression	98 100		
5.3 CONCLUSIONS	103		
SUMMARY AND CONCLUSIONS	104		
Bibliography			

List of Figures

- Fig 1.1 The simplified schematic representation of oxygenic photosynthesis of thylakoids.
- Fig 1.2 Schematic representation of ETC pathway from H₂O to NAD⁺ in thylakoid membranes.
- Fig 1.3 Electron microscopy showing a structure of megacomplexes consisting of PSII-LHCII
- Fig 1.4 Structures of PSI-LHCI complexes from Cyanobacteria to higher plants.
- Fig 1.5 The Cryo-EM projection map of PSI-LHCI structure from C.reinhardtii.
- Fig 1.6 Thylakoid lipids bounded with the monomeric form of cyanobacterial Photosystem II
- Fig 1.7 The iron uptake pathway from Chlamydomonas. The pathway is same as higher plants.
- Fig 1.8 Schematic structure of *C.reinhardtii* cell having the thylakoid membranes.
- Fig 2.1 Representation of *C. reinhardtii* cultured in TAP medium with agar and growth.
- Fig 2.2 Baseline corrected FTIR spectra showing absorption bands for lipid, protein.
- Fig 3.1 Growth curve, morphology and, RT fluorescence results of C. reinhardtii -Fe cells.
- Fig 3.2 Chl a florescence from PAM and OJIP transients in control & -Fe cells with DCMU.
- Fig 3.3 Blue native PAGE of thylakoid membranes isolated from control, -Fe cells.
- Fig 3.4 Immunoblots of PSII and LHC proteins content from control and Iron deficient.
- Fig 3.5 Immunoblots of major LHC II proteins Lhcb1, LHCb2, CP29, CP26 and Lhcbm5.
- Fig 4.1 Growth, Fv/Fm and, Morphology of C.reinhardtii under from +Fe, -Fe, RC1, 2G-Fe.
- Fig 4.2 The OJIP Chl a fluorescence transients in dark-adapted C. reinhardtii.
- Fig 4.3 Visible circular dichroism of (+Fe), (-Fe), RC1, 2G-Fe, RC2.
- Fig 4.4 Blue Native-PAGE of membrane supercomplexes from cells grown under -Fe, C, RC.
- Fig 4.5 SDG fractions from isolated thylakoid of +Fe, -Fe, RC1, 2G-Fe, RC2. 0.8% β-DM.
- Fig 4.6 Absorption and CD spectra from volume 200 μL collected from fractions (F1, F2, &F3).
- Fig 4.7 Immunoblots of PSII core, OEC complex and, LHCII proteins- C -Fe, RC1, 2G-Fe RC2.
- Fig 4.8 Immunoblots of PSI core and LHC1 proteins from C, -Fe, RC1, and 2G-Fe and RC2.
- Fig 4.9 Fv/Fm with ROS and Fv/Fm activity decreased with increased ROS in C. reinhardtii.
- Fig 4.10 Protein aggregation from *C.reinhardtii* cells grown under C, -Fe, RC1, 2G –Fe and, RC2.
- Fig 5.1 Growth and biomass measurements from iron sufficient (+Fe) and iron deficiency (-Fe).
- Fig 5.2 Confocal bright field images from C.reinhardtii cells stained with Nile Red fluorescence.
- Fig 5.3 Fluorescence spectroscopy and total lipid content analysis of *C.reinhardtii*.
- Fig 5.4 FTIR analysis of carbon storage in C. reinhardtii under iron deprivation and ratios.
- Fig 5.5 TAG content from TLC and semi-quantitative analysis of TAG content from TLC.
- Fig 5.6 Mono saturated fatty acid composition from C, -Fe, Rc1, 2G-Fe and, Rc2 conditions.
- Fig 5.7 1st stage and severe iron deficiency from 0-72 h expression studies of DGAT2A&PDAT1.

List of Tables

- **Table 1.** Chlorophyll a fluorescence OJIP test parameters.
- **Table 2.** The parameters of FTIR wavenumbers of each functional group.
- **Table 3.** Molecular mass quantifications from fragmentation irons and ions for fatty acid.
- **Table 4.** Gradient conditions for sample measurements for all the conditions.
- **Table 5.** Fatty acid measurements and identification through LC/MS.

ABBREVIATIONS

77K 77 degree Kelvin = -196 degree Celsius

BN-PAGE blue-native polyacrylamide gel electrophoresis

CET cyclic electrone transfer around PSI

DCMU 3-(3, 4-dichlorophenyl)-1, 1-dimethylurea

Chl chlorophyll

DBMIB 2, 5-dibromo-3-methyl-6- isopropyl-p-benzoquinone

ETC electrone transfer chain between PSII and PSI

 $F_{\rm m}$ maximum fluorescence in the dark-adapted

 F_{o} minimum fluorescence in the dark-adapted

F_v/F_m ratio of variable to maximal fluorescence

DDM n-dodecyl β-D-maltoside

kDa kilo daltons

LHCII light harvesting complex II

LHCI light harvesting complex I

NPQ non-photochemical quenching

TAG triacylglycerol

ATP adenosine try phosphosphate

MGDG monogalactosyldiacylglycerol

DGDG di galactosyl diacylglycerol

SQDG sulfo quinovosyl diacylglycerol

FTIR fourier transform infrared

OEC oxygen evolving complex

P680, P680* reaction centre Chl of PSII and its excited singlet state

PSI photosystem I complex

PSII photosystem II complex

RC reaction centre

 Q_A and Q_B primary and secondary plastoquinone electron acceptor of

PSII

SDGUC sucrose density gradient ultracentrifugation

SDS-PAGE sodium dodecyl sulphate-polyacrylamide gel electrophoresis

LD lipid droplet

Fe²⁺ iron element

NADPH nicotinamide adenine dinucleotide phosphate

ROS reactive oxygen species

Fd ferredoxin

DTT dithiothreitol

CD circular dichroism

PDB protein data bank

Cyts cytochromes

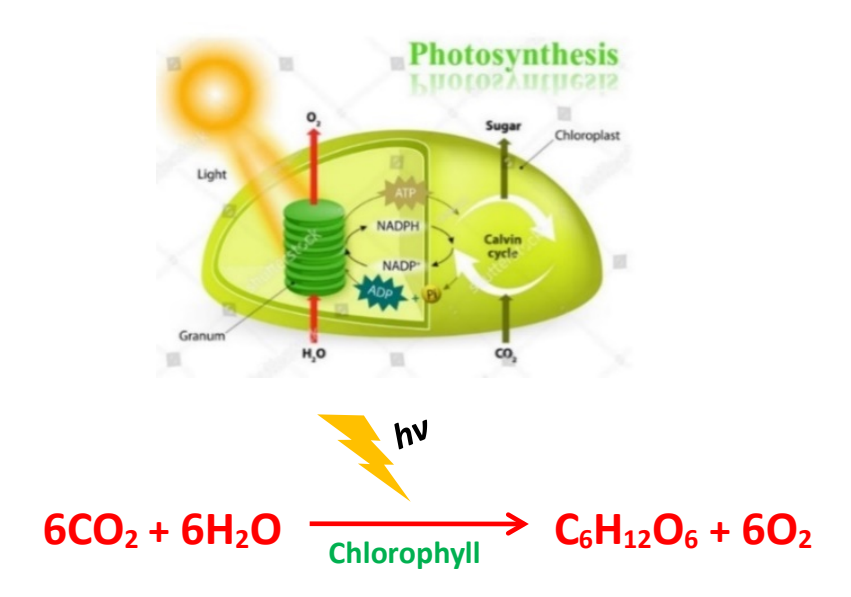
MLDP major lipid droplet protein

N nitrogen

P phosphate

Introduction

Chapter 1



1.1 Photosynthesis

Oxygenic photosynthesis is the most important photochemical reaction on Earth. It describes the process by which photosynthetic organisms such as higher plants and cyanobacteria convert the stable inorganic raw materials into biologically usable organic compounds in the presence of sunlight. All of our food and energy derives from this unique photosynthesis process (Fig. 1.1). The net primary productivity of photosynthesis is estimated at 85 - 120 Gt carbon/year (Imramovsky et al., 2011). Thus, understanding the basic and applied aspects of photosynthesis is essential to provide food and energy for an exponentially growing world population as well as to a wide range of sciences and technologies. During photosynthesis, oxygenic photosynthetic organisms use light energy from the sun to convert carbon dioxide (CO₂) and water (H₂O) into energy rich carbohydrates.

Molecular oxygen (O₂) is released into the atmosphere as a by-product during this process. The solar radiation used in this process is known as 'photosynthetically active radiation' or PAR, which is between the 400 –700nm (Alados et al., 1996). The overall equation shown above can be expressed on an oxidation-reduction scale where H₂O is the initial electron donor in oxygenic photosynthesis. Electrons are then passed through a series of protein complexes before finally reducing the electron carrier NADP⁺ to NADPH. The catalysts of this reaction are membrane proteins embedded in the thylakoid membranes that also act in the formation of a proton gradient across the thylakoid membranes. The adenosine triphosphate (ATP) synthase uses the energy from the proton motive force (PMF) to synthesize ATP from adenosine diphosphate (ADP) and inorganic phosphate (Pi) (Bolton, 1977). The capture of energy from sunlight and storage in these universal

energy-storing molecules is commonly referred to as the light reactions. The energy stored in the form of ATP and NADPH is subsequently used to fix atmospheric CO₂ into carbohydrates in a process called Calvin-Benson- Bassham cycle (CBB). The CBB cycle is catalysed by soluble proteins, notably Ribulose-1, 5-Bisphosphate Carboxylase/oxygenase (RuBisCO) which is the utmost abundant protein on the planet (Griffiths, 2006). Oxygenic photosynthesis occurs in both prokaryotic cells (cyanobacteria and prochlorophytes) and in eukaryotic cells that originally acquired photosynthesis via the primary endosymbiosis event with a prokaryotic cell that later originated as chloroplast (Wallin, 1993). The sunlight funnels its energy to the photosystem (PS)II and further it transfers the electron through electron transfer chain (ETC) to reduce NADP⁺ to NADPH. The main complexes involved in the electron transport chain of oxygenic photosynthesis are PSII, cytochrome (Cyt) b6/f complex and PSI (Fig. 1.1). Also, two-electron carrier molecules namely plastoquinone (PQ) and plastocyanin (PC) mediate electron transport between these membranes embedded protein complexes. The proton motive force generated with electron transfer is used to drive the ATP synthesis by the ATP synthase complex, an F-type ATPase also located in the thylakoid membrane (Falkowski and Raven, 1997).

1.2 Light harvesting and energy transfer in photosynthesis

The process of oxygenic photosynthesis starts with the absorption of light by pigment molecules surrounding PSII (Fig. 1.2). This light energy is then transferred through pigment molecules in the form of excitation and it reaches a 'special pair' of chlorophyll molecules (P680) located at the centre of PSII, also known as the reaction centre (Vredenberg and Duysens, 1963). At the special pair, excitation energy causes an electron to be donated to a molecule of pheophytin – a modified chlorophyll molecule.

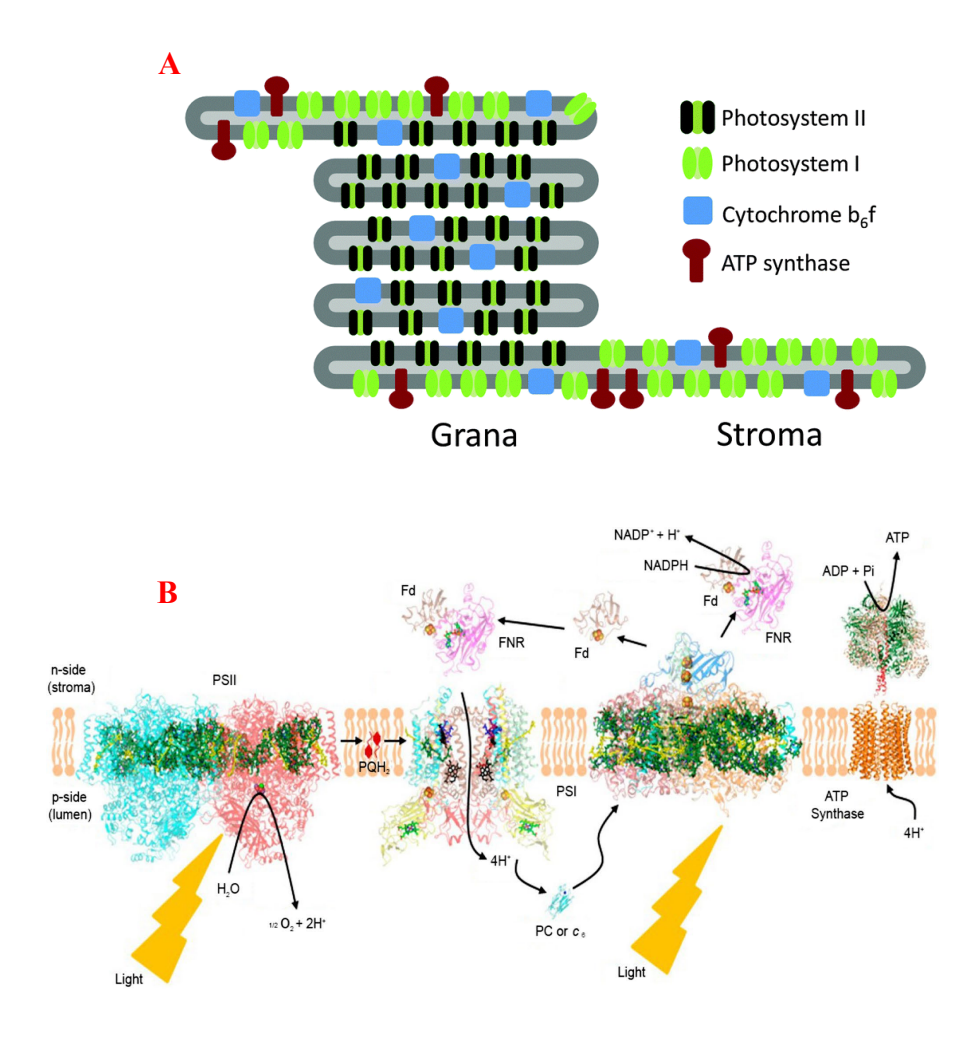


Fig. 1.1 The simplified schematic representation of oxygenic photosynthesis process. (A) Sketch of the thylakoid membrane composed of stacked grana membrane enriched with PSII-LHCII complexes and unstacked stromal membranes with PSI-LHCI complexes. (B) PSII includes major subunits D1 and D2, bind chlorophyll P680 and components of the electron transport chain, 4 manganese atoms facilitate splitting of the water molecule. The Cyt *b6/f* contains seven subunits and includes 2 cytochromes (b₆ and *f*) and an iron-sulphur protein (Fe-S). PSI contains over seven subunits and binds chlorophyll P700 in addition to several other electron carriers. Electrons are transferred to NADPH via soluble ferredoxin (Fd) using ferredoxin-NADP+ reductase (FNR). The ATP synthase complex uses the proton gradient generated by electron transport to synthesize ATP (Adapted from Cramer, 2019).

This first redox reaction results in the oxidation of the P680 pigment to form P680⁺ and reduction of pheophytin to pheophytin. The electron is then transferred to the next electron carrier in the form of a quinone (Q_B) bound to the D₂ subunit which is a core protein of PSII. This transfer takes place in 10⁻¹⁰ µs, minimizing the risk of the electrons being back transfer to the special pair and being wasted as heat before subsequent transfer to a loosely associated quinone molecule (Q_B). Two high-energy electrons are needed to reduce Q_B to QH₂, in this process two protons taking up from the chloroplast stroma. The reduced quinone (plastoquinol) diffuses through the thylakoid membrane towards the Cyt *b6/f*. Photooxidation of H₂O at the oxygen-evolving complex (OES), located luminal side of PSII restores the electrons lost in this process (Hill, 1937). Electrons are passed from the OEC to the oxidized P680⁺ via a tyrosine side chain situated on the D1 bound with Ty_Z subunit of PSII (Nelson and Yocum, 2006). The reaction at the OEC can be summarized as the following:

$$2H_2O + 2A \longrightarrow 2AH_2 + O_2$$

Four electrons are needed to balance this equation. However, the reaction centre only has enough reducing power to reduce one electron at a time. At the centre of the OEC resides a manganese-calcium oxide cluster in a cubane-like structure (Umena et al., 2011), which serves to temporarily store reducing power until four manganese atoms have been reduced and splitting of H₂O can proceed. Each PSII monomer contains more than 1,300 water molecules forming hydrogen-bonding networks that may serve as channels for protons, H₂O or oxygen molecules (Ferreira et al., 2004). The OEC is located on the luminal side of the membrane and it maintains the proton gradient across the thylakoid membrane as well as supplying electrons to PSII. Two electrons are transferred from PSII to the Cyt *b6/f* complex via reduced

membrane- plastoquinones, soluble form. The Cyt *b6/f* complex provides approximately two-thirds of the protons to drive the synthesis of ATP (Hasan et al., 2013). The action of cyclic electron flow from PSI via ferredoxin, the complex also plays a major function in balancing the ratio of NADPH and ATP. Electrons flow through an iron-sulphur centre located in the Fe-S protein to Cyt *f* before being passed to a second electron carrier, plastocyanin (Green and Parson, 2003). Firstly, two protons are extracted from the stromal side and transferred via plastoquinol to the lumenal side. Secondly, another plastoquinol binds to the complex, transferring an electron to plastocyanin via the iron-sulphur centre. Finally, uptake of two more protons from the stromal side regenerates the plastoquinone. Overall, four electrons are transferred from the stroma to the luminal side of thylakoid membranes.

Electrons can also be passed from PSI via ferredoxin in a process known as cyclic electron transport (Barber et al., 1997). PSI accepts the electrons from PC and transfers them either to NADPH (noncyclic electron transport) or back to Cyt *b6/f*. Similar to PSII, PSI is a transmembrane protein complex containing reaction centre (P700) along with antenna chlorophylls, phylloquinine, and iron-sulfur proteins serve as intermediate redox carriers. Upon excitation of the special pair of reaction centre pigments (P700), an electron is donated to a chlorophyll molecule (A₀) and then onto phylloquinone (A₁) before transfer through three iron-sulphur centres (4Fe-4S), F_x, F_A and F_B. The electron carrier in the chain (Fx) reduces ferredoxin. An electron from plastocyanin oxidizes P700⁺ to regenerate P700. The flow of electrons through the transfer chain of oxygenic photosynthesis and an increase in the redox potential of electrons upon excitation at PSII and PSI is formally referred as the z-scheme (Senge et al., 2014).

1.3 The photosynthetic machinery of the thylakoid membrane

1.3.1 Structure and function of PSII-LHCII complex

The PS II is a multimeric protein-pigment supramolecular complex located in the thylakoid membranes of plants and cyanobacteria. During the light reactions of photosynthesis, PSII uses light excitation energy to split H₂O into electrons and protons where O₂ is evolved as a by-product (Barber, 2003) (Fig. 1. 3). This complex releases the oxygen which gives life on the earth. So far from higher plants, C₂S₂M₂-type PSII– LHCII structure has been reported. The recent study of PSII structure was resolved at resolutions of 3.8 to 3.37Å (Shen et al., 2019). The overall structure of *C.reinhardtii* PSII-LHCII complex is a heterodimer with two-fold symmetry which consists of two PSII core proteins (C₂), least 27-28 subunits organized in 2 moieties, core proteins surrounded by antenna system (Caffarri et al., 2009). The PSII core is consists of two proteins, D1 (PsbA) and D2 (PsbB) which have the reaction centre P680 and both arranged in a heterodimeric form (Rutherford and Faller, 2003). The P680, upon light absorption is excited. The excited chlorophyll molecule donates an electron to the initial electron acceptor pheophytin (Phe) which sequentially transfers the electron to primary electron accepter, Q-A located at D2, Q-A further transfer the electron to secondary electron acceptor plastoquinone, Q_B, site on D1 (Debus et al., 1988).

The electron transfer is mediated by iron (Fe²⁺) molecule which is located between Q_A and Q_B sites of PSII (Fig. 1.3). However, the oxidized P680⁺ is again reduced by amino acid residue, tyrosine which is present at Tyr161 position of the D1 subunit designated Y⁻_Z which in turn reduced by an OEC cluster, where photolysis of water takes place (Styring et al., 2012). Two antenna proteins, CP43 and CP47 form an intrinsic antenna with CP43 also binding the manganese centre of OEC complex. The primary role of the peripheral antenna is to absorb the light energy and transfer the

excitation energy to the reaction centre chlorophyll molecules thereby regulate the photosynthesis process via photo-protective mechanism (Schmid, 2008).

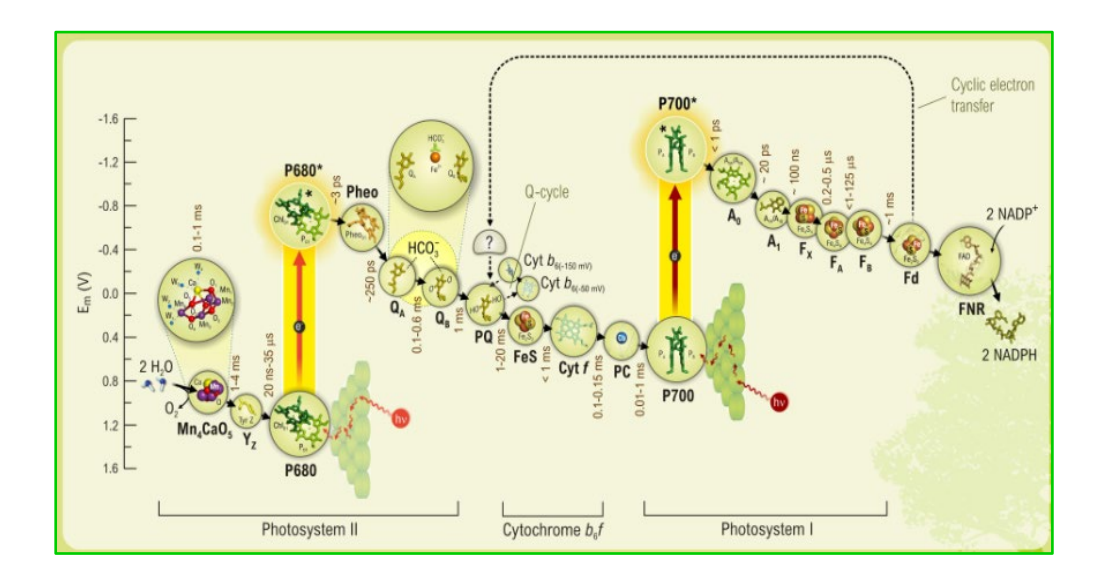


Fig. 1.2 Schematic representation of ETC pathway from H₂O to NAD⁺ in thylakoid membranes. Mn₄O₅Ca is an oxygen-evolving complex (OEC), which participates in the splitting of 2 H₂O molecules in four H⁺, four e⁻ and one O₂. Transfer of excitation energy through centre Chl P680 and P700 operates the entire process. The photon that was captured by P680 and it gets excited P680* which transfer the energy from its light antenna complex to pheophytin. Q_A, a tightly bound molecule which accepts and transfers an e⁻ at a time. Q_B which is loosely bound, a movable molecule which accepts and transfers 2 electrons and protons at a time. Q_BH₂, reduced Q_B and shuttling the 2 electrons and protons within the hydrophobic core to Cty *b6/f* complex. Plastocyanin (PC) is a highly motile copper containing protein. P700 is an excited state of Chl reaction of PSI which transfers an electron to Ao. Phylloquinone is represented A. Fx, F_A, F_B, are the mobile proteins contains iron-sulphur centres. F_D is a ferredoxin-NADP oxidoreductase which enables the NADP⁺ to accept 2 electrons and a proton. Carbon fixation reactions occur in the stromal side of the chloroplast. Rubisco enzyme participates in carbon fixing reactions under dark conditions and it has large and small subunits (Adapted from Govindjee et al., 2017).

It is composed of 6 different or individual protein subunits which belong to the light-harvesting multigene family which are coordinated with Chl *a/b* and pigment xanthophylls in different ratios (Jansson, 1999). The complete light-harvesting complex consists of two strongly bound (S-LhcIIs) trimers, another two moderately bound (M-LhcIIs) trimers and two N-LhcIIS (Naked) trimers forming a C₂S₂M₂n₂-type complex (Fig. 1.3). In additions to this, each PSII-LHCII monomer consists of at least 99 cofactors: 189 Chl, 53 carotenoids, two pheophytins, 12x beta-carotene, 2x plastoquinone, one heme, one bicarbonate, 20x lipid, the OEC (Mn₄CaO₅) cluster (including 2 Cl⁻ ions), and 1 non-heme Fe²⁺ and 2 putative Ca²⁺ ions per monomer (Shen et al., 2019). In plants and algae, two other OEC extrinsic proteins, PsbP (23 kDa) and PsbQ (17 kDa) are found and these two proteins play a role in the water-splitting reaction by optimizing the levels of Ca²⁺ and Cl⁻ ions in the cell (Debus, 1992).

All oxygenic photosynthetic organisms have the manganese clusters which are stabilized by an extrinsic OEC protein encoded by the gene known as *psbO*, a molecular mass of 33 kDa and this subunit (PsbO) is attached on the luminal side of thylakoid membranes. The extrinsic subunits of the oxygen-evolving complex are formed by four subunits (PsbO, PsbP, PsbQ, and PsbR) which are present in higher plants as well as in *C.reinhardtii* complex (Shu et al., 2017). The PSII structure of cyanobacteria contains 35 Chl *a* molecules, 2 pheophytins and 12 beta-carotene molecules (Loll et al., 2005). In *C.reinhardtii*, the light-harvesting complexes (S, M, and N-LCHII) are encoded by *lhcbm1* to 9 genes and divided into 4 groups based on their sequence homology: type I (LhcBM3, LhcBM4, LhcBM6, LhcBM8, and LhcBM9), type II (LhcBM5), type III (LhcBM2 and LhcBM7), and type IV (LhcBM1) (Minagawa and Takahashi, 2004). The peripheral structure of the antenna of *C*.

reinhardtii shares the common features as those of algal and plant LHCI complex (Qin et al., 2019; Suga et al., 2019). In *C.reinhardtii*, the LHCB5-Cr-CP26 consists of 13 Chl binding sites and three carotenoid binding sites which are similar to the plant CP26 whereas Cr-CP29 has 13 Chl and 3 carotenoids but lacking pigment molecule at Chl *b* 614 which is present in the plant. Also, two protein subunits, CP26 and CP29, are closely associated with the PSII core complex.

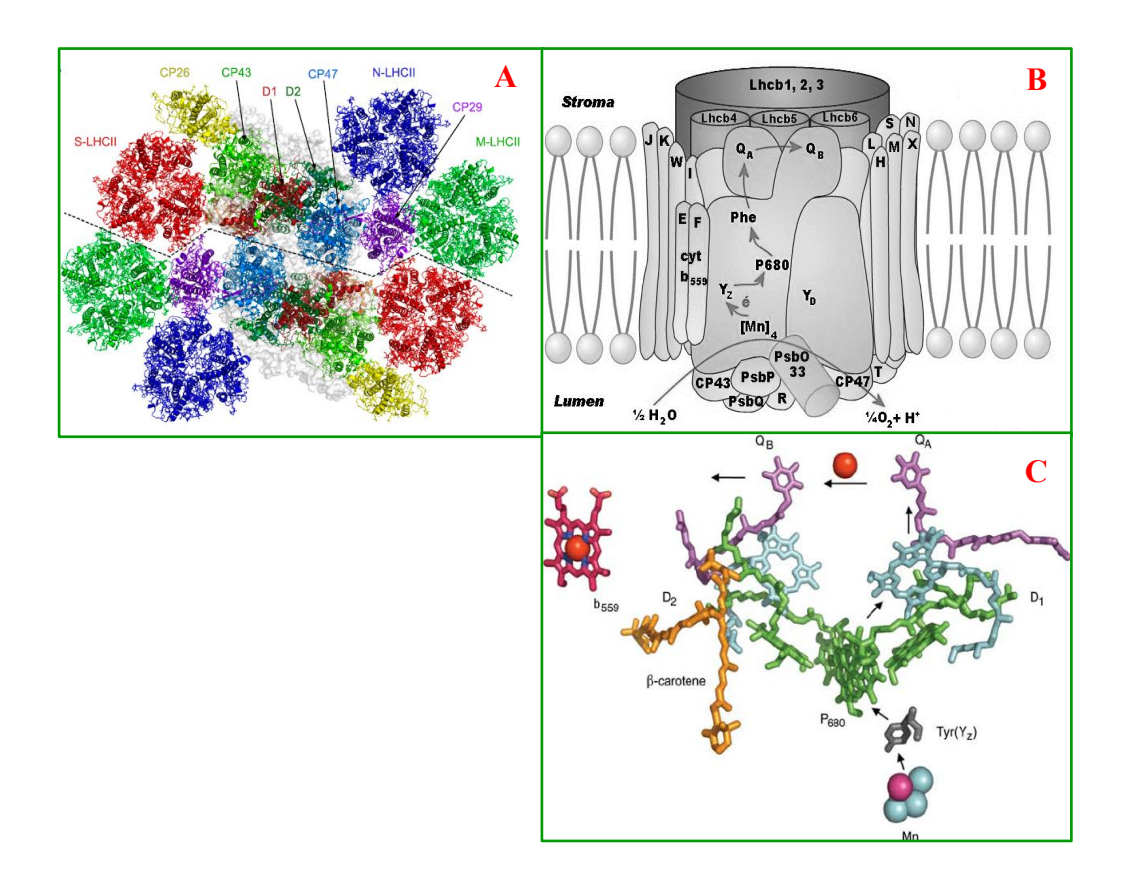


Fig. 1.3 Cyo-electron microscopy showing a structure of megacomplexe consisting of PSII-LHCII dimers. (A) The representation of PSII is composed of core proteins along with LCHII complex. Inner antenna Lchb4, lhcb5 and, Lhcb6 which are close to the core reaction centre (D1 and D2 heterodimer complex), composed of monomeric Chl *a/b*, carotenoids, and outer subunits, (Lhcb1, Lhcb2 and Lhcb3) exists as trimers which are showing with black colour (B). Electron transfer e⁻ mediated by Q_A and Q_B, primary electron acceptors and oxidized P680 is re-reduced by Tyn (Y_Z) which is in turn reduced by OEC complex (C). (Adapted from Nelson, 2006 and Sheng et al., 2019).

1.3.2 Cytochrome *b6/f* complex

The Cyt b6/f complex is a platoquinol-plastocyanin reductase present in thylakoid membranes of higher plants, green algae, and cyanobacteria. It transfers the electrons from plastoquinone to plastocyanin (Berg et al., 2007). It has a central role in oxygenic photosynthesis which links to the PSII to PSI and converting the solar energy into a transmembrane proton gradient for ATP generation (Tikhonov et al., 2014). It is a dimer in its structure of two different monomers and each monomer consists of 8 subunits. Each monomer contains 4 huge subunits: a Cyt f with a c-type cytochrome, a Cyt b6f with the iron group, a Rieske iron-sulphur protein contains a 2Fe-2S cluster and a subunit IV; and four small subunits are named as PetG, PetL, PetM and PetN (Whitelegge et al., 2002). The total molecular weight of Cyt b6/f complex is of 217 kDa (Whitelegge et al., 2002). The crystal structure of Cyt b6/f complex have been reported from C.reinahrdtii, M.laminosus, Nostoc sp PCC 7120 and Spinach leaves (Stroebel et al., 2003; Yamashita et al., 2007; Baniulis et al., 2009; Malone et al., 2019). Cyt b6/f complex mediates the electron transport between the PSII and PSI reaction centre by reducing the soluble plastocyanin or Cyt c6 (Smith et al., 2004). The inter-membrane space within the Cyt b6f complex contains lipids, which provides directionality to heme-heme electron transfer (Hasan and Cramer, 2014).

1.3.3 Structure and function of PSI-LHCI complex

PSI is a large multi-subunit protein complex located in thylakoid membrane known as plastocyanin-ferredoxin oxidoreductase which is crucial for oxygenic photosynthesis (Jolley et al., 2005; Amunts et al., 2007) (Fig. 1.4).

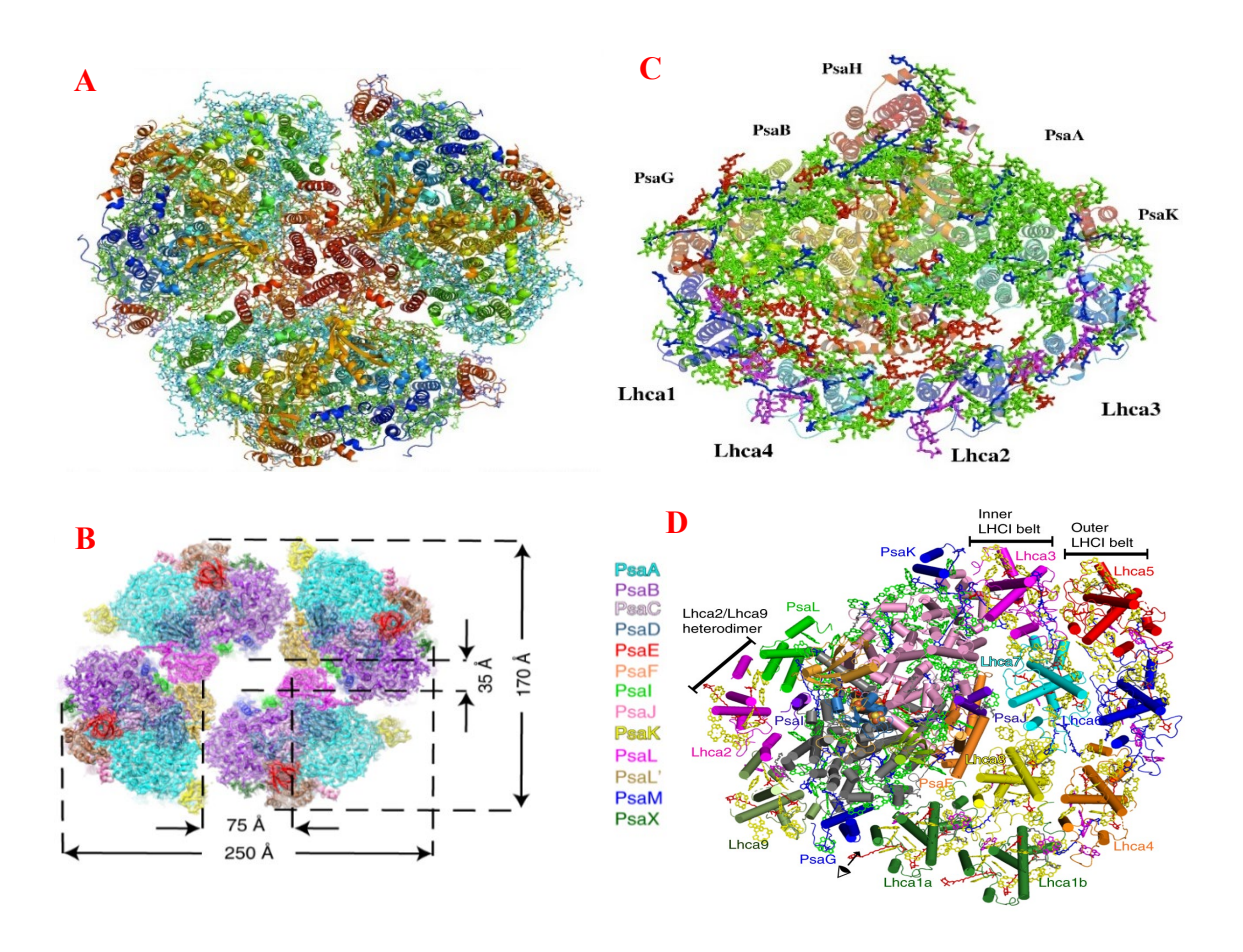


Fig. 1.4 Structures of PSI-LHCI complexes from Cyanobacteria to higher plants. (A) Showing the structure trimeric form of PSI cyanobacteria. (B) Recent crystal tetrameric structure of PSI from Cyanobacteria. (C) Structure of PSI-LHCI supercomplex from the higher plant, Pea and PDB 5L8R, with Chla in green, chlb in magenta, carotenoids in blue, and lipids in red colour. (D) PSI-LHCI structure from *C.reinhardtii* showing two layers of LHC belts around core proteins. (Figures were adapted from Nelson, 2006; Caspy and Nelson, 2018; Zheng et al., 2019; Qin et al., 2019).

The crystal structure of thermophilic cyanobacterium Synechococcus elongates PSI has been resolved at a resolution of 2.5 Å. According to the structure, the PSI complex has 12 protein subunits, 127 cofactors which include 96 chlorophylls, two phylloquinones, three Fe₄S₄ clusters, 22 carotenoids, four lipids, Ca²⁺ and 201 H₂O molecules (Jordan et al., 2001). PSI of cyanobacteria is existed in a trimeric form and it consists of 36 protein subunits, and 381 cofactors are attached with non-covalent bonds. The PSI crystal structure from the higher plant, pea (*Pisum sativum*) has been resolved at 2.6 Å resolution and it reveals that the PSI complex is consists of 16 protein subunits, 240 ligands, 36 lipids, and more than 200 H₂O molecules (Mazor et al., 2017). Both PSI and LHCI, together contain 200 chlorophyll molecules, three Fe-S clusters and two phylloquinones (Ben-Shem et al., 2003). PSI has two core homologous subunits, PsaA and PsaB, binding to P700, A₀, A₁, and F_x. The Fx is a 4Fe-4S centre is bound by 4 cysteines, two provided by PsaA and two by PsaB. PsaC, PsaO, PsaH and PsaE form a docking site for ferredoxin on the stromal side, while PsaN forms the plastocyanin docking site on the luminal side (Fromme et al., 2001). 12 iron atoms are present per PSI monomer.

The light-harvesting complex of PSI is diverse among other photosynthetic organism eg., cyanobacteria and land plants even though conserved core complex. PSI complex from cyanobacteria exists as a trimer in which each monomer shares the light energy to achieve the maximum efficiency to harvest the light energy (Kubota-Kawai et al., 2018). Also the PSI structure from the filamentous cyanobacterium, *Anabaena* sp. PCC7120 reported that which forms the tetramer and dimer instead of trimer complex (Watanabe et al., 2011). A recent study showed the formation of tetrameric PSI under high light conditions, with increased content of PSI-bound carotenoids such

as myxoxanthophyll, canthaxanthin and echinenone in cyanobacteria (Li et al., 2019). The crystal structural was resolved the tetrameric PS I structure at a resolution of 2.37 Å from cyanobacteria Anabaena sp. PCC 7120. According to this structure, there are four PS I monomers, organized in a dimer form in two distinct interfaces (Zheng et al., 219). In *C. reinhardtii*, PSI oxidizes plastocyanin or cytochrome c6 (*Cyt c6*) and reduces ferredoxin, which eventually generates NADPH via Fd-NADP-oxidoreductase (FNR) and it is involved not only in linear electron transfer reactions but also involved in cyclic electron transfer reactions (Nelson and Junge, 2015). The reducing components, NADPH and ATP are used to fix acetate or CO₂ into starch. Figure 1.5 showing the structure of PSI-LHCI complex from Cyanobacteria to higher plants. Recently, the tetrameric structure has been reported in Cyanobacteria under high light condition (Zheng et al., 2019). The core antenna of PSI is bound to LHCI forms the crescentshape close to PsaF/PsaJ of the core complex. Overall 10 LHC proteins were identified which are similar to plant PSI-LHCI complex. Reports from 3D model analysis explain the structural arrangement of PSI-LHCI and its physiological role in C. reinhardtii (Yadavalli et al., 2011). Recent reports showed that determination of the full configuration of 10 LHCI subunits in the green algal PSI-LHCI supercomplex by identification of their cross-linked chemical cross-linking, products immunodetection and mass spectrometry and suggesting that the two copies of LHCA1 and one copy of each of the other eight LHCI subunits (Fig. 1.5). Overall 10 LHCI subunits are present in PSI-LHCI supercomplex in *C.reinhardtii* (Ozawa et al., 2018).

A recently published crystal structure explains that each Lhca protein is bind to 14-17 molecules of chlorophylls (Chl) and 3-5 carotenoids (Su et al., 2019). The most distinguishing feature of the structure of green algal LHCI is the existence of two

layers. inner LHC1 belt is heterotetramer composed The a and Lhca1a/Lhca8/Lhca7/Lhca3 and the outer LHC1 belt is composed of Lhca1b/Lhca4/ Lhca6/Lhca5 from PsaK side. The heterodimer, Lhca2/Lhca9, which binds to the opposite side to the LHCI belt in between PsaL and PsaG (Suga et al., 2019). The ATP synthase consists of two portions, the Fo portion which is embedded in the transmembrane region, and the F1 portion is perturbed into the soluble stroma (Soares et al., 2008). The F_1 portion consists of the subunits, alpha (α), beta (β), gamma, delta, and epsilon. The F_O region of ATP synthase consists of subunits a, b (x2) and c (x10-15). Protons pass across the membrane from the intermembrane space to the matrix, down the concentration gradient generated by the electron transfer chain through the cring of the F_O region is attached to the central asymmetric part, composed mainly of γ subunit, causing it to movable within the α_3 β_3 of the F_1 thereby the 3 catalytic binding sites are involved in a series of changes that leads to ATP synthesis (Junge and Nelson, 2015).

The rate of Calvin-Benson-Bassham cycle reactions is saturated during the excess light condition and it leads to more production of ATP and NADPH when compared with their metabolic demand and it creates ATPase limitation from lack of ADP substrate, which reduces the return of H⁺ to the stroma and causes the acidification of luminal side (Rees et al., 1992). A major photo-protective mechanism, nonphotochemical quenching (NPQ) is activated when luminal pH goes down. In *C.reinhardtii*, NPQ activity requires LHCSR1 and LHCSR3 proteins to trigger the quenching state to sensing low luminal pH in the membranes (Peers et al., 2009).

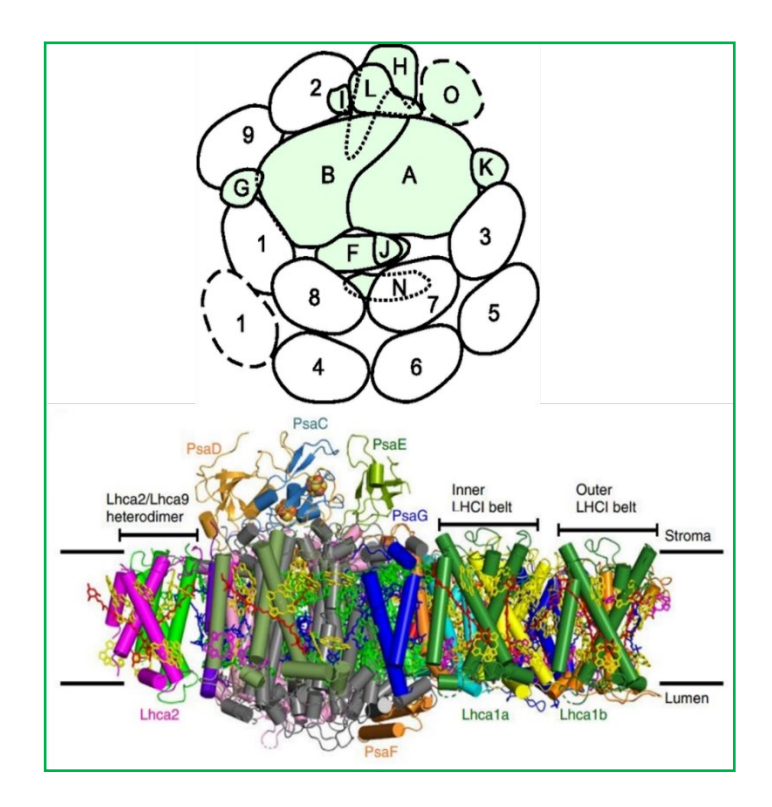


Fig. 1.5 The representation of PSI-LCHI structure from *C.reinhardtii*. A, Cryo-EM projection map of dimer structure of PSI-LHCI, LHCA2 with red in colour and LHCA9 with pink in colour which is overlaid on the PSI-LHCI. B, Schematic structure of PSI with LCHI complexes, PsaA and Psab are core proteins of PSI. C, Cryo-EM structure of pea plant PSI-LHCI complex which showing that PsaA, B, C, E, G, and F. The LHC1 proteins in inner LHC1 belt and outer LHC1 belt towards the stromal side. (Adapted from Ozawa et al., 2018 and Suga et al., 2019).

1.4 Structure and function of thylakoid membrane (polar) lipids

Membrane lipids are involved in the formation of the double-layered surface of all living cells. This non-polar bilayer avoids the diffusion of ions across the membrane which enables in the formation of a proton motive force for photochemical activities. The lipids, various proteins, receptors and ionic pores present in the membrane controls the entry and exit of other molecules as part of the metabolism (Fig. 1.6). The membrane lipids are highly conserved from cyanobacteria to higher plants which suggest that these lipids are essential for membrane integrity and proper function and maintenance of the photosynthetic machinery. Chloroplast consists of three layers, outer and inner membranes along with thylakoid intermembrane space, where photochemical and electron transport reactions are carried out. Thylakoid membranes constitute of the photosynthetic machinery, PSII, PSI, Cyt *b6/f* complex and, ATP-synthase subunits (Garab et al., 2017). Apart from these complex proteins, the chloroplast thylakoid membranes of plant and cyanobacteria are mostly composed of 4 unique lipid classes.

The first and most abundant galactolipid is monogalactosyldiacylglycerol (MGDG), second most is digalactosyldiacylglycerol (DGDG), and the third one is the sulfoquinovosyldiacylglycerol (SQDG) which is a sulphur containing lipid and the last one is phosphatidylglycerol (PG). The abundant uncharged lipids in thylakoid membranes are, MGDG is about 50% and DGDGD is 25% respectively (Dorne et al., 1990). The two galactolipids, MGDG and DGDG are predominant in thylakoid membranes of chloroplasts, and essential for the proper function of photosynthesis (Kobayashi et al., 2007). The remaining occupied with SQDG and PG. The sole phospholipid is PG which is present in cyanobacteria and another one is phosphatidylinositol (PI) is present in a minor constituent in the thylakoid membranes (Wada and Murata, 1998; Kobayashi, 2016).

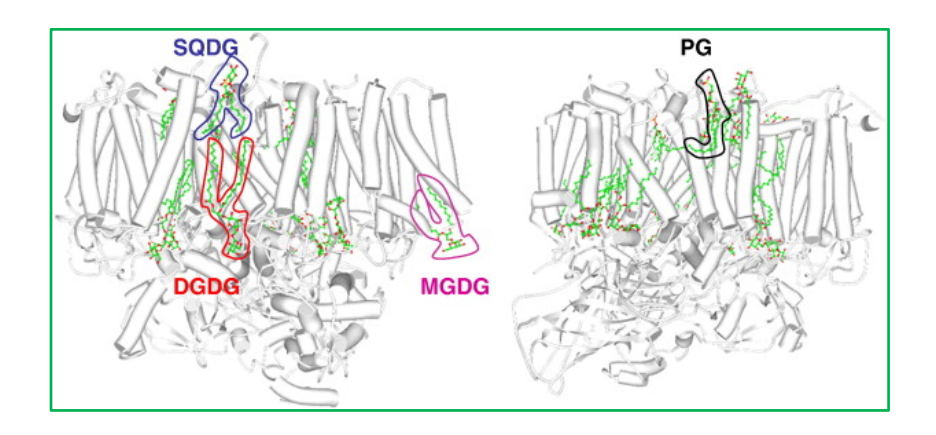


Fig. 1.6 Thylakoid lipids associated with the monomeric form of cyanobacterial Photosystem II from *Thermosynechococcus elongates*, (PDB ID: 3KZ1). The image was visualized using Protein Workshop to show chloroplast lipid ligands. Examples of sulfoquinovosyldiacylglycerol (SQDG), mono and digalactosyl diacylglycerol (MGDG, DGDG) phosphatidylglycerol (PG), are circled with respective colour (Adapted from Guskov et al., 2009 and Boudière et al., 2014).

The recent PSI-LHCI complex crystal structure from *C.reinhardtii* consists of 15 lipids of three types were identified and they are PG, DGDG and MGDG (Suga et al., 2019). The PSI core consists of 4 lipids, one is PG846, which is linked with PsaA, PG847 with PsaA, DGDG 850 with PsaB and last one is PG851 with PsaB which are distributed in a pseudo-C₂ symmetrical form (Suga et al., 2019). The galactolipids are synthesized at the chloroplast envelop membranes. In Tobacco and *Arabidopsis*, the enzyme MGDG synthase, *MGD1* is localized at inner envelope of the chloroplast where it produces the predominant part of MGDG (Awai et al., 2001). The knock (*MGD1-1*) out mutant of Arabidopsis shows in decreased 40% MGDG thereby severe loss in thylakoid membranes and also sequential degradation of galactolipids (Kobayashi et al., 2007).

The reports have been shown that the number of thylakoid membranes were decreased with altered architecture in partial deficiency of MGDG lipid in *Arabidopsis*, tobacco and maize (Wu et al. 2013; Fujii et al., 2014). MGDG also plays an important role in photoprotective nonphotochemical quenching and its ability to mediate solubilisation of violaxanthin, binding of violaxanthin de-epoxidase to the thylakoid membrane (Jhans et al., 2009). However, the complete absence of MGDG (~95 %) causes the loss of PSII activity and thereby the formation of immature photosynthetic supercomplexes (Kobayashi et al., 2013).

In vitro analysis reveals that MGDG is required for LHCII oligomerization and dimerization of PSII and also enhances the energy coupling between LHCII and PSII core proteins (Schaller et al., 2011; Kansy et al., 2014). The outer chloroplast envelope harbours two DGDG synthase complexes and is named as DGD1 and DGD2 syntheses (Froehlich et al., 2001; Kelly et al., 2003). The enzyme DGD1 synthesizes the major proportion of DGDG, whereas DGD2 is active under phosphate limitation for supplying the intermediate of lipids for cell survival. The similar results were observed in the MGD1 mutant of tobacco in reduced levels of Cyt b6f protein complex and bottleneck in the electron transport (Wu et al., 2013). The most important galactolipid, DGDG is required for the proper maturation or maintenance of the thylakoid membranes. The deficient DGDG mutant of A.thaliana, showed strong bends in thylakoid membranes of leaf chloroplasts. DGDG is essential for the proper maintenance of structure and function of PSII especially on donor side and involved in trimerization of LHCII (Steffen et al., 2005; Hölzl et al., 2009). The development of the thylakoid membrane is also affected by the loss of PG and SQDG in plants. In pea plants and spinach leaves, the degradation of PG in thylakoid membranes hampers the electron transport system in PSII thereby without affecting the PSI activity (Droppa et al., 1995).

Characterization of PG-deficient mutant of Synechocystis reveals that PG is required for the proper regulation of electrons from the primary Q_A to the Q_B at the PSII acceptor side, for the maintenance of the activity of OEC complex at the PSII donor side, and the activity of the PSI complex, and finally involved in trimerization (Domonkos et al., 2004; Sakurai et al., 2007). The results from *Chlamydomonas* mutants also suggested that PG is required for the synthesis of D1 and CP47, LHCII trimer formation, state transition ability, and the activity of OEC complex (Dubertret et al., 1994; Maanni et al., 1998; Pineau et al., 2004). The loss of SQDG causes the decreased grana stacking which leads to major curling in thylakoid membranes (Yu and Benning 2003). In summary of this, galactolipids, (MGDGD and DGDG) are acidic lipids, (PG and SQDG) involved in proper maintenance of thylakoid membranes, stabilization of PSII dimer, the proper function of PSI, LHCII complex and, the activity of oxygen evolving complex. Apart from above membrane lipids, the extraplastidic membrane lipids are very important for the function of cellular metabolism and they are diacylglyceryl-N, N, N-trimethylhomoserine (DGTS), phosphatidylinositol (PI) and phosphatidylethanolamine (PE). DGTS lipid is the major class of lipid in C.reinhardtii (Moellering et al., 2009). A major difference between plants and algae is like C. reinhardtii contain DGTS, which is to substitute for the phosphatidylcholine (PtCho) found in plants (Moore et al., 2001). In C. reinhardtii, the biosynthesis of DGTS is located at ER and synthesis catalysed by an enzyme known as Chlamydomonas betaine lipid synthase (BTA1_{Cr}) (Riekhof et al., 2005).

1.5 Algal biofuels

Development of new biofuel production methods is expected to become important with increasing population in the coming years. Large-scale domestic biofuel production appears to be feasible, reducing the cost of imported petroleum and petroleum-based fuels and improving sustainability energy. Diminished fossil fuel supplies and global warming due to anthropogenic CO₂ emissions have generated massive developments in renewable energy. Microalgal biomass for biofuel has been a focus of efforts, however, it is relatively high cost and low yield; biotechnological improvements are the major implications for the viability of microalgae as a biofuel source. Microalgae are the third generation of material for biofuel production. The edible feedstock (first generation), organic waste products and land grew energy crops (second generation), which compete with food crops for arable land (Moore, 2008). The conversion rate of light energy into useful high-energy compounds is higher in microalgae relative to the first generation of biofuels (Melis, 2009).

Another major advantage of algal derived biofuels is the ability to accumulate biomass rapidly (Imramovsky et al., 2011). The major challenge associated with the process of biofuels from viable algae is depending upon the ability to produce algal biofuels at the economic scale (Starckx and Senne, 2012). The production of biofuels is associated with high lipid production from photosynthetic green algae (Griffiths and Harrison, 2009) but to reach the production of lipids, all the steps linked with the efficient production of algae at large scale level. The land area required to displace sizable fractions of petroleum use with biofuels would be reduced if using algae as a feedstock.

1.6 Abiotic stress

Generally, stress is divided into two primary groups: biotic and abiotic. Biotic is nothing but when biological living organisms such as weeds, insects, and pathogens that damage other living systems whereas abiotic stress is non-living system that affects the living organisms in a specific environment. Abiotic stress includes many factors which affect the environment. The main abiotic stress factors are extreme temperature, salinity, drought, nutrient deprivation (P, N, S, Fe, Zn, Cu, Mn), high light, cold, heavy metals, wind etc...

1.6.1 Iron homeostasis in Chlamydomonas

The iron is available in the form of ferrous oxides (Fe²⁺) and which is relatively abundant in the earth's crust. It is present mostly insoluble form as ferric oxides (Fe³⁺) in water surface and neutral to alkaline soil. The limited bioavailability of iron Fe²⁺ creates a major problem to photosynthetic organisms and estimations indicates that there is 40% growth inhibition occurs in ocean phytoplankton (Moore et al., 2002). The main pathway for iron uptake is same from land plants to Chlamydomonas (Fig. 1.7). The iron uptake is a ferroxidase-dependent ferric transporter complex and it consists of the ferroxidase (FOX1) and ferric transporter (FTR1). The enzyme FOX1 is a copper dependent enzyme which catalyses the oxidation of Fe(II) to Fe(III) which is similar to yeast, the enzyme Fet3p and in humans Ceruloplasmin (Herbik et al., 2002; La Fontaine et al., 2002). The FOX1 protein is react with enzyme permease, FTR1, which transfer the ferric iron which is brought by FOX1 into the cytoplasm (Terzulli and Kosman, 2010). FOX1 protein quickly responds when low concentration of iron that effects on cells physiology and it acts as a robust marker enzyme for iron status in the cell. Green algae and

plants have two iron rich compartments, chloroplast and mitochondrion. They have numerous iron dependent proteins which are essential in the electron transfer pathways in their cells. Iron containing proteins involved in various biochemical processes such as detoxification of reactive oxygen species, fatty acid metabolism, and other biosynthetic pathways. The complexes involved in electron transfer reactions are dimers of PSII, Cyt $b_6 f$, monomer of PSI and, linear electron flow from PSII to ferredoxin requires 30 iron ions (if includes plastocyanin and cytochrome c_6 31 iron atoms are required) (Blaby-Haans and Merchant, 2013). However, the respiration reactions requires more iron than photochemical reactions. At the same time, in all oxygen evolving photosynthetic organisms, chloroplast is the major sink for iron where iron acts as a cofactor in many iron-dependent proteins of the thylakoid membranes (Glaesener et al., 2013).

1.6.2 Methods for creation of iron deficiency in Chlamydomonas

There are three common methods generally used to create less iron nutrition in the laboratory. The first is by using chemical chelators to limit the available iron in the medium. Two compounds, 2,2'-dipyridyl and Bathophenanthroline disulfonic acid are rottenly used to chelate the iron from yeasts cells, *S. cerevisiae* (Jo et al., 2009). Studies from the plant, *A. thaliana* have used as chelators such as ferrozine which chelates the iron (Lanquar et al., 2005; Yang et al., 2010). The ferrozine and ethlenediamine-N,N'-bis (2-hydroxyphenyl) acetic acid have been used for Chlamydomonas to chelate the iron in the medium (Rubinelli et al., 2002). However, iron chelators, they will also bind to other metal ions along with iron, so again it is a severe problem for growth (Kroll et al., 1957; Stookey, 1970).

This technique has not been used for Chlamydomonas. In *A. thaliana IRT1* is a mutant of iron transporter which was used to study the iron nutrition on lateral root development and its gene expression (Wang et al., 2007; Giehl et al., 2012). In the yeast double mutant, the *fet3 fet4* lacking both high and low affinity iron transport pathway and thereby they are very sensitive under less or more of iron concentration (Dix et al., 1994). The third and best approach is to omit or control the addition of an iron which we added to the medium.

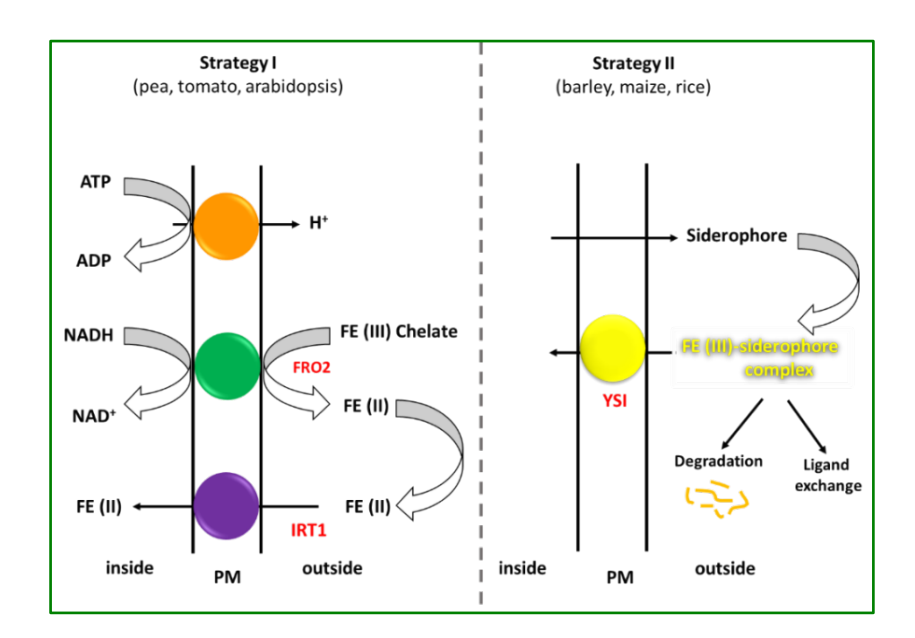


Fig. 1.7 The iron uptake pathway from Chlamydomonas. The pathway is same as higher plants. It is simply known as fungal like a pathway, ferroxidase-dependent ferric transporter complex (FOX and FTR1 complex). The enzyme, FOX1 expressed abundantly in iron-deficiency (Adapted from Guerinot and Yi, 1992; Glaesener et al., 2013).

1.6.3 Role of iron (Fe²⁺) in photosynthesis

Iron deficiency is major abiotic stress from ocean to land plants. It constitutes a promising factor leading to reduction of growth of aquatic organisms and the reduction of crop yield. Generally, low bioavailability makes it deficient for life on the earth. In nature, it is predominantly found in the form of Fe³⁺ oxides at biological pH which is insoluble from oxygen-rich surface waters and neutral to alkaline soil (Guerinot and Yi, 1994). Estimations have been shown that iron limits phytoplankton growth up to 40% of the ocean and that 30% of the land is too alkaline to optimal iron uptake and also suggesting the poor iron bioavailability affects the consequential impact on the food chain, oxygen release and, carbon sequestration (Chen and Barak, 1982; Moore et al., 2002). Organisms like plants and algae have developed a complex system for iron uptake and adjusting their metabolomics pathways to survive even in low iron concentrations (Walker and Connolly, 2008). Plants have developed two strategies for iron uptake to avoid iron deprivation. The non-graminaceous monocots and dicots use the strategy I for iron uptake whereas grasses strategy II (Curie et al., 2001) (Fig. 1.7). The major part of iron is believed to present in both organelles, chloroplast and mitochondria (Briat et al., 2007). Among all photosynthetic complexes, PSI complex has more iron content (12 Fe per PSI) and it is more prone to iron deficiency in C. reinhardtii and Oryza sativa (Yadavalli et al., 2012a&b). Also, reported that most of the PSI complexes have been destabilised in Fe deficiency. Normally in iron limitation, chlorosis (loss of chlorophyll) is the early symptom that occurs in all photosynthetic organisms (Price, 1968). Chlorosis is attributed to inhibition of chlorophyll biosynthesis which involves iron containing enzymes/proteins and it ultimately leads to changes in chloroplast ultrastructure and decreased abundance of photosynthetic machinery (Spiller and Terry, 1980). Iron mainly participates in electron transfer reactions which

are operated during the photosynthesis process. Usually, ROS production is one of the major threatening factors that limits the growth of photosynthetic organisms (Yadavalli et al., 2011a&b). The iron deficiency response in *C. reinhardtii* includes a hierarchy for iron allocation within organelles and importantly, acetaldehyde dehydrogenase (ADH1), is induced under low iron level and it attenuates the remodelling of the photosynthetic machinery in *C. reinhardtii*. Iron deficiency stimulates the expression of stress-related proteins such as NDA2, LHCSR3, and PGRL1 in *C. reinhardtii* (Höhner et al., 2013). These findings suggest that iron involved in the regulation of bioenergetic pathways and is sensitive to the cellular and metabolic and/or redox status of the chloroplast.

1.7 Strain C.reinhardtii

C.reinhardtii is a single, eukaryotic alga and it has a unique system for investigating how photosynthetic organisms response to low level of iron concentration. The response of plants to iron deficiency can be evaluated by checking the nutritional profile of each cell, tissue type. However, C.reinhardtii generally grown in liquid cultures and exposure to nutrients can be more homogenous. The organism, Chlamydomonas is very convenient and easy to grow in in vitro conditions and also to elucidate the fundamental aspects of photosynthesis (Rochaix, 2002), in specific to metal metabolism (Merchant et al., 2007). It has been well documented that thylakoid membranes are arranged in appressed and non-appressed regions and their functional organization have been studied extensively in wild type and their mutants impaired in various photosynthetic regulatory mechanisms (Fig. 1.7).

It has distinct pyrenoid where CO₂ fixation occurs and dark reactions take place (Harris, 2001). Galactolipids are essential for proper formation and organization of thylakoid membranes and also proper function of complexes involved in electron

transfer reactions. The present study with *C.reinhardtii* strain, wt CC125 has been used as a model organism for studying the strategy of iron starvation (Fig. 1.8). Several reports have shown that under iron limiting conditions in *C.reinhardtii*, the electron flow from Q_A to Q_B site of PSII complex is down regulated (Msilini et al., 2011a; Yadavalli et al., 2012a). However, LHC proteins are deferentially affected in C.reinhardtii cell in low iron levels (Yadavalli et al., 2012a). The main components of LHCI proteins drastically reduced which leads to down regulation of LHCI complex whereas the overall abundance of LHCII protein are remaining fairly effected (Hippler et al., 2001). Further, the same reports on the N-terminal processing of Lhca3 protein is a key step which induces a conformational change that activate the remodelling of LHCI complex (Naumann et al., 2005). The reports on the remodelling of bioenergetic pathways that change the proteomic levels due to iron limitation (Naumann et al., 2007). The recent studies have been shown that alteration of their pigments and proteins that ultimately decreases the PSI-LHCI complex with iron deficiency in C.reinhardtii (Yadavalli et al., 2012a). Recent PSI-LHCI crystal structure from C.reinhardtii has elucidated that there are ten Lhca proteins which are arranged in two layers of the belt (Suga et al., 2019). To characterize the photochemistry and organization of thylakoid membranes under severe iron deficiency in C.reinhardtii can be answered for several questions related to Fe importance.

We have focused on the effect of iron deficiency on electron transfer mechanism, functional and biochemical characterization of PSII-LHCII supercomplexes. Further, we have studied the restoration of photosynthetic activity, their supercomplexes, and degradation or remodelling of thylakoid membrane lipids and expression of enzymes/proteins involved in lipid accumulation for the understanding of lipid biosynthetic pathways for biofuel production under iron

starvation. Further, their recovery conditions are also studied for understanding the role of iron nutrition in *C.reinhardtii*.

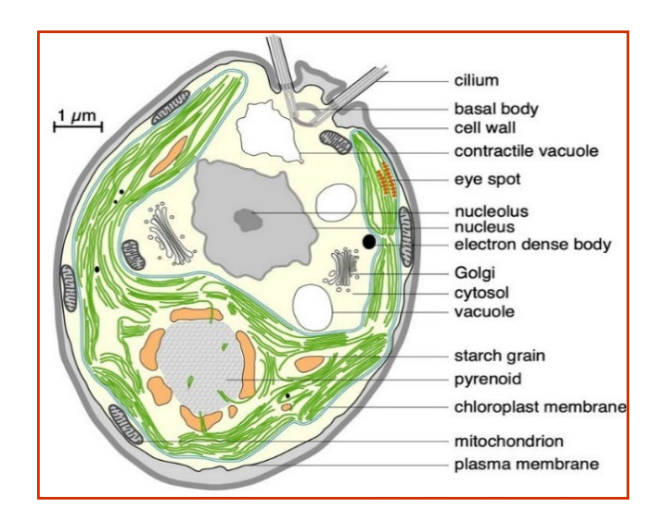


Fig. 1.8 Schematic structure of *C.reinhardtii* cell. (Adapted from Mec Cormick lab)

1.8 Objectives of the study

In this study, we have characterised the changes in photosynthetic apparatus, alteration of membrane lipids and lipid accumulation by using biochemical and biophysical methods in *C.reinhardtii* under iron starvation. To accomplish our major goals of the study, we have designed the following objectives.

Objectives

- 1. Photochemistry and biochemical characterization of PSII-LHCII supercomplexes under iron starvation.
- 2. Recovery of photosynthetic activity and apparatus from severe iron deficiency condition.
- 3. Alteration of thylakoid membrane lipids and lipid accumulation under iron starvation.

Experimental procedures

Chapter 2



2.1 Description of C. reinhardtii

C. reinhardtii wild-type CC125 strain is a motile unicellular alga, generally, shape in the oval. The culture was obtained from the Chlamydomonas resource center, University of Minnesota, USA. This strain originated from an isolate made near Amherst, Massachusetts, in 1945. The genus of Chlamydomonas, consisting of about 325 species, all are unicellular flagellates, found in stagnant water and on damp soil, in freshwater, seawater, and even in snow as "snow algae" (Hoham et al., 2002) Chlamydomonas is used as a model organism to study molecular biology, especially studies of flagellar motility and chloroplast dynamics, bioenergy, and genetics. C. reinhardtii is of interest for producing biopharmaceuticals and biofuel, as well as being a valuable research tool in making hydrogen.

2.2 Culturing of C.reinhardtii

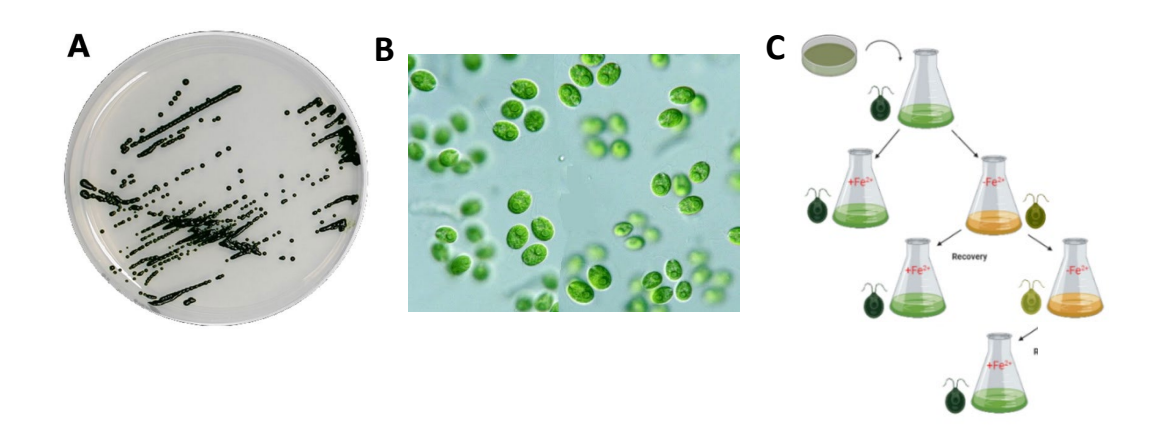


Fig. 2. 1 (A) Representation of *C. reinhardtii* cultured in TAP medium with agar and growth. (B) Showing the bright filed microscopic image from the cell and cell size is around 10 μm (C). Methodology for iron deficiency in *C.reinhardtii* cells.

Cells of *C. reinhardtii* wild type strain was grown in a Tris-acetate phosphate medium (TAP) under continuous illumination at 50 μ mol photons m⁻² s⁻¹ at 25 ± 2 °C (Fig. 2.1). The seed culture was grown up to mid-logarithmic phase and approximately 3.0 x 10⁶ cells were collected and washed thrice with TAP(-)Fe medium. These cells were inoculated into 800 mL of TAP(-)Fe medium and allowed to grow for 72 h (1st stage of iron deficiency). The 1st stage of iron deficiency of cells (3.0 x 10⁶) was inoculated again into TAP(-)Fe deficiency medium (2nd stage of iron deficiency) as well as TAP (+)Fe medium for recovery (RC). RC1 was grown up to 72 h. For recovery condition, the same number of cells were collected and added to the TAP (+) Fe medium and this was represented as RC2. All the flasks were washed with 10% HCl and autoclaved before the preparation of TAP (-)Fe medium. Cell culture has been maintained in TAP solid medium containing 1.5% of Agar (MERCK) in TAP media. Culture steaking has done every 15 days and all the plates were kept at cool white fluorescent light (80 μ mol photons m⁻² s⁻¹ at 22 ± 2 °C).

2.3 Spectrophotometric measurements

Spectrophotometric measurements of cell density were taken using a PerkinElmer spectrophotometer (USA). Absorbance value at a wavelength of 750 nm (A₇₅₀ nm) was used to measure the cell density of *C. reinhardtii*. For each measurement, 1 mL of sample was loaded into a 10 mm width polystyrene cuvette (Eppendorf, USA). 1 mL of media was used as a blank for the spectrophotometer at the appropriate wavelengths. The fractions collected after sucrose density gradient and used for measuring the room temperature absorption spectra. All the fractions were recoded from 400-750 nm with a scan of 100 nm min⁻¹ by using UV-3600 Shimadzu spectrophotometer.

2.4 The fast OJIP Chlorophyll a fluorescence measurements

Chl *a* fluorescence transients were measured with the Plant Efficiency Analyser (PEA) at room temperature. In Handy PEA fluorescence instrument (Hansatech Instruments Ltd., UK), activating light is provided by an array of three high intensities light-emitting diodes, which are focused onto the cell surface to provide uniform illumination. The diodes provide red light at a wavelength of 650 nm and an intensity of 3000 μ mol photons m⁻² s⁻¹, which is readily absorbed by the chloroplast. 1 mL of actively grown cells were taken for measurements. Then each cell suspension was kept in dark for 30 min at room temperature. 10 μ M of Diuron (DCMU) was used for inhibitor treatment. The fluorescence measurements were taken after 30 min of dark incubation and followed by the fluorescence measurements were taken as described in Kodru et al. (2015). The fluorescence transient at 20 μ s is designated Fo and the maximum fluorescence yield (Fm) occurs around 200 ms. The difference between Fo and Fm is known as variable fluorescence (Fv).

The fast fluorescence kinetics was recorded from 10 μ s to 1 s. The initial fluorescence (F_O) was set as O (30 μ s), L (150 μ s), K (300 μ s), J (20 ms) and I (30 ms) are the intermediates (F_L and F_K, respectively) and P (300 ms) as the maximum fluorescence (F_M). The fluorescence transients were double normalized in between F_O (30 μ s) and F_K (300 μ s) represented as V_{OK} [V_{OK} = (F_t-F_O)/ (F_K-F_O)] to explain the possibility of fluorescence rise at an early step at 30 μ s. Subsequently, the difference in transients (D_{VOK}) concerning a reference was calculated for each sampling date to reveal the value called as L-band. Similarly, the transients were double normalized between F_O and F_J represented as V_{OJ} [V_{OJ} = (F_t-F_O)/ (F_J-F_O)], and the difference between transients denoted as D_{VOJ} was determined for each sample to assess the band

called K-band. The ratios Fv/Fo and Fv/Fm are used to assess photosynthetic efficiency. O-J-I-P kinetics were visualized by using Biolyzer HP 3 software (for calculating the JIP test parameter that quantifies energy flow through PS II) by Bioenergetics Laboratory, University of Geneva, Switzerland).

Table 1. Chlorophyll *a* fluorescence OJIP test parameters

Formulae	Description of the OJIP test parameter	
$\begin{array}{ccc} Fm & & Maximum \ fluore \\ K_N & & \end{array}$	Minimum fluorescence value after the onset of actinic light illumination at 30µs Maximum fluorescence value after the onset of actinic light illumination Non-photochemical de-excitation rate constant Photochemical de-excitation rate constant	
K_P ABS/RC = MO (1/V _J) (1/ ϕ_{Po}) center (RC)	Absorption flux (for PSII antenna chls) per reaction	
ETO/RC = MO (1/VJ) ψ o DI _O /RC = (ABS/RC) - (TRO/RC)	Electron transport flux per RC (at $t = 0$) Dissipated energy flux per RC (at $t = 0$)	
$RC/CSm = \psi_0 (VJ/MO) - (ABS/CSm)$ (at t = tFM)	Density of reaction centers per excited cross-section	
ABS/CSm = FM (at $t = tFM$) approximated by FM	Absorption flux per excited cross section,	
$TR_O/CSm = \phi_{Po} \text{ (ABS/CSm) (at t = tFM)}$ approximated by FM	Trapped energy flux per excited cross section,	
$ET_O/CSm = \phi_{Eo} (ABS/CSm) $ (at t = tFM) approximated by FM	Electron transport flux per excited cross section,	
$DI_O/CSm = (ABS/CSm)-(TRO/CSm)$ (at t = tFM approximated by FM	Dissipated energy flux per excited cross section,	
PI (ABS) = (RC/ABS) $(\phi_{Po}/(1-\phi_{Po}))$ $(\psi_{O}/(1-\psi_{O}))$	(o)) Performance index on absorption basis	

2.5 Chlorophyll *a* fluorescence induction measurements

Pulse amplitude modulated-PAM 101 fluorometer (Walz GmbH, Effeltrich, Germany) was used to monitor the Chl *a* fluorescence under different stress conditions. PAM was connected to a Data Acquisition System 100 controlled by WIN CONTROL v2.08 software (Heinz Walz GmbH, Germany). *C.reinhardtii* cells were collected from respective conditions and adjusted to an equal density of 3 x 10⁶ cells mL⁻¹ or based on equal chlorophyll content. The cells were kept for dark adaptation for 20 min before

fluorescence measurements. The two LED arrays provided the actinic light (AL) at 650 nm and which was with illuminating the cell suspension applied for 1 ms, after measuring light (ML) 460 nm was turned for measuring and continued for 5 min and later turn off the AL. The maximal fluorescence from the dark adopted state (Fm) and during the time course of actinic illumination (Fm') and the subsequent dark relaxation period was determined by saturation (1400 μ mol photon m⁻² s⁻¹) light pulse was applied at 1 min intervals. The maximum quantum efficiency of PSII [Fv/Fm = (Fm – Fo)/Fm] was assessed after 20 min of dark incubation. Subsequently, fluorescence rapid light curves (RLCs) were obtained using eight different actinic light intensities (145, 221, 344, 536, and 830 μ mol photons m⁻² s⁻¹ for 30 s each). Subsequently, the actinic light (250 μ mol photons m⁻² s⁻¹) was maintained for 5 min, before a final saturating pulse was applied. The fluorescence RLC parameters were calculated according to Kosourov et al., (2007).

2.6 Room temperature fluorescence measurements

The fluorescence spectra were measured with a Perkin-Elmer LS55 spectrofluorimeter. The excitation at and emission spectral widths were fixed at 6 nm, respectively. The Low temperature (77 K) emission spectrum is used to measure the chlorophyll sites, and sensitive to monitor the changes in both PSI and PSII. This spectrum also reveals fluorescence maxima at 680 and 705 nm which are attributed to PSII and PSI respectively whereas, at room temperature, we can measure PSII changes. Here we have measured the PSII changes with iron deficient conditions at RT fluorescence measurements. We have kept the Chl fluorescence excitation at 436 nm and the emission wavelength was between 650 nm to 780 nm. The room temperature fluorescence emission spectra were measured as described by Msilini, et al. (2013).

Measurements were collected based on Chl content, protein content, and an equal number of cells from all the samples and we got similar results. Therefore, we showed the data with 10 μg mL⁻¹ Chl content for RT measurements.

2.7 Total ROS measurements

Total ROS produced by *C. reinhardtii* cells during iron deprivation was measured using the fluorescent dye 2', 7'-dichlorofluorescein diacetate (DCFH-DA) (Sigma). Logarithmic-phase cells were centrifuged at 1500 x g, 20 °C for 5 min, resuspended in an equal volume of fresh TAP medium, and then incubated in 5 μM DCFH-DA for 1h in the dark at 25 °C. After dark exposure, the cells were washed twice with TAP (-Fe) or TAP to remove excess dye. The fluorescence was measured using a Microplate reader (Tecan M250) at an excitation of 485 nm and an emission of 530 nm. The amount of total ROS was calculated by using the equation:

Total ROS =
$$(F_{TAP} - (-Fe_{TAP}))$$

2.8 Quantification of neutral lipids

The cells were fixed with 0.25% (v/v) glutaraldehyde and stored at 4 °C until measurement. A Nile Red solution (1 mg mL⁻¹ Nile Red) in Acetone (Merck) was added to each sample, and the mixture was incubated for 20 min at room temperature. Then excess dye was removed by centrifugation at 3000 rpm at RT. The fluorescence was measured with an excitation at 530 nm and emission at 604 nm with help of EnSpire plate reader (Teccan, MPRO infinite 200, USA). Total NR bound to neutral lipids was calculated from background (autofluorescence from Chlorophyll- without NR) fluorescence. Bellow formula has been used for fluorescence calculation.

Total NR fluorescence = (Background fluorescence – whole-cell fluorescence)

2.9 Fourier-transform infrared spectroscopy (FTIR)

Fourier-transform infrared spectroscopy (FTIR) can be used to measure the infrared absorption attributed to specific molecular vibrational modes (Murdock and Wetzel, 2009). Macromolecular groups including, proteins, lipids, carbohydrates, and nucleic acids, can be quantified by measuring their characteristic absorption bands (Table 2.) (Dean et al., 2010). Samples were collected and pelleted from 10 mL of liquid culture. The cell pellet was washed with 1 mL of dH₂O and then the total pellet was dried at RT for 24 h. For FTIR measurements, we have taken equal dry weight from all the samples. The OMNIC (Brucker, U.S.A) and AutoPRO (Technologies) software associated with programmed to take a baseline measurement in an empty well (60 scans) and then measure all other wells containing samples (60 scans). The following table showing the wavenumbers for respective molecule identification.

Table 2. Showing the parameters of FTIR wavenumbers of each functional group.

Wavenumber (cm ⁻¹)	Assignment
3000-2800	νC-H of saturated CH
~2925	νC-H of lipids
~1740	νC=O of ester groups, primarily from lipids and fatty acids
~1650	νC=O of amides from proteins (amide I band)
~1540	δN –H of amides from proteins (amide II bands)
~1455	δas CH3 and δas CH2 of proteins
~1398	δs CH3 and δs CH2 of proteins, and vs C-O of COO- groups
~1250-1230	vas P=O of phosphodiester groups of nucleic acids and phospholipids
~1200-900	vC–O–C of saccharides
~1075	vSi–O of silicate frustules

vas, asymmetric stretch; vs symmetric stretch; δas, asymmetric deformation; δs, symmetric deformation.

For analysis of spectra, previously published peak attributions were identified in *C.reinhardtii* (Stehfest et al., 2005; Pistorius et al., 2009). All spectra were baseline corrected using the automatic baseline function in the OMNIC software to minimize differences between spectra due to baseline shifts (Fig. 2.2). Spectra were then scaled to the peak height of the amide II band (1545 cm⁻¹). Lipid accumulation was expressed as a lipid: amide I ratio using the peak height measured at either 2921 cm⁻¹ or 1741 cm⁻¹, attributed to lipids, and at 1655 cm⁻¹ attributed to amide I (protein).

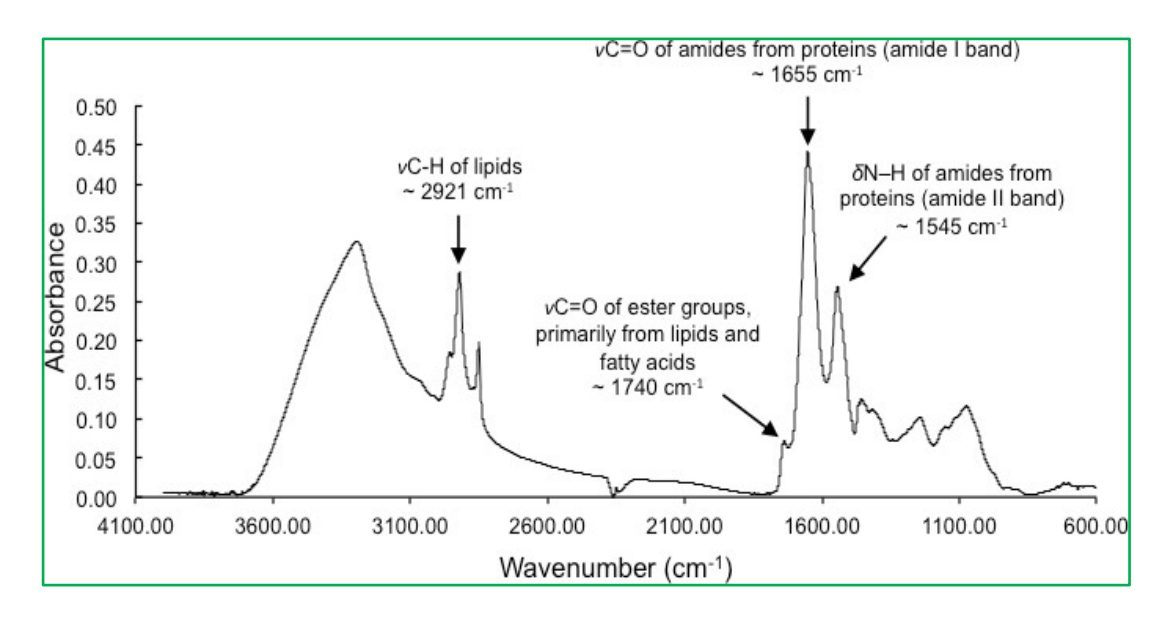


Fig. 2.2 Baseline corrected FTIR spectra showing absorption bands used for lipid, protein, and carbohydrate analysis: lipid peaks at \sim 2920 cm⁻¹ and \sim 1740 cm⁻¹; amide I peak at \sim 1655 cm⁻¹ amide II peak at \sim 1545 cm⁻¹. Carbohydrate bonds at 1210 cm⁻¹.

2.10 Lyophilisation for dry weight measurements

Total dry weight (DCW) was measured after lyophilisation. An equal volume (30 mL) of algal culture was collected by centrifugation at 2000 x g for 10 min at RT. The cell pellet was washed with distilled water to remove the excess nutrients and again centrifuged at the same above centrifugation for 5 min and the final cell pellet was freeze in liquid nitrogen before keeping in lyophilization. Each tube was sealed with parafilm and kept in a lyophilizer (USA) at -109 °C for 12 h and pressure was at 0.002

Chapter 2

psi. Total dry weight was quantified by taking the weight of the tube with dry pellet minus weight of the empty tube. Follow the simple calculation below

$$DW = (w2-w1)/v$$

Where w1 is the empty tumbler weight, w2 is the dried cell pellet weight, and v is the initial volume of the sample.

2.11 Quantification of total lipids

The dried cells of *C. reinhardtii* were used for total lipid content measurements. The lipid content was quantified in terms of the percent of dry biomass accounted for by lipids. The dry powder (20 mg) was pre-crushed with 1 mL of n-hexane and then transferred into a 10 mL glass tube, and 3 mL of n-hexane and 1.5 mL of isopropanol were added to the same tube. The tube was shaken at 100 rpm for 24 h. The 30 ml of distilled water was then added to the tube. The tube was shaken for 1 min and then centrifuged at $5,000 \times g$ for 5 min. The upper n-hexane layer containing the lipids was collected on a pre-weighed Eppendorf tube (1.5 mL), dried at room temperature overnight at RT, and then dried at $50 \,^{\circ}$ C for 1 h. The collected lipids were then weighed. Finally, the total lipid content was calculated and expressed in (%).

2.12 Extraction of lipids by Bligh & Dyer method

Total lipids were extracted as described by Bligh and Dyer, (1959) method and 20 mg dried algal sample was resuspended in 1.5 mL of chloroform/methanol (MERK) (2:1, v/v) and vortexed for 2 minutes and 50 μL of 1 M KH₂PO₄ (SRL, India) for extraction of polar lipids whereas for extraction of neutral lipids, 50 μL of 0.9% KCL added then vortexed for the 30s. The tube was centrifuged at 3000 x g, 25 °C for 5 min for phase separation. Among three phases, the upper phase is a mixture of water and methanol,

the second phase is cell debris containing proteins, nucleic acids, starch, and third, the lower phase is chloroform with lipids. We have collected the lower chloroform phase without disturbing the other two layers. This was repeated three times and the upper layer was collected and pooled. The extracts were dried via purging with N_2 gas (commercially purchased) and 20 μ L of chloroform or hexane or methanol whichever you needed for Thin-layer chromatography (TLC). Generally, chloroform is preferable. The samples were sealed with parafilm and stored at -20 °C for further analysis.

2.13 Isolation of thylakoid membranes

The method for isolation of thylakoid membranes from *C.reinhardtii* was adapted and modified from (Subramanyam et al., 206). The thylakoid membranes were isolated from cells grown at mid-logarithmic phase. The cell pellet was washed with 0.3 M sucrose, 5 mM MgCl, 5 mM HEPES, and centrifuged at 3000 x g for 10 min and sonicate the cells. Protease inhibitors, 1 mM 6-Amino caproic acid, 1 mM benzamidine hydrochloride were mixed in the solution for thylakoid isolation. The sonication was performed for 10 min at pulses on for 12s and pulses off for 47s. The supernatant was again centrifuged at $1000 \times g$ for 2 min and collected the supernatant and then collected supernatant was transferred in to separate tube and centrifuged at $10,000 \times g$ for 10 min. The pellet was washed with 0.3 M sucrose, 5 mM HEPES, 5 mM CaCl₂, 10 mM EDTA and centrifuged at $10,000 \times g$ for 10 min. The final pellet was resuspended in 0.2 M Sorbitol, 5 mM Tris–HCl (pH 7.5), 5 mM CaCl₂. The isolated thylakoid membranes were then frozen in liquid nitrogen and stored at $-80 \,^{\circ}$ C until use.

2.14 Quantification of total Chlorophyll

The total Chl was measured spectrophotometrically after extraction with 80% (v/v) acetone (MERK). 1 mL of cells was collected and transferred into a 1.5 mL tube. The cell-free media was removed by centrifugation at 2500 x g for 10 min at 25 °C and added the 1 mL of 80% acetone, vortexed and kept in the dark for 20 min at -20 °C. The samples were centrifuged at 10, 000 x g for 10 min. The total chlorophyll was calculated according to Porra et al. (1989) by taking the absorbance at 645 nm (A645) and 663 nm (A663) with a spectrophotometer (PerkinElmer, USA). The total chlorophyll (chlorophyll a + chlorophyll b: Chl a+b) concentration (μg /mL) was calculated as follows:

Chlorophyll a (mg/mL) = 12.7 x A663 - (2.69 x A645) dilution factor.

Chlorophyll b (mg/mL) = (22.9 x A645) - (4.68 x A663) dilution factor.

Total Chlorophyll (Chl a + b) (mg/mL) = $(8.02 \times A663) + (20.12 \times A645)$ dilution factor.

The total protein quantification was carried from thylakoid membranes by the Bradford method (Braford et al., 1976).

2.15 Sucrose density gradient separation method

The isolated thylakoid membranes were solubilized in 1% n-Dodecyl β -D- Malstoside (DDM) (Sigma) with 0.8 mg mL⁻¹ Chl and incubated for 10 min in dark at 4 °C. This is then centrifuged at 10,000 rpm for 10 min. The supernatant of 150 μ L was loaded on a sucrose density gradient [0.1-1.4 M sucrose, 5 mM Tricine-NaOH (pH 8.0), 0.5M betaine and 0.05% β -DM] and centrifuged at 288,000 x g with an SW Ti41 rotor was used to separate the supercomplexes (swing bucket rotor-Beckman Coulter, USA) at 4° C for 17 h (Subramanyam et al., 2006;

Takahashi et al., 2006). Three fractions were obtained and named fractions, F1, F2, and F3. The F1 (LHCII), F2 (PSII-LHCI/PSI-LHCI) F3 (PSI-LHCI), so for our experiments, we have collected 200 μL volume of sample equally from each fraction from top to bottom and carefully transferred into a 96 well plate to quantify the band intensity. The density of each fraction was taken at 675 nm. These fractions, F1, F2, and F3 were then used for absorption and CD spectra measurements.

2.16 Circular dichroism studies

Room temperature (RT) visible circular dichroism spectra were used and recorded with JASCO-1500 spectropolarimeter (Japan). The measurements were taken in the visible region (400–750 nm) with a path length of 1 mm for cells, thylakoids, and sucrose density fractions. The bandwidth was kept at 4 nm and 1 nm as the data pitch. Each sample was measured based on equal protein concentration, 20 µg mL⁻¹. Each spectrum was subtracted with a solution containing 0.2 M sorbitol, 5 mM Tris–HCl (pH 7.5) and 5 mM CaCl₂ for baseline correction and scanned with three accumulations at a scan speed of 100 nm min⁻¹.

2.17 BN-PAGE and 2D SDS-PAGE

Thylakoid membranes were taken based on chlorophyll and solubilized with 1% n-dodecyl β-D-maltoside (Sigma) at 4 °C for 10 min. A solution containing protease inhibitors were used 1 mM 6-Amino caproic acid, 1 mM Benzamidine hydrochloride. After solubilization, the mixture was centrifuged at 18000 x g under 4 °C for 18 min. Then, 7 μg of chlorophyll was loaded into each lane, and the gel was run at 4 °C with increasing voltage as described by Schägger and von Jagow, (1991) and Madireddi et al., (2014). In addition to this, native protein standard markers (Amersham, Cat no: 17044501) were also loaded on the gel to calculate the molecular weight of the

supercomplexes. Colloidal coomassie blue (CBB) staining was used to stain the gel. For two-dimensional gel separation, BN-PAGE gel was sliced into small and transferred to a 15 mL falcon tube for solubilization. The solubilization was done for 8h at RT with solubilized with 0.15 M Tris (pH-6.8), 10% glycerol, 2% SDS, 2.5% Mercaptoethanol. After solubilization, the gel was placed on 12 % SDS gel with a thin layer of stacking gel and sealed with Agarose (1.5%) which is dissolved in 0.15 M Tris-Buffer (pH-6.8). The gel was run initially at 50 v and then increased to 75 v till the end. The gel was stained with CBB solution.

2.18 Protein extraction

The *C.reinhardtii* cells were collected at mid logherthemic phase by centrifugation at $1800 \times g$ for 10 min and the pellet was transferred into 1.5 mL Eppendorf tube for wet weight measurement. Approximately 100 mg of wet tissue was taken for protein isolation. The cell pellet was solubilized with 0.1M Tris, pH 6.8, 0.1 M DTT, and 4% SDS and vortexed for two cycles with 30 s of time. Tubes were allowed to heat for 5 min at 95° C and then waited for RT. The supernatant was collected by centrifugation at 8000 x g for 10 min. The total protein was quantified by the Broad ford method. Individual polypeptides were separated on a 12% or 15% Bis-tris gel with an equal concentration of protein $(10 \mu g)$ for each lane.

2.19 Immunoblots

Proteins were transferred onto the nitrocellulose membrane by using a trans blot system (Bio-Rad) according to Towbin et al. (1979). The nitrocellulose membrane was incubated with primary antibodies (LhcII, LhcI, PSII and PSI) raised in rabbits and the dilution of antibodies is as follows: For PSII-LhcII complex, PsbA and PsbB (1:5,000): CP47 (1:2000): PsbO (1:5,000): LhcSR3 (1:1000): Ferredoxin (1:1000): Cyt b6 (1:5,000): AtpC (1:10,000): LhcB2 (1:5,000): CP29 (1:10,000): CP26 (1:10,000) and

Lhcbm5 (1:5,000). For PSI-LHCI complex, PsaA and PsaC (1:1000): PsaD, PsaH and PsaG (1:10,000): PsaF (1:10,000): (all these antibodies purchased from Agrisera, Sweden). The LHCI antibodies were followed the following dilutions, Lhca1 (1:5,000): Lhca3 (1:5,000): Lhca5 (1:300): Lhca6 (1:300): Lhca7 (1:250) and Lhca8 (1:350), (These antibodies were raised in our laboratory and reported (Yadavalli et al., 2010)). The lipid biosynthetic enzymes, acyl-CoA: diacylglycerol; acyltransferase (DGAT2A, 1:1000) and, phospholipid: DAG acyltransferase (PDAT1, 1:250) were tested for expression of their proteins (Boyle et al., 2012). The major lipid-droplet protein (MLDP) was used for identification (1:250). Subsequently, the secondary antibodies (Agrisera, Sweden) Anti-Rabit (1:10,000) conjugated with horseradish peroxidase were used for Chemi-luminescence (Bio-Rad) signal on the membrane. Histone3 (H3 (1:5,000) was used as a loading control. The images were recorded using a Bio-Rad Touch Imaging Chemi Doc System.

2.20 Protein aggregation

To see the protein aggregation in Fe starvation, the proteins were loaded on to the gels an equal volume of protein (5 μ g) and after running the electrophoresis the top of the gel (a bit of stacking and including part of about 1 cm of the running gel) was carefully sliced for all the lanes. These gels were made to small pieces, lyophilized and further, these lyophilized samples were denatured by using 2% β -mercaptoethanol for overnight and placed on to the gel. The gels were run in the electrophoresis field. The gels were transferred onto the nitrocellulose membrane using a trans-blot system as mentioned above. We have probed the PsaA of PSI and PsbA of PSII antibodies were used to see their protein abundance in the form of aggregation.

2.21 Thin layer chromatography

The identification of the TAG was performed by TLC. The samples (10 μ L) were applied to the silica gel TLC plate (Silica gel 60, F254, MERK) by spraying using a Linomate 5 (Camag, USA). The TLC was separated using a solvent mixture containing hexane/ether/acetic acid (70:30:1, v/v/v) as the solvent system. All the solvents used from MERK. Triolein (Sigma) standard was dissolved in CHCl₃ for mg mL⁻¹ concentration. The developed TLC plates were air-dried and visualize the separated TAG expose to iodine vapour at 37 °C for 2 min (Yang and Wittkopp et al. 2015). More Iodine exposer is led to the creation of unsaturation at lipids on the TLC. So the preferable time for Iodine staining is below 2 min. For each plate, 5 μ g of Triolein standard was used as a Triacylglycerol (TAG) standard. The TAG content was quantified by grey semi-quantitative analysis using Image J (v 1.45, NIH).

2.22 Liquid chromatography/ Mass spectrometry (LC-MS) measurements

Based on the modified HPLC separation method was used and analysed (Jouhet et al., 2017). Total lipid extracts containing fatty acids from all the conditions were dissolved in 100 μL (0.1%) of Acetonitrile. Fatty acid, C:17 (Sigma) was dissolved in 0.1% Acetonitrile at a concentration of 1 μM for the stock, and a concentration of 0.5 μM was added into all the samples as an internal standard. The samples were kept for lipid extraction for 30 min at 800 rpm at RT and then the vacuum evaporated at 45 °C for 15 min. The derivatization was done with n-Butanol for 20 min at 60 °C, then again vacuum evaporated at 65 °C for 15 min. The lipids were re-extracted into acetonitrile, 0.1%, and formic acid. From each sample, a 10 μL volume of the sample was injected into LC/MS. The organic buffer consisting of acetonitrile/ 0.1% formic acid (Buffer-A) and aqueous buffer composed of water with formic acid (Buffer-B) run for 2 min

with 0.0 - 0.2 min flow rate was at 0.1 mL/min 20% of buffer-B. The organic phase from the 0.2-1 flow rate was at 0.5 mL/min with 100% organic buffer and then 1-1.5 min for 0.1 mL/ min of flow rate organic buffer with 20% buffer-B. In the end 1.5-2 min for a run with a flow rate of 0.1 mL/ min buffer of 100% aqueous phase. Lipid classes were separated using the LC/MS (Shimadzu 5045) system was used for lipid identification.

MS Conditions for detection of mass from all the conditions.

Source: ESI, Nebulizing Gas: 2.5L/min, Heating Gas: 10L/min, Drying Gas flow: 10L/min. Interface Temperature: 300 °C, DL Temperature: 250 °C, Heat Block

Temperature: 400 °C

MRM masses: Table 3.

Table 3. For molecular mass quantifications from fragmentation irons and their ions for each fatty acid.

Analyte	Internal Standard (IS)	Precursor [amu]; [M+H]	Product [amu]
C14:0	² H ₃ C14	428.2	85.1
C14:1	² H ₃ C14	426.2	85.1
C14:2	² H ₃ C14	424.2	85.1
C14:3	² H ₃ C14	444.2	85.1
C16:0	² H ₃ C16	456.3	85.1
C16:1	² H ₃ C16	454.3	85.1
C16:2	$^{2}\text{H}_{3}\text{ C}16$	470.3	85.1
C16:3	$^{2}\text{H}_{3}\text{ C}16$	472.3	85.1
C18:0	$^{2}H_{3} C18$	484.3	85.1
C18:1	$^{2}H_{3} C18$	482.3	85.1
C18:2	² H ₃ C18	489.3	85.1
C18:3	² H ₃ C18	498.3	85.1
C18:4	² H ₃ C18	500.3	85.1

Table 4. Gradient conditions for sample measurements for all the conditions.

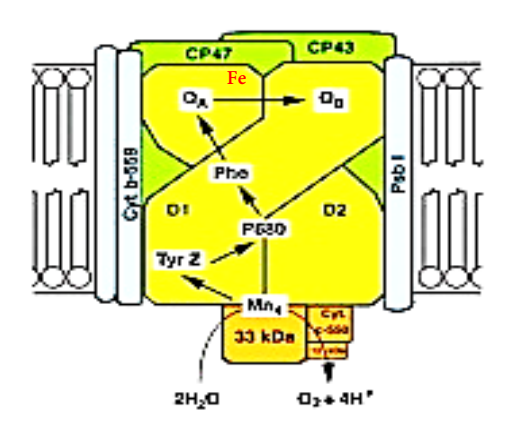
Time in min	Flow rate	% B
0.35	0.1ml/min	100
0.36	0.5ml/min	100
0.75	0.5ml/min	100
0.76	0.1ml/min	100
1.0	STOP	

2.23 Transmission electron microscopy

Cells were fixed with 2% glutaraldehyde diluted with 0.1 M phosphate buffer (pH = 7.2) for 2 h and glutaraldehyde was removed by washing for three times at RT. The tubes containing the samples were transferred to pure embedded in the resin to harden the resin for 24-48 h at 56 °C. Ultrathin sections with a thickness of 90-110 nm were cut with ultramicrotome (Leica Ultra UCT). All the sections were kept on to 400 mesh copper grids (Sigma).

Photochemistry and biochemical characterization of PSII-LHCII supercomplexes under iron deficiency in *C. reinhardtii*

Chapter 3



3.1 INTRODUCTION

Transition metals like copper (Cu), manganese (Mn), and iron (+Fe) they can donate and accept electrons, making these metals suitable cofactors in enzymes that catalyze redox reactions in the biological systems. In particular, iron is used as a cofactor in numerous biochemical pathways and therefore which is an essential nutrient for living organisms. The cells contain heme-, iron-sulfur proteins that function in the respiratory and operation of energy transfer reactions in photosynthesis. So all these reactions require relatively high levels of iron as a co-factor. The chronic limitation of iron in the ocean and on earth crust leads to decrease in the photosynthesis that ultimately reduces the growth of photosynthetic organisms. Iron deficiency in photosynthetic organisms leads to chlorosis (loss of chlorophyll), which is leads to inhibition of photosynthetic electron transport and ultimately loos of photosynthetic machinery (Spiller and Terry, 1980).

Iron is a cofactor mainly in the PSII, PSI, Cyt b6/f complex, and Cyt c6 (Yadavalli et al., 2012a). Among all photosynthetic proteins, the PSI (12 Fe per PSI) consists of more iron. The reports have been shown that PS I is the prime target due to high Fe content and these changes were observed under Fe deficiency in Cyanobacteria (Straus, 2004). Fe deficiency causes the photosynthetic electron flow which leads to a decrease in the protein content of PSI complex (Strzepek and Harrison 2004). The alteration of pigment-protein complexes and formation of an additional pigment-protein complex around PSII in cyanobacteria is known as Iron deficiency-induced protein (IdiA) and it role in protection of PSII particularly at the acceptor side from the damage (Michel et al., 1996; Michel and Pistorius, 2004). Similarly, in the way another protein has been found A: IsiA, Iron stress induced protein to protect the PSI (Boekema et al.,

Chapter 3

2001). Iron deficiency induces the expression of *isiA* gene product is known as *isiA* ring around PSII which consists of CP43' protein forms 18 subunits around the trimeric PSI core (Andaluz et al., 2006). Fe deficiency in green alga *C.reinhardtii* leads to decreased energy transfer between Lhc complex and RC (Moseley et al., 2002b; Naumann et al., 2005). The results have been showed that the reduced content of chlorophyll and thereby inhibition of PSI-LHCI supercomplexes formation which leads to decreasing the photosynthetic efficiency in *C. reinhardtii* (Yadavalli et al., 2012a). Further, the photoautotrophic green alga *Dunaliella salina*, expressed a homolog protein with iron deficiency known as Tidi-LHCI antenna with coupled to the PSI reaction centre (Varsano et al., 2006). The measurements from the P700 (P700+) after the termination of FR-light have shown that cyclic electron flow around PSI were decreased from iron deficient conditions (Msilini et al., 2013b). The PsaC and PsaD, the core proteins of PSI were decreased by 50% whereas the PsaE protein were degraded from Fe deprivation in rice (*Oryza sativa*).

The dissociation of LHCI subunits from PSI complex which is may be due to increased levels of reactive oxygen species, which is reported by the increased content of ROS (Yadavalli et al., 2012b). Iron deficiency causes the decreased electron transport chain and it leads to decreased abundance of photosynthetic proteins partcularly a decrease in the PSII quantum yield and PSI protein content level in higher plants (Andaluz et al., 2006; Timperio et al., 2007b; Msilini et al., 2011). Further, iron deprivation associate with antenna proteins of two photosystems were significantly affected in *C. reinhardtii* (Naumann et al., 2005). So from this study we have focused on PSII during the iron deficiency in *C. reinhardtii* and most of the studies were described on PSI. Ours results explain about the changes in the cell morphology,

functional aspects of photochemistry, thylakoid organization and, protein profile of PSII associated LHCII complexes.

3.2 Results and discussion

3.2.1 Growth analysis and morphological changes

It is well known that iron (Fe) is an essential element for electrons transfer reactions which ultimately promotes the plant growth and nutrition. The effect of Fe deficiency on photosynthetic level, particularly at PSII is not well understood. Growth pattern analysis was monitored by optical density (OD₇₅₀) and morphological changes has been observed from confocal microscopy (Fig. 3.1A). The control and iron deficient growth under optimal conditions for up to 6 days. The control cells exhibits optimal growth (OD₇₅₀ value 0.942 ± 0.021) where as iron deficient cells showed decreased growth pattern (0.395 \pm 0.014) up to 4 days of growth. Control cells were found to more active with high optical density than the iron deficient cells. It is indicating that iron deficient cells showed reduced growth when compared to control condition (Fig. 3.1A). Previously we have reported that Fe deficiency induces severe damage to the PSI photochemistry which leads to congestion in electron transport in C. reinhardtii and as well as in rice (Yadavalli et al., 2012 a&b). The chlorophyll was excited at 488 nm in between emission range of 600-700nm. The control cells reveal normal in size (10 μm) whereas the cells in rosette shape in iron deficiency condition which is called as palmelloids- formation of daughter cells with in the parent cell (Fig. 3.1B), which is a characteristic feature of algae when grown under abiotic stress conditions as reported (Neelam and Subramanyam, 2013). The previous reports explains that the palmelloid formation in C. reinhardtii is due to either loss of flagella or membrane gelatinizations after exposer with the environmental stress (Lürling and Beekman, 2006). Our results are also suggest that the palmelloid formation in iron deficiency due to cell wall abnormality in *C.reinhardtii* cell (Fig. 3.1A). In control condition, the cell size is measured as 10-12μm, whereas as 4-6μm cell size when cells grown from Fe deficiency which clearly show that the cell size has been reduced under Fe deficiency condition.

3.2.2 Analysis of fluorescence emission spectra

The RT fluorescence emission spectra recorded from thylakoid membranes of control cells showed the major peak at 683 nm and this 683 nm peak is originated mainly from PSII, while the long wavelength emission is assigned to PSI-LHCI with the contribution of vibrational satellites of PSII (Ferroni et al., 2011). The RT fluorescence emission spectra of thylakoid membranes from iron deficiency shows a significant increase of maximum fluorescence at 683 nm than control cells. This highlights that the energy transfer from Q_A to Q_B of PSII is hampered. These results indicates that an increase in fluorescence maximum at 683 nm is due to the block of an energy transfer from four Chl *a* to PSII complex (Fig. 3.1D).

The exact reason behind this a non heme iron present between Q_A and Q_B and it is bounded by His-215 and His-272 on D1 and on the other hand His-213 and His-268 on D2 pocket (Diner and Petrouleas, 1987). This is well supported by the work done on UV-B effect on cyanobacteria *Spirulina platensis*, this increased emission spectra is due to uncoupling of energy transfer from Chl *a* to PSII (Kolli et al., 1998). The same concentration of iron was add to four days of iron deficient cells and further the cells were left for the growth for 32 h and measured the RT fluorescence emission spectrum from the isolated thylakoid proteins. Their recovery cells showed the emission spectra equals to the control and this indicates the iron is very important for the proper transfer of energy from PSII complex.

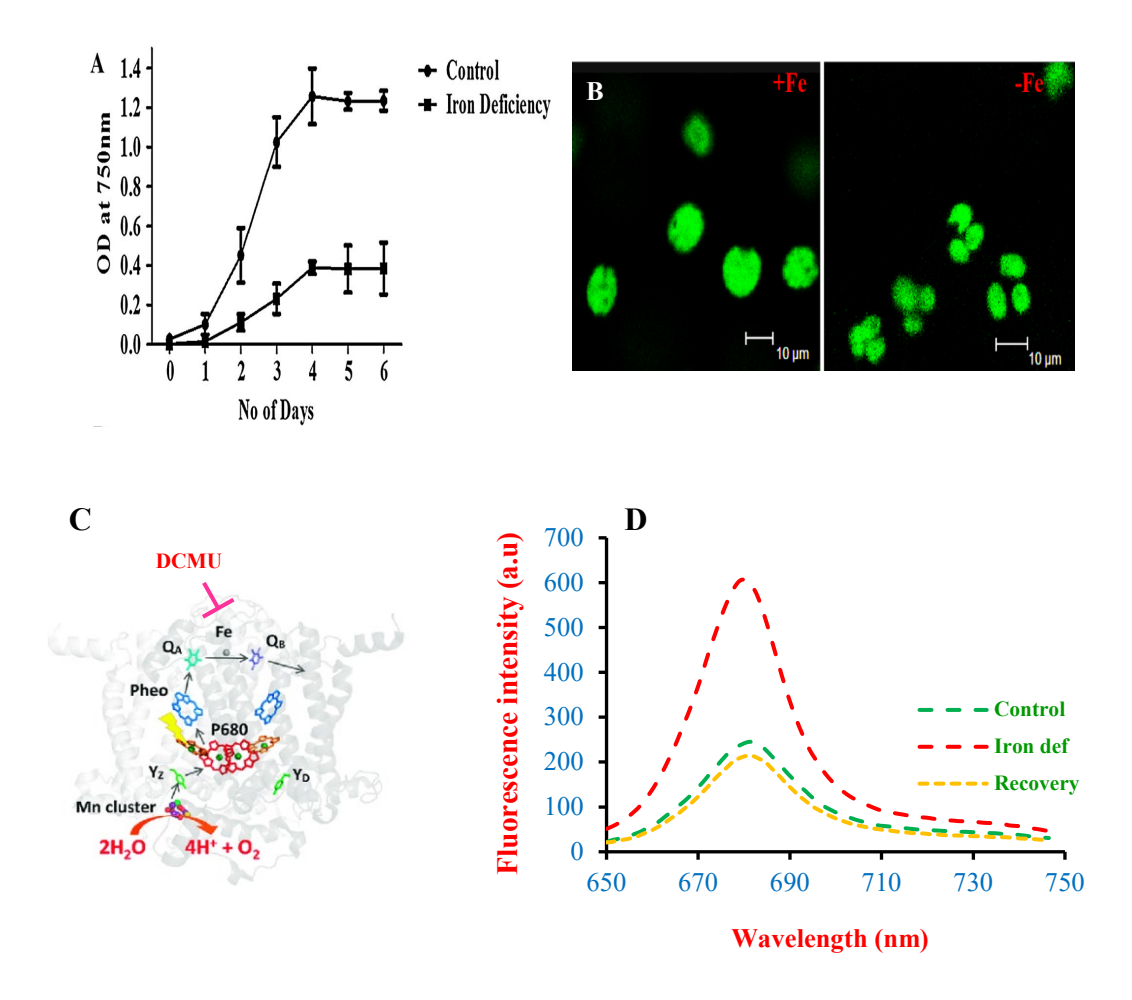


Fig. 3.1 (A) Growth curve of *C. reinhardtii* cells in control (+Fe) and Iron starvation (-Fe) grown for 6 days O.D at 750 nm. (B) Confocal microscopy images of *C. reinhardtii* showing altered cell size and cell morphology as forming palmelloid when grown under control (+Fe) and Fe starvation conditions. All images were taken equal magnification of 10 μm. (C) The binding site of DCMU at Q_B - Q_A of D1 protein which is core protein of PSII. (D) Room temperature florescence emission spectra of the *C. reinhardtii* cells grown under control, iron deprivation and repelled conditions. Measurements were performed with equal Chl concentration of $10\mu g/ml$. Each curve is the average of 3 different measurements.

3.2.3 Analysis of transient Chl a fluorescence

The various abiotic stresses can analysed with help of Chla fluorescence transients and these can be analysed by the JIP test. During the time course, the fluorescence data show significant differences at three phases of OJIP transients and Chla fluorescence in between control and iron deficient condition (Fig. 3.2). In control (+Fe) cells, the OJIP phases are very clear and have attained maximum fluorescence which indicates the efficient electron transport in the non-cyclic, which constitutes PSII, Cytb6/f, and PSI in a sequential manner. The initial fluorescence level Fo was decreased at 24 h under iron deficiency, however after 72 h of growth, it been recovered to the control level (Fig. 3.2B). The electron transport beyond QA can be blocked by DCMU. In DCMU -Fe deficiency cells the maximum P phase level was close to the F_m value of untreated cells (Fig. 3.2B). The onset of control cells show the Fv/Fo (2154 \pm 56.23) and Fv/Fm (0.743 ± 0.023) values to increase where as decreased values after prolonged iron deficiency (Fv/Fo = $824\pm\ 21.10$, Fv/Fm = $0.512\pm\ 0.031$) (Fig. 3.2C). In the absence of iron, there is a decline in Fv/Fm with the amplitudes of the O-J and I-P phases indicates that the OEC got damaged and it fail to provide the further electrons to PSII to reduce the quinone acceptors of the photosystem. Thus because of lack of Fe there is decreasing in the maximal fluorescence.

We have confirmed by addition of DCMU to cells which shows a decline of JIP phases under iron deficiency. This is due to immediate onset of stress condition there by cell couldn't able to cope up with the iron deficiency. However, the three phases of OJIP transient can be see with a slight reduction in I peak (Fig. 3.2B). Also, the P phase which corresponds to maximum fluoresce which is significantly decreased even in DCMU treated cells that indicates the acceptor side of PSII also impair. In the

overall, these results suggest that iron deficiency causes the impairment of both acceptor and donor side of PSII.

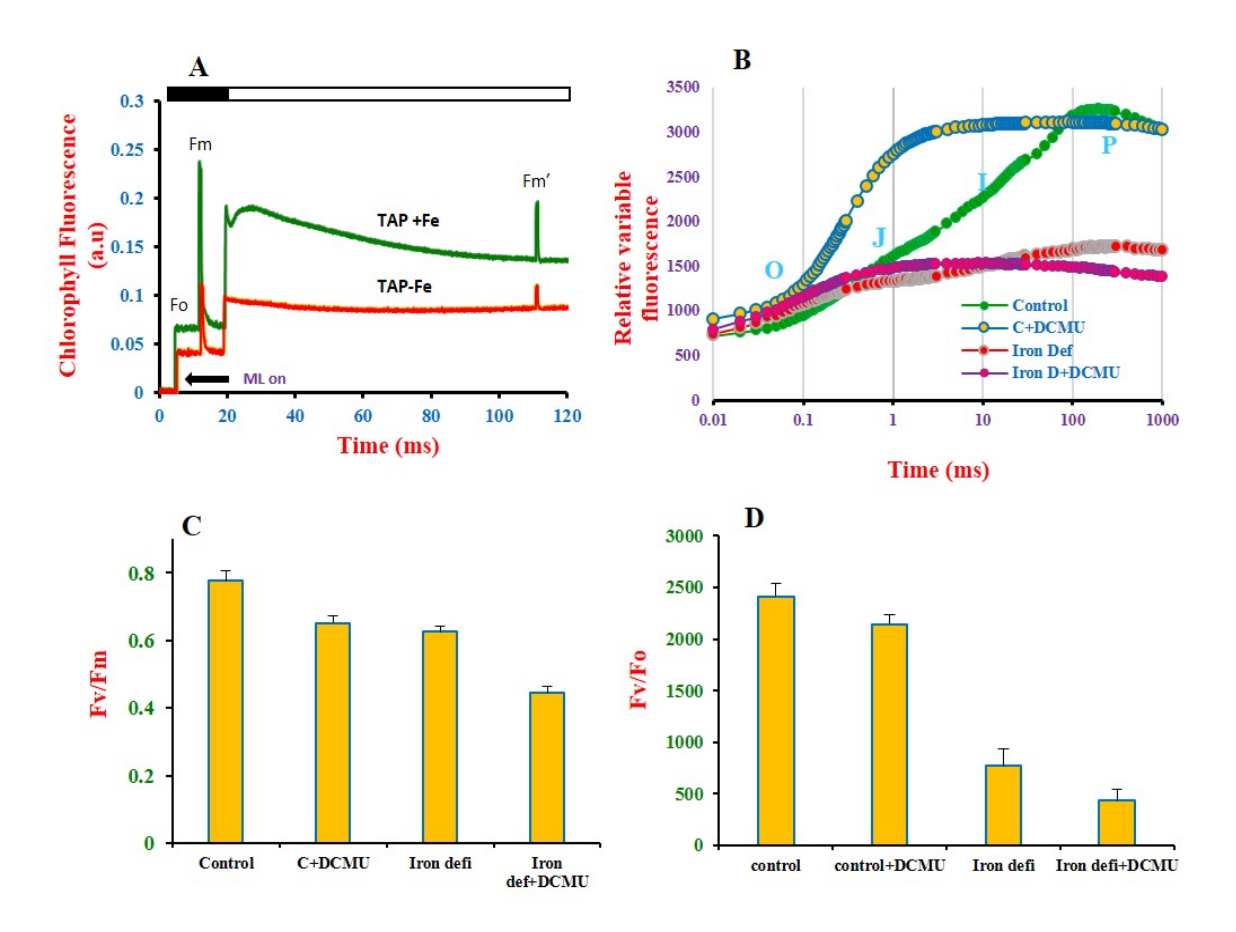


Fig. 3.2 (A and B) Chl *a* florescence from PAM and OJIP transients in control and control with DCMU for 10 min in darkness, with 10 μM concertation. Iron starved (-Fe) and Fe starved cells with DCMU and repelled conditions of *C. reinhardtii* cells. (C) And (D) Fv/Fm values of respective conditions. Excitation of samples was with 3000 μmol photons m^{-2} s⁻¹ 650 nm light. All the measurements done with three separate cultures. Chl*a* fluorescence PAM measurements were done with 1400 μmol photons m^{-2} s⁻¹ actinic light and measuring light at 150 μmol photons m^{-2} s⁻¹. Saturation light was kept at 15000 μmol photons m^{-2} s⁻¹ for duration of 0.5s.

This is well accepted with reports stated that the OJ phase indicates the reduction of Q A while JI could represent a further closure of PSII reaction centres with accumulation electrons in Q_AQ_{2B} stage (Kodru et al., 2015). A decline in Fo has also been show in lettuce plants under iron deficiency condition (Msilini et al., 2011a). This indicates that in the absence of DCMU, Fe deficiency cells have the maximum of peak in the 0.2–2 s time range (P) not all PSII reaction centers were closed, and thus the Fv/Fm and Fv/Fo were decreased (Fig. 3.2 C&D). In addition to damage to PSII, reduced electron flow through PSII may occur as a consequence of the retardation of the transfer of electrons from the reaction centre to the PQ pool. Growth after 72 h of Fe-deficient conditions resulted that the first stage of inhibitory action was detected as increase of the amplitude of the OJ phase of the Chl fluorescence induction with a decline of JI, which agrees well with the treatment of pea leaves with DBMIB is an artificial quinone causing the IP phase to disappear (Schansker and Strasser, 2005). The JI phase was previously shown to be matching to O-J phases, the sum of the amplitudes of OJ and JI indicating the complete reduction of Q_A (Kodru et al., 2015). By 72 h of Fe deficiency, the level of I peak of iron-stressed cells approaches 90% of maximum fluorescence (F_m).

3.2.4 Separation of supercomplexes from thylakoid membranes

The separation of membrane supercomplexes were carried out by BN-PAGE and it has been used for the separation of thylakoid membranes complexes from control and iron deficiency of C. reinhardtii cells. The thylakoid membranes were solubilized with a mild detergent like β -dodecyl maltoside (β -DM), we were able to separate the supercomplexes of C. reinhardtii as reported previously Madireddi et al. (2014). The results obtained from control shows where the PSI-LHCI, PSII-LHCII, PSII RCC dimer, ATP synthase, Rubisco, Cyt b6f, PSI monomer, PSII RCC, LHC trimers and

LHC monomers were separated. However, the significant differences has been observed from iron deficiency condition (Fig. 3.3A). The major supercomplexes PSII-LHCII and PSI-LHCI were completely disorganized (Fig. 3.3 A lane 2) and also, PSII reaction centre dimer, ATP synthase, and Cyt *b6f* complexes were not assembled in iron deficiency cells. It is clear that if the Chl biosynthesis or protein synthesis is retarded and it cause disorganization of supercomplexes of PSI and PSII. The monomeric form of PSI, PSII and LHC's were existing but some extent they were increased (Fig. 3.3A).

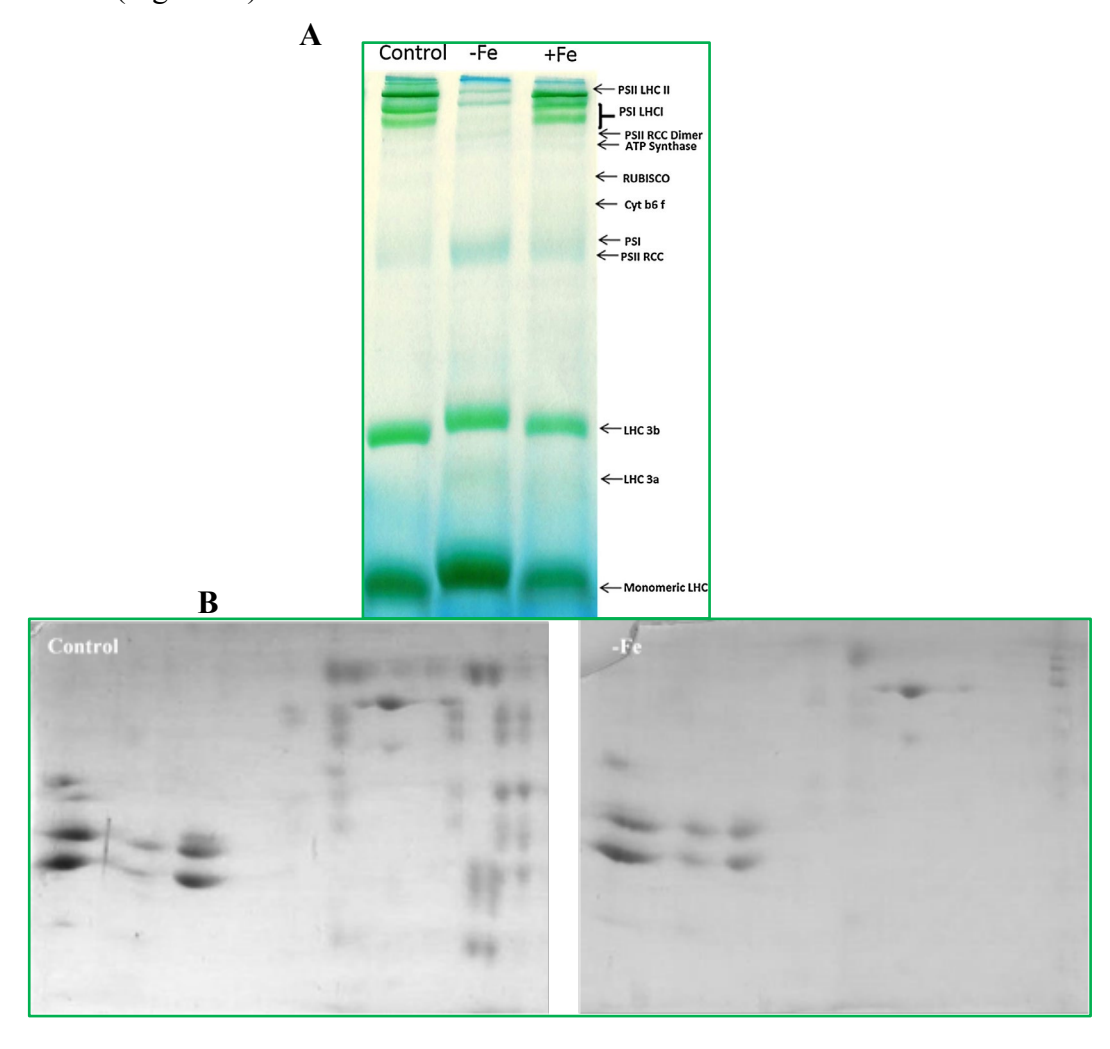


Fig. 3.3 (A) Blue native PAGE of thylakoid membranes isolated from control, iron deprivation and iron replenished after deprivation were solubilised with $1\%~\beta$ –DM and separated by BN-PAGE, and complexes were identified according to previous literature. Equal amount of chlorophyll ($10~\mu g$) was loaded into each lane. (B) Individual proteins were separated by second dimensional gel electrophoresis from each lane of BN-PAGE.

supercomplexes was not formed besides by addition of iron and it restored after 32 hours. Thus, iron plays an important role in formation or organization of supercomplexes. Subsequently, a pronounced iron deficiency resulted in a reduction of light harvesting complexes content in both PSI and PSII (Timperio et al., 2007; Yadavalli et al., 2012a&b). The BN-PAGE gel slices were solubilized and placed on second dimension to separate the individual proteins. The wild type supercomplexes were separated into individual proteins and they were normal in the control condition (Fig. 3.3B). Surprisingly, both PSII-LHCII and PSI- LHCI proteins were decreased under iron deficiency conditions. Though the LHCs are present, but they were not forming supercomplexes with PSI and PSII. Hence, the excited electron transfer is impaired due to iron deficiency in *C. reinhardtii* cells.

3.2.5 Protein profile of PSII reaction centre changes in Fe deficiency

We have separated the thylakoid proteins of both control and iron deficiency thylakoids on SDS-gels and transferred onto PVDF membrane. The blots were probed for detection of PSII core and LHCII antibodies. Fig. 3.4, the core proteins of PSII shows that core antenna proteins CP43 and CP47 are significantly altered in their content. Further, reaction centre protein, D1 has been changed whereas no change in D2 protein content. The oxygen evolving complex is important for donation of electrons after splitting of water molecule to reaction the centre PSII. Among all water oxidation subunits, PsbO protein content has been reduced significantly. However, PsbP is not changed in iron deficiency conditions (Fig. 3.4). These results are suggesting that iron nutrition is indirectly involving in the donation of electrons from oxygen evolving complex. Further, the protein accumulations of PSII was characterized to see the

abundance of proteins in Fe deficiency. It is expected that excitation energy transfer from PSII to PSI is hampered due to less accumulation of reaction centre proteins.

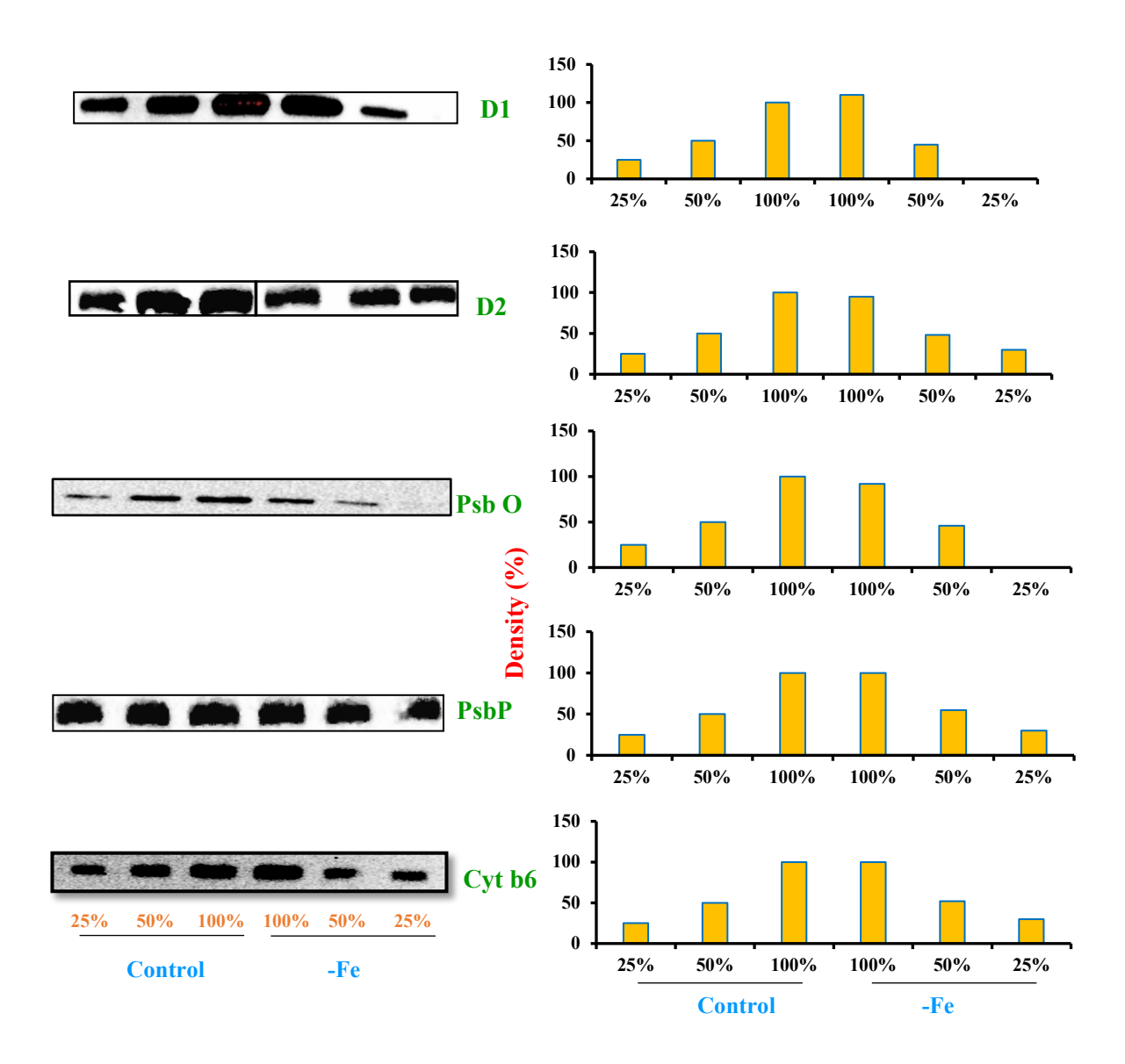


Fig. 3.4 Immunoblots of PSII and LHC proteins content from control and Iron deficient. Equal chlorophyll was loaded with different dilutions (25, 50 and 100%) as a positive control and separated by SDS gel electrophoresis. PSII core proteins D1, D2, OEC (PsbO & PsbP). Each band density was quantified with Image J software and measurements were expressed in (%).

3.2.6 Light harvesting complex (LHCII) protein profile changes in PSII

On the earth, LHCII protein is the most abundant membrane protein. It is well participates in the harvesting of sunlight and transferring of excitation energy to the core complex during the photosynthesis. Here, we have investigated the abundance of LHCII proteins under Fe deficiency condition to understand the level of harvesting energy. Interestingly, the major LHCII trimer subunits (Lhcb1 and Lhcb2) contents were reduced whereas, the minor subunits CP26 and LhcBm5 were not significantly. These results show that changes in LHCII protein level would hamper the efficiency of light harvesting capacity and reduce the light energy transfer to the reaction centre. Additionally, the LHCII proteins (Lhcb1, Lhcb2, CP26, CP29, and LhcBm5) were majorly reduced in iron depleted cells which indicates that light harvesting capacity was minimized (Fig. 3.5).

However, CP29 other minor subunits have remarkably changed under Fe deficiency. Generally, plants change their antenna size depending on the light environment to optimize light harvesting capacity (Anderson and Andersson, 1988). PSI appears to be the first target of iron deficiency (Moseley et al., 2002), perhaps because of its high Fe content as the electron transfer involves 12 iron atoms. The phototrophic cells maintain efficient photosynthetic systems, but still lose overall photosynthetic activity at the beginning of iron deficiency (Terauchi et al., 2010). Hence, our data is well agreement with our studies that under photoheterotrophic conditions the photosynthesis is vulnerable to iron deficiency. In our case, the PSII also damaged remarkably apart from PSI when iron is depleted. Hence, the PSII photochemistry is impaired.

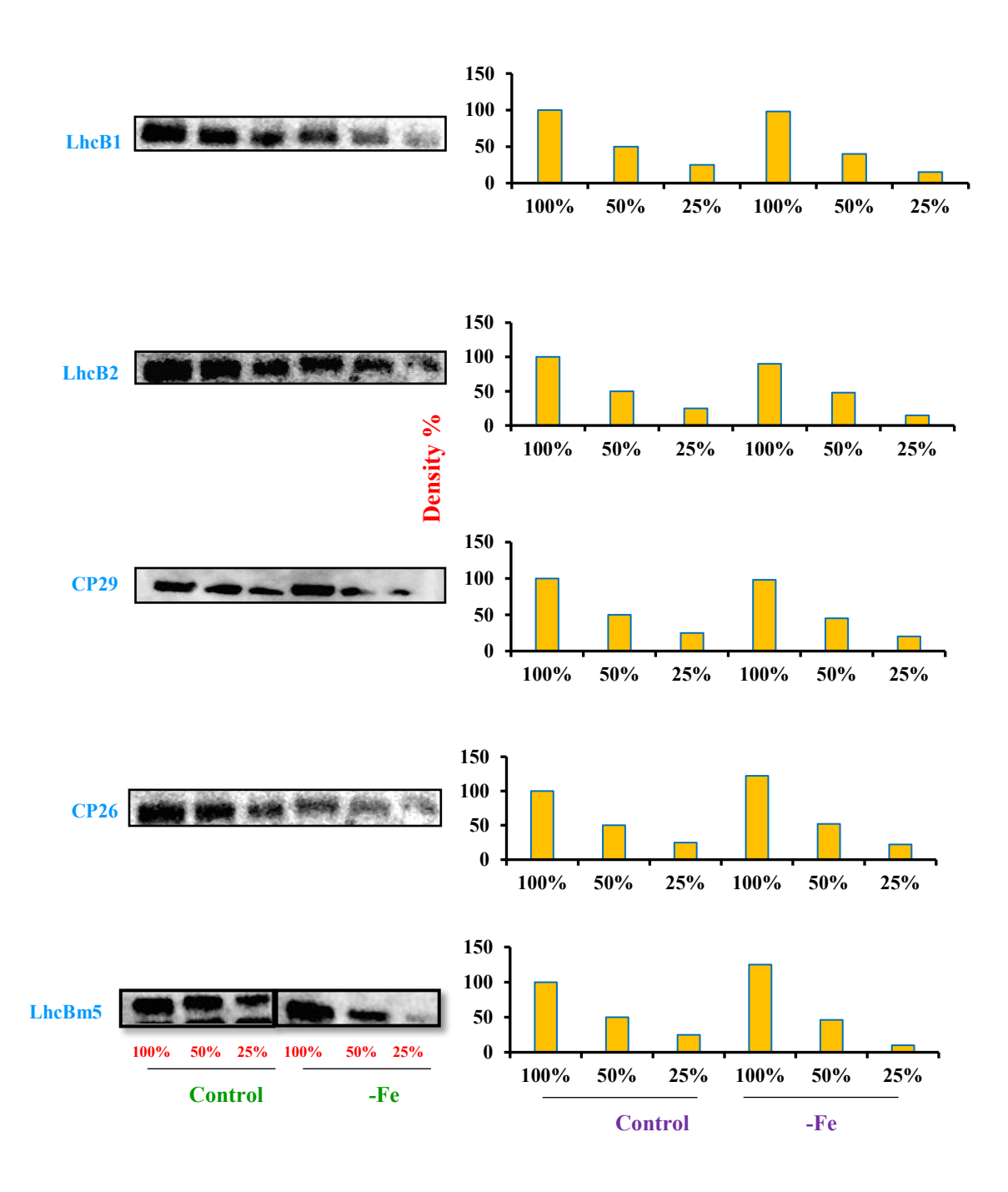


Fig. 3.5 Major LHC II proteins Lhcb1, LHCb2, CP29, CP26 and Lhcbm5 are detected. The adjacent bar diagram were developed by Image J software to show the quantity of protein present. Each band density was quantified with Image J software and measurements were expressed in (%).

3.3 CONCLUSIONS

In summary of the study the cell size has been reduced in iron deficiency condition. The complete depletion of iron affects the PSII photochemistry, which indicates the electron transport from Q_A to Q_B is impaired. Also, suggest that both acceptor and donor side of PSII has been damaged. In addition, the organization of supercomplexes were disturbed due to lack of iron. So iron is functionally important for the proper organization of thylakoid membranes in the chloroplast. The differential degradation or damage of LHCII proteins was observed. This could be the loss of chlorophyll biosynthesis in the *C.reinhardtii*.

4.1 RESULTS AND DISCUSSION

4.1.1 Growth, total chlorophyll and, cell morphological analysis

Growth, cell morphology, and total chlorophyll were analyzed from the cell grown under control (+Fe), iron deficiency 1st generation (-Fe), the second generation of iron limiting condition and their recovery conditions called as RC1 (recovery from one-time depletion of iron) and RC2 (recovery from second generation depletion of iron), respectively (Fig. 4.1). Growth was monitored by cell count which started from 24 h to 96 h under the above conditions. The control cells have shown optimal growth up to 96 h. The growth had decreased by 50% in iron deficiency and also 70-80% in severe iron stress conditions (2nd generation of iron deficiency) when compared to control (Fig. 4.1A). Our studies are in agreement with our previous studies that the growth decreases to 50% in *C.reinhardtii* under iron deficiency conditions (E. R. Devadasu et al., 2016). However, in the second generation of iron deficient conditions, the growth decreased to 75-80%. Nevertheless, regrowth was observed in their recovery (RC2) condition and it was reached almost to the control (+Fe) condition.

This shows that cells are in dormancy state having a very low metabolic state. It also suggests that iron is the main nutrient for *C.reinhardtii* growth. However, decreased chlorophyll content was observed in iron deficiency and severe iron deficient conditions (Fig. 4.1B). In control cells, the (10.6±0.166 mg/mL) optimal level of Chl content was present whereas the decreased Chl content in iron deficient (4.247±0.554 mg/mL) as well as severe iron deficiency (1.723±0.272 mg/mL) conditions. The Chl content has recovered up to the optimal level (9.53±0.806) in RC1 as well as in the RC2 condition (7.04±1.033). Iron is essential and is required for Chl biosynthesis which is revealed by the recovery of RC1 and RC2 conditions that indicates the Chl content was again resynthesized, even from severe iron starvation. The reduction in growth and Chl

suggest that the Chl biosynthesis is very slow due to lack of Fe. We have observed morphological changes through confocal microscopy. The control cells were normal in shape, however, the iron deficient as well as the severely iron deficient cells appeared as rosette shape and formed a palmelloid (Fig. 4.1C). The palmelloid formation in algae is a characteristic feature of abiotic stress conditions (Neelam & Subramanyam, 2013).

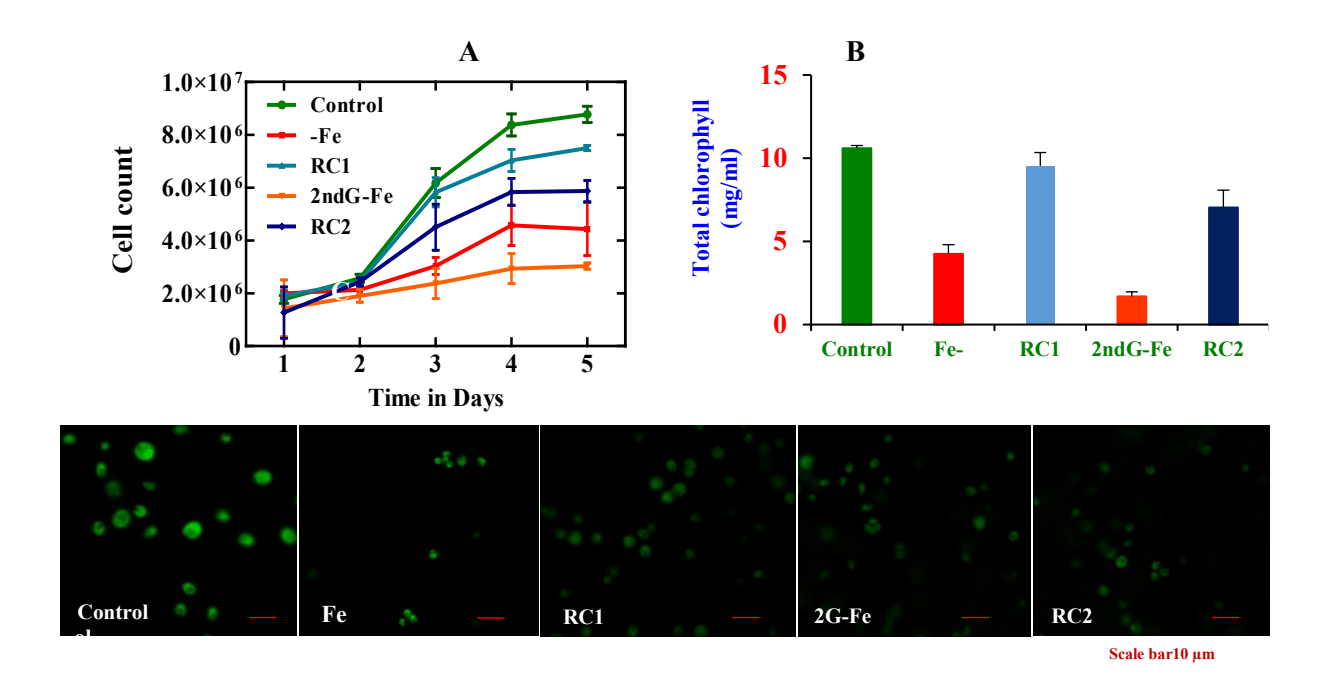


Fig. 4.1 (A) Growth analysis of *C.reinhardtii* under iron starvation course up to 5 days from Control, -Fe, RC1, 2G-Fe, and RC2 conditions. Growth was monitored by daily cell count basis. (B) The total chlorophyll was quantified from the cells after 4th day growth. (C) Cell morphology was studied with confocal microscopy and an equal (10 μ m) scale was maintained for all images. All the experiments were carried out with three individual times.

4.1.2 Analysis of chlorophyll a fluorescence transients and OJIP-test

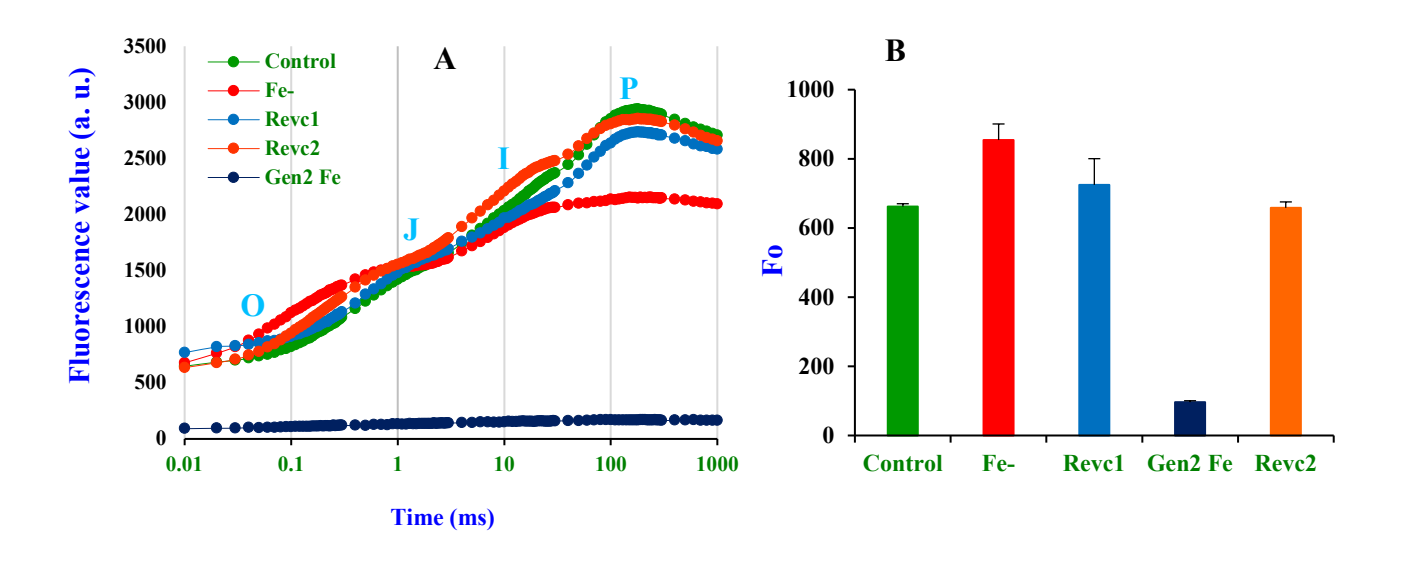
Fig. 4.2 depicts the comparison made among the raw OJIP transients measured from control as well as severe iron deficiency and their recovered cells after 72 h of growth. When dark-adapted oxygenic photosynthetic cells are exposed to actinic light for Chl a fluorescence kinetics (FI) as the Kautsky Curve (Papageorgiou, Tsimilli-Michael, & Stamatakis, 2007). Chl a fluorescence analysis explains the main changes of PSII bioenergetics and simultaneous alterations in photosynthetic processes (Fig. 4.2A). The O–J phase is associated with the reduction of Q_A i.e., reduction at acceptor side of PSII, the J–I phase was raised due to accumulation of Q_A Q_B and subsequent Q_A to Q_{A2} (Q_B loosely bound molecule). The raise at I to P phase in the fluorescence explains the variable fluorescence, Fv is due to reduction of PQ pool, and phase P, express the rate of utilization of potential energy from incident light. The Fo and Fm extreme values were associated with the conformational parameters of NPQ de-excitation constant (K_P), and photochemical de-excitation constant (K_P).

The initial fluorescence value F_O has decreased in severe iron deficient conditions, this due to several reasons which includs an increased number of inactive RCs that would decrease the Q_A , primary reduction. It could be structural damage leads to a decreased excitation energy transfer from antenna complex to RCs which leads to decreased at F_O (Fig. 4.2B). The difference in the Chl a fluorescence from the periodic day intervals was normalized to a region between 50 μ s to 300 μ s. The resulting kinetic difference of V_{OK} (ΔV_{OK}) which allowed to assess the band called L-band (Fig. 4.2E). However, on the first stage and severe iron stress conditions the appeared L-band showed slightly higher whereas recovery (RC2) has a slight decreased positive peak at 0.15 ms whereas in RC1 is similar to control (Fig. 4.2E). The higher change in the L-

band amplitude (150 μs) suggests that both iron deficient cells were capable of disconnection of LHCII from PSII complex which maintenance the energetic connectivity (Strasser and Stirbet, 1998). In similar way, the variable fluorescence was normalized at 50 μs and at 2 ms (Voi) are shown in Fig. 4.2E to explain the changes at Voi under iron deficiency condition allowed to analyse and assess the band known as K-band and it appeared between 0.25 and 0.30 ms (Fig. 4.2F). However, the raise in K-band due to the reduced efficiency of OEC thereby no further electrons from OEC to the PSII acceptor side towards to PSI (Strasser, 1997) (van Heerden and Krüger, 2007). To show the evidence, we have observed the PsbO protein level by western blot and it showed that there was change content of PsbO protein that indicates that OEC complexes have damaged in-turn the energy transfer could have been impaired. The previous studies on elevated temperatures show a rise in the positive side of K-band is because of damage of acceptor side of PSII (Srivastava et al., 1997).

Severe iron deficiency induce the changes in biophysical parameters obtained from the fluorescence transients and JIP-test (Fig. 4.2D). The reduction in FM value corresponded to an increase in non-photochemical de-excitation constant (K_N) and also decreases in photochemical de-excitation rate constant (K_P). The reduced parameters, Fv/Fm, area between Fo and Fm, RC/ABS, Fv/Fo, sigmoidal component (Fig. 4.2D) were observed in the first stage as well as severe iron stress condition suggested that the loss of active reaction centers results in decreased electron transport from RCs to PQ pool (Strasser et al., 2000). The reduced in photosynthetic activity (Fv/Fm) are also caused by non-photochemical quenching in the iron stress consition (Fig. 4.2C) The formation of inactive reaction centers in the first stage and severe iron deficiency condition is linked with the higher value parameters of non-photochemical deexcitation processes (K_N). Similar results were observed in *C.reinhardtii* cells treated

with salinity condition where the inhibition of PSII leads to decreasing the variable Chl fluorescence (Neelam & Subramanyam, 2013). The OJIP fluorescence transients also show the important parameters related to photochemical reactions which are useful to give the information about structural and functional PSII aspects and out of them, we focused on selected parameters which we gave at (Table 1) those are useful to compare the PSII behaviour of Chlamydomonas under iron stress condition (Goussi et al., 2018). The inference is drawn from Chl *a* fluorescence that the photochemical activities were dramatically changed due to the loss of Fe in Chlamydomonas cells. However, the photochemical activities were almost restored when Fe is supplemented to these severe Fe deficiency cells.



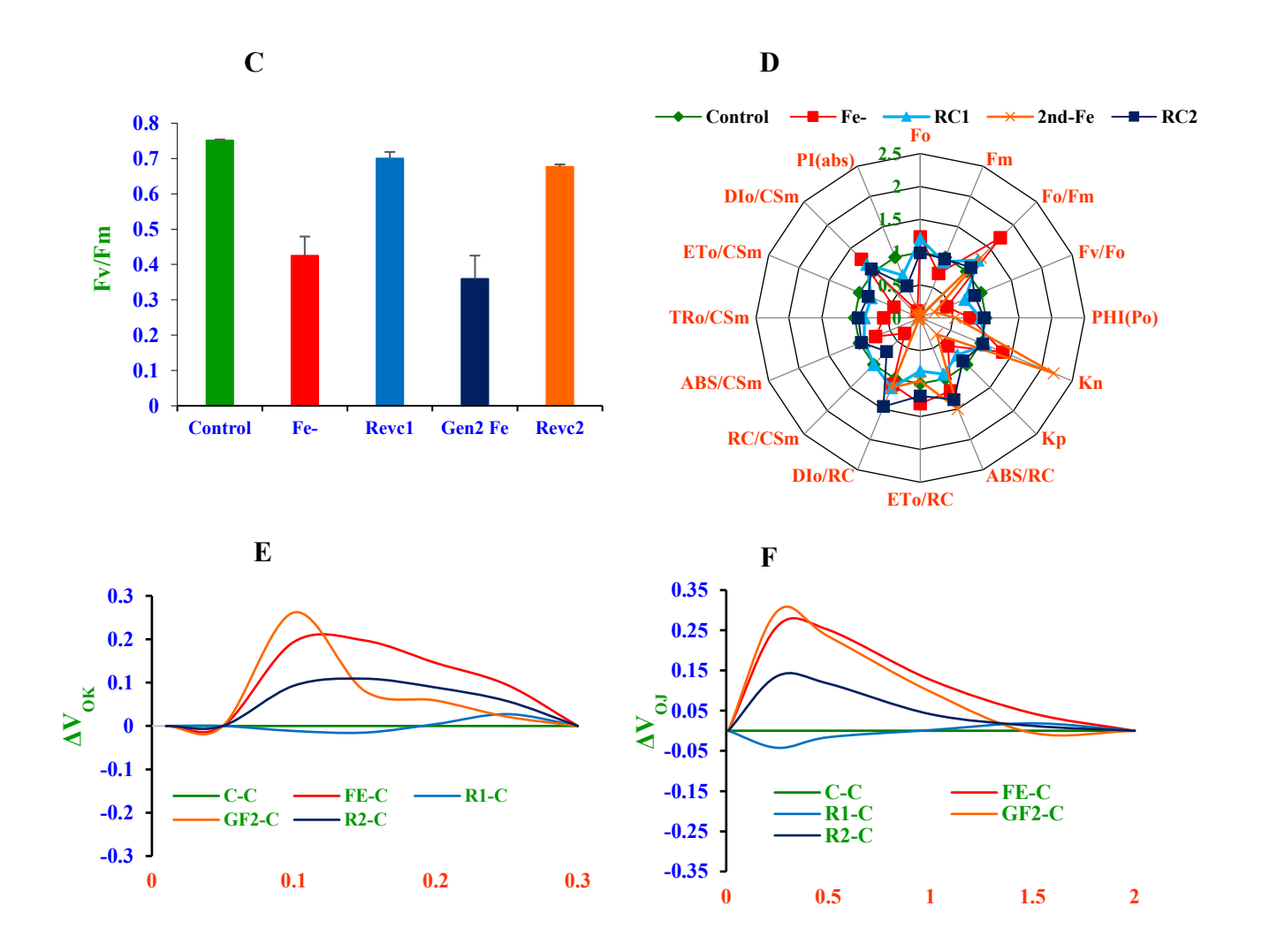


Fig. 4.2 The OJIP Chl *a* fluorescence transients (log time scale) recorded in dark-adapted *C. reinhardtii* under control, iron deficient (-Fe), recovery (RC1), 2nd generation of iron deficiency (2nG-Fe) and, recovery (RC2) stress conditions. (A) Raw Chl *a* fluorescence transients curves exhibiting fluorescence intensity (Ft) recorded between 0.1 and 1000 ms time (a.u. = arbitrary units). (B) OJIP-test curves were double normalized between FO and FK phases: $V_{OK} = (Ft - F_O)/(F_K - F_O)$. (C) The kinetic difference of V_{OK} [DV_{OK} = (Ft - F_O)/(F_K - F_O)] showing L-band at (0.15 ms) and curves represented as control is in green, -Fe is in red, RC1 is in blue, 2nd Generation –Fe is in an orange and, Recovery (RC2) in purple color. (D) Variable fluorescence transients double normalized between F_O and F_J phases: $V_{OJ} = (Ft - F_O)/(F_J - F_O)$. (E) In the inset, the kinetic difference of V_{OJ} [DV_{OJ} = (Ft - F_O)/(F_K - F_O)] showing K-band was obtained and labeling has given the same as above. All measurements were done after 72 hours of growth and the experiments were conducted in three individual times (n=3). (F) Radar plot showing the changes in Chl *a* fluorescence transients from dark-adapted *C. reinhardtii* cells under progressive –Fe stress conditions. All the parameters are deduced from the OJIP-test analysis. Measurements were taken for each sample three times.

4.1.3 Circular dichroism spectra analysis from thylakoid membranes

Identification of the pigment-protein complexes that are involved in the formation of the chiral macro domain organization which typically gives intense CD signals. We have used thylakoid membranes isolated from the control, 1st stage of iron deficiency as well as 2nd generation iron deficient cells and their recovery conditions (RC1 and RC2, respectively) for understanding the complexity of thylakoid membranes (Fig. 4.3). We have measured the CD in the range of 400-750 nm. The studies from CD visible region (400-750 nm) were divided into Soret and "psi-type" regions (Győző Garab and Van Amerongen, 2009). The spectra are mainly dominated by the psi-type bands: the positive at 694 nm and negative band at around 679 nm, which are raised due to association of Chl a molecules with chiral domains of photosynthetic complexes and the band at 506 nm which can be attributed to carotenoids bound in a long-range structure (Győző Garab and van Amerongen, 2009). The minor bands below 500 nm, as well as the band at (-)657 nm, originates from excitonic interactions (Parson & Nagarajan, 2003). The two major bands at 694 and 679 nm are raised due to dimers of Chl which explains the excitonic interaction of Chl a in thylakoid membranes, whereas peak at 657 nm in the negative region is due to Chl b (Fig. 4.3A).

The CD spectra measured showed Qy region, there are two negative peaks at 646 and 694 nm and one positive peak at 679 nm, similar to previous reports (Nagy et al., 2014). The two major bands, at (+)679 and (-)694 nm have originated from Chl a dimers caused by the excitonic interaction of Chl a in the chloroplast, while the negative peak at 654 nm is characteristic of Chl b (Breton, 1984). In the Soret region, the positive band at 506 nm attributes from Chl a, while the negative peak at 483 nm is characteristic of Chl b (Fig. 4.3A). The (+)506 and (-)483 nm CD bands were decreased in severe iron deficient conditions due to decreases in the amount LHCII trimers in the number

of PSII-LHCII supercomplexes (Dall'Osto et al., 2006). The positive bands around 506 and 483 nm are attributed to chlorophyll-carotenoid interactions. The values were calculated by 694/679 nm psi-type band at different iron stress conditions, the psi-type band significantly altered in first and sever iron deficient conditions whereas in recovery conditions these peaks are almost equal to the control (Fig. 4.3B). However, in 2nd generation recovery, the cells have not adapted like the control. The CD spectra of thylakoid membranes isolated from severe iron deficiency and its recovery conditions and their different CD bands are compared in Table 3.

The psi-type difference CD bands at CD₆₉₄₋₇₅₀ and CD₇₅₀₋₆₇₉ have originated from PSII chiral domain and the band CD₅₀₆₋₆₂₀ has reported due to β-carotene located within PSII core (Gyozo et al., 1988; Toth et al., 2016). The CD₄₈₃₋₄₇₃ region demonstrated the interaction of LHCII protein-protein within the trimers which affect the peripheral Chl b and neoxanthin molecules. The CD₄₈₃₋₄₇₃ value has decreased in 1st and 2nd generation iron deficient conditions, whereas in their recovery conditions (RC1 and RC2), the value had increased. This is due to decreased interaction of proteinprotein LHCII trimers as well as Chl b and recovery conditions showed the values were close to the values obtained from the control thylakoid membranes. This indicates that iron is playing an important role in the reorganization of thylakoid membranes. The band CD₆₃₀₋₇₅₀ associated with Chl b interaction within LHCII monomers (Garab et al., 1991; Dobrikova et al., 2003). The $CD_{483-473}$ band and $CD_{630-657}$ bands explain about the trimeric and monomeric stability of LHCII complexes. In the thylakoid membranes, the spectra region at CD₆₉₄₋₆₅₇, CD₇₅₀₋₆₇₉, and CD₅₀₆₋₆₂₀ were decreased in the 1st generation of iron deficiency and also in severe iron deficiency condition when compared to control. In their recovery conditions, (RC1 and RC2) gave spectra similar to that of the control. The results from CD signals indicate that structural changes were

observed due to interactions between chlorophylls and carotenoids (protein–protein interactions) in LHCII trimmers. This could affect the excitonic interactions of pigments from different protein complexes and lipid–protein environments which ultimately changes the spectral alterations. These data explain that the impairment of the organization of the photosynthetic supercomplexes and macro-organization upon iron deficient conditions, whereas the photosynthetic complexes were completely restored when Fe is supplemented with these deficient cells (Fig. 4.3C). The changes from protein–pigment complexes and their interactions were reformed when the cells grown under recovery conditions. This implies that iron is very important for the integrity of thylakoid membranes.

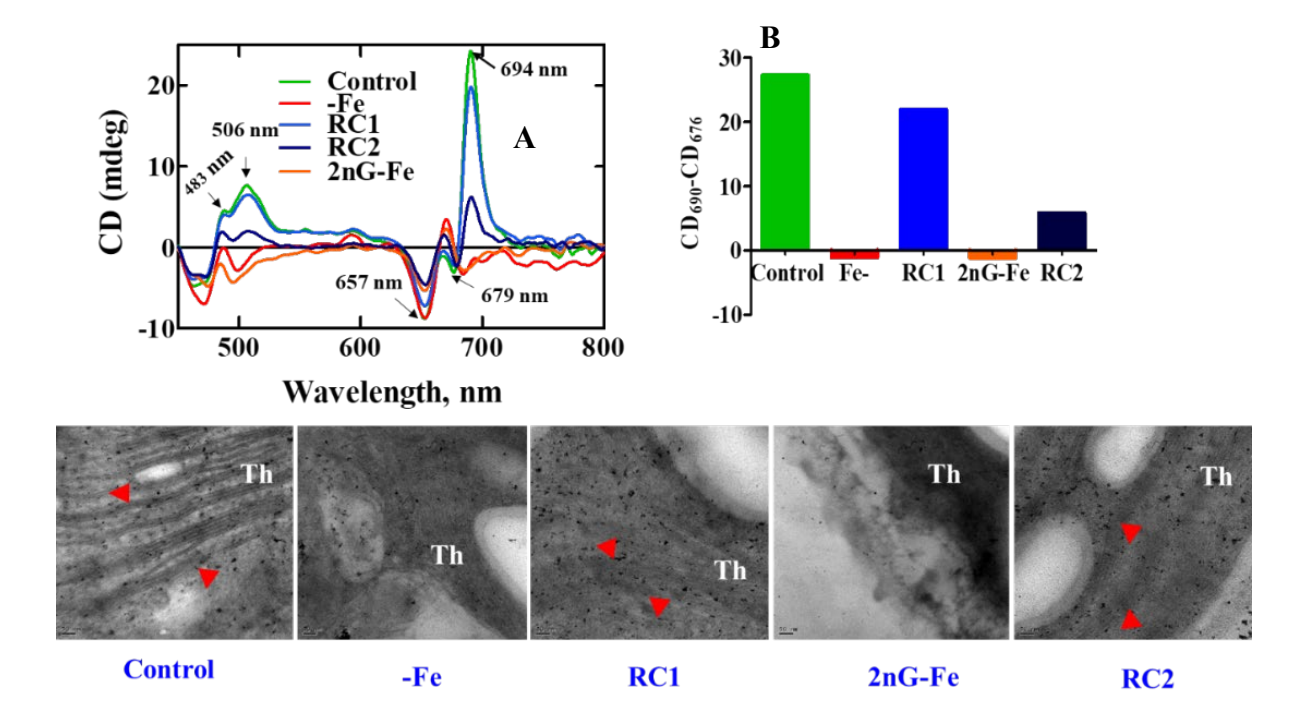


Fig. 4.3 (A) Visible circular dichroism spectra of control (+Fe)-green, iron deficiency (-Fe) red, RC1-blue, 2^{nd} G-Fe - orange and RC2 - purple in colours as represented. (B) The amplitude of psi-type CD bands in the region (CD₆₉₀-CD₆₇₆). Spectra were measured with equal (30 μ g/mL) chlorophyll based. (C) Transmission electron microscopic analysis of thylakoid stacks and their organization in the chloroplast.

4.1.4 Thylakoid membranes supercomplexes analysis by BN-PAGE

Additionally, we have analyzed the membrane supercomplexes from thylakoid membranes using BN-PAGE. This method is used for the separation of native membrane supercomplexes from the chloroplast. The investigation of the photosynthetic complexes were identified through BN-PAGE (Ossenbühl et al., 2004). Here, the supercomplexes were isolated and separated from thylakoid membranes of control, iron deficient, severe iron deficient condition, and their recovery cells. The non-ionic detergent β-dodecyl maltoside was used as a solubilizing agent. The data explains that the PSII-LHCII, PSII dimerization, and PSI-LHCI complexes were disassembled in both iron and severe iron deficient conditions. The monomeric core proteins of PSI and PSII were also affected severely with iron deficiency (Fig. 4.4).

One of the trimers from the whole LHCII complex is almost diminished and the monomer content was also decreased in iron deficient condition. However, these LHCII trimers are resynthesized in recovery conditions (RC) (Fig. 4.4). Moreover, the supercomplexes separated from the sucrose density gradient is the agreement with the change in supercomplexes. These results indicate that the PSII and PSI organizations are damaged under iron deficient conditions, which leads to decrease in the total photochemical yield. The native protein profile shows that PSI RC dimeric proteins, PsaA, and PsaC are affected, indicating that PSI is more prone to an iron limiting condition. The protein Lhc3b of LHCII trimer complex which is severely affected/demised. The other LHCII complexes, trimer and monomer complexes were also disorganized, which suggest that there is an impairment of efficiency of an excitation energy transfer at PSII RCs. Hence, there is a decline in Chl fluorescence, supercomplexes, and pigments are due to disordering in their organization under severe

iron deficiency. However, in the recovery process, all these complexes were restored in cells of both first and second generation of iron deficient cells, indicating that iron is essential for the formation of all the above supercomplexes.

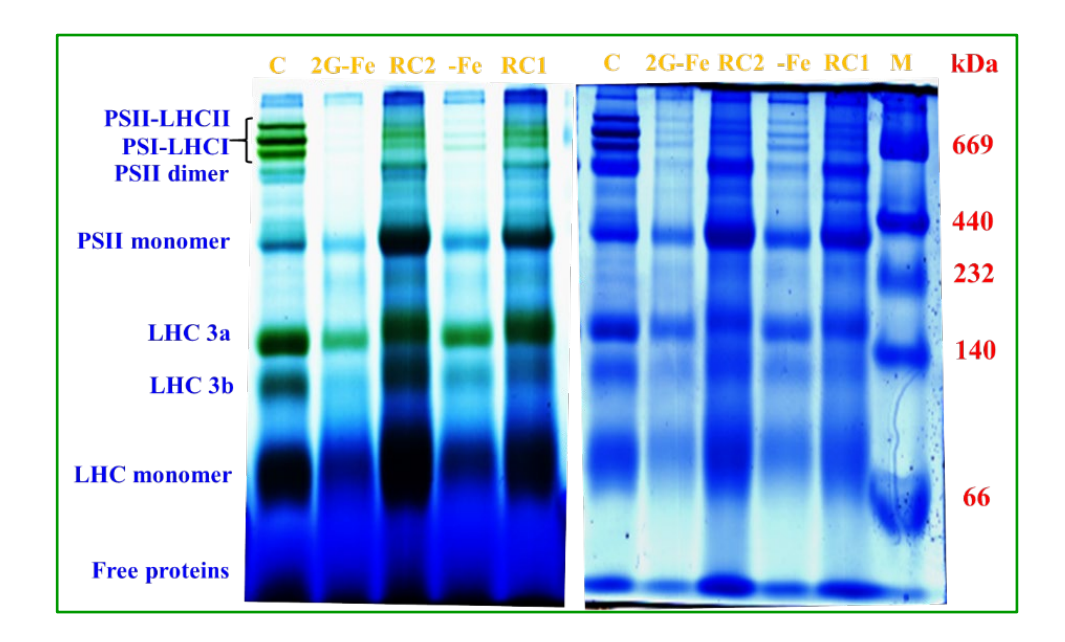


Fig. 4.4 Membrane supercomplexes were isolated from cells grown under iron deficient as well as control and their recovery conditions (8 μg of Chl/per well) and separated through Blue Native-PAGE. (B) The same gel stained with colloidal CBB stain and they labelled as (PS I) II (PSII-RCC Monomer), IL (PSI LHC I Complex), IIL (PSII LHC II Complex), II2 (PSII Dimer), A (ATP Synthase), L3a L3b (LHC Trimers), L (LHC Monomers) and free proteins.

4.1.5 Characterization of supercomplexes from sucrose density gradient

The supercomplexes were separated by using a sucrose density gradient centrifugation. The isolated thylakoid membranes were solubilized with β-DM and loaded onto the gradient with an equal amount of chlorophyll (0.8 mg/mL Chl). After the centrifugation, different green fractions were found in the 1st iron deficient as well as severe iron deficient conditions and their recovery (RC1 and RC2) conditions along with control (Fig. 4.5A). These fractions were designated as F1 (LHCII), F2 (a small proportion of PSI-LHCI complex with PSII), F3 (consists of larger PSI-LHCI-LHCII supercomplexes), (Subramanyam et al., 2006; Yadavalli et al., 2012). For our study, all the fractions were collected and density was measured at 675 (Fig. 4.5B).

The intensity of F3 band containing PSI-LHCI supercomplexes was diminished or completely absent in 1st iron deficiency as well as in severe iron deficiency condition. However, these F3 band was recovered in RC1 and RC2 which are same as in control (Fig. 4.5). The increased density of F3 fraction of RC2 conditions indicates the resynthesis of PSI-LHCI supercomplex. These results also supports blue native gels and absorption spectra, which show the complete absence of PSI-LHCI supercomplexes (Fig. 4.4). Similar results were observed from *C.reinhardtii* cells treated with salt stress with the complete loss of PSI-LHCI supercomplexes (Subramanyam et al., 2010; Yadavalli et al., 2012). These results imply that PSI-LHCI complexes are more damaged due to iron deficiency than the iron sufficient condition.

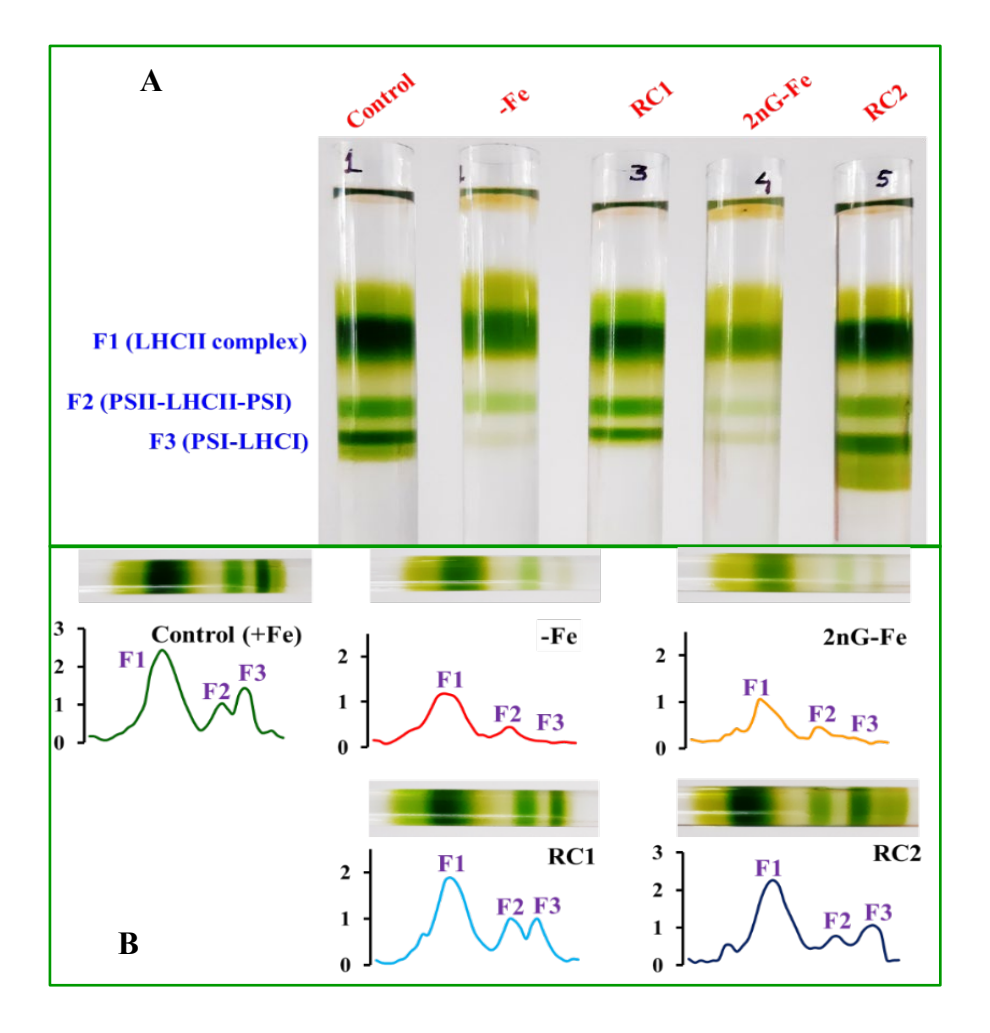


Fig. 4.5 (A) Sucrose density gradient separation of membrane supercomplexes from isolated thylakoid membranes of control (+Fe), -Fe, recovery-RC1, severe iron starvation (2G-Fe) and, recovery-RC2. Thylakoid membranes were solubilized with 0.8% β-DM and equal chlorophyll (150 μ g/per tube) was loaded on top of the tube. (B) The absorption of each fraction of the sample was taken at 675 nm from plate reader and each fraction was labelled as F1, F2, and F3. SDG separation was done with three individual experiments.

Chapter 4

To study the absorption cross-section of LHCII, PSII-LHCII-LHCI and, PSI-LHCI supercomplexes under iron deficient conditions, we have used three different band fractions for the absorption and visible CD spectra to understand the pigment-pigment and pigment-protein interactions (Fig. 4.6). Literature shows that the F1 band arises mostly from LHCII, F2 from PSII-LHCII-little fraction of PSI-LHCI and F3 mostly from PSI-LHCI-LHCII complexes (Yadavalli et al., 2012). The absorption spectra of F1 fraction which have major peaks at 675 nm and 652 nm in the red region and 439 nm and 472 nm in the blue region, originates mainly due to LHC complex. The major peaks at 675 nm and 652 nm are due to Chl a and Chl b, respectively which are significantly decreased in 1st as well as 2nd generation iron deficient conditions whereas the same peaks were observed in their respective recovery (RC) conditions. These results indicate that the LHC complexes were marginally decreased in iron deficient conditions, but the LHC complexes were restored, upon re-addition of iron. Similarly, the F2 fraction shows the major peaks at 675 nm, 439 nm and a minor peak at 470 nm and 420 nm corresponds to PSII-LHCII-LHCI and F3 fraction show the two major peaks at 678 nm and 469 nm and a minor peak at 439 nm which is characteristic absorption spectra of PSI-LHCI supercomplex (Subramanyam et al., 2006).

The F3 fraction (PSI-LHCI) supercomplexes were damaged in both 1st and 2nd generation iron deficient conditions whereas the increased peaks at 678 nm, 469 nm and, 439 nm from their recovery conditions, indicate re-synthesis of PSI-LHCI supercomplexes (Fig. 4.6C). All the complexes were severely affected due to Fe deficiency conditions, whereas all these complexes were almost restored upon readdition of iron. Similarly, these fractions F1, F2, and F3 were also used to measure the visible CD spectra, they also follow the same trend. The F1 green band obtained from the sucrose density gradient originates from LHCII complexes (Fig. 4.6D). In which in

Chapter 4

the red region, the spectra are characterized by the band peaks at (-)-653, (+)-669, and (-)-685 nm, which are associated with the Qy exciton states of Chl b and a, this data is an agreement with the previous report (Subramanyam et al., 2006; Akhtar et al., 2015). The dominant peaks for LHCII band (F1) shows (+)-439, (+)-446, (-)-473, and (-)-493. In the blue region, the spectra have a more complex structure due to the abundance of Chl and carotenoid transitions. Similarly, the F2 band arises from PSII-LHCII, a bit of PSI-LHCI, their CD bands at Qy exciton states of Chl a and b (+)-691, (+)-669, (-)-653 and blue region showing the dominating peaks at (-)-465 and (+)-446 (Subramanyam et al., 2006). Further, F3 band fraction is attributed to PSI-LHCI supercomplexes (Subramanyam et al., 2006), the CD peaks show the excitation states of Chl a and b (+)-689, (+)-674, and (-)-653, in the blue region the dominant peaks are (-)-465 and (+)-446.

In Fe severe starvation (2nd generation), the peaks have been predominantly diminished in both CD and absorption spectra. However, band 3 (F3) which corresponds to PSI-LHCI complexes were more prone to Fe starvation compared to LHCII (F1). The severity of damage follows as PSI-LHCI>; PSII-LHCII> LHCII. This implies that iron is more abundant in PSI-LHCI complexes, compared to PSII-LHCII complexes. In all these complexes the pigment-pigment excitation coupling is significantly altered. Due to Fe deficiency, these complexes have been destabilized or they have not synthesized under severe Fe deficiency. When the severe Fe deficiency cells were re-supplemented with Fe, all the above mentioned supercomplexes were restored. This emphasizes that the cells were in dormancy, during iron starvation. Similarly, the blue native gels are also in agreement with the sucrose gradient separation data that supercomplexes were lost in Fe stress conditions but restored upon re-addition of iron.

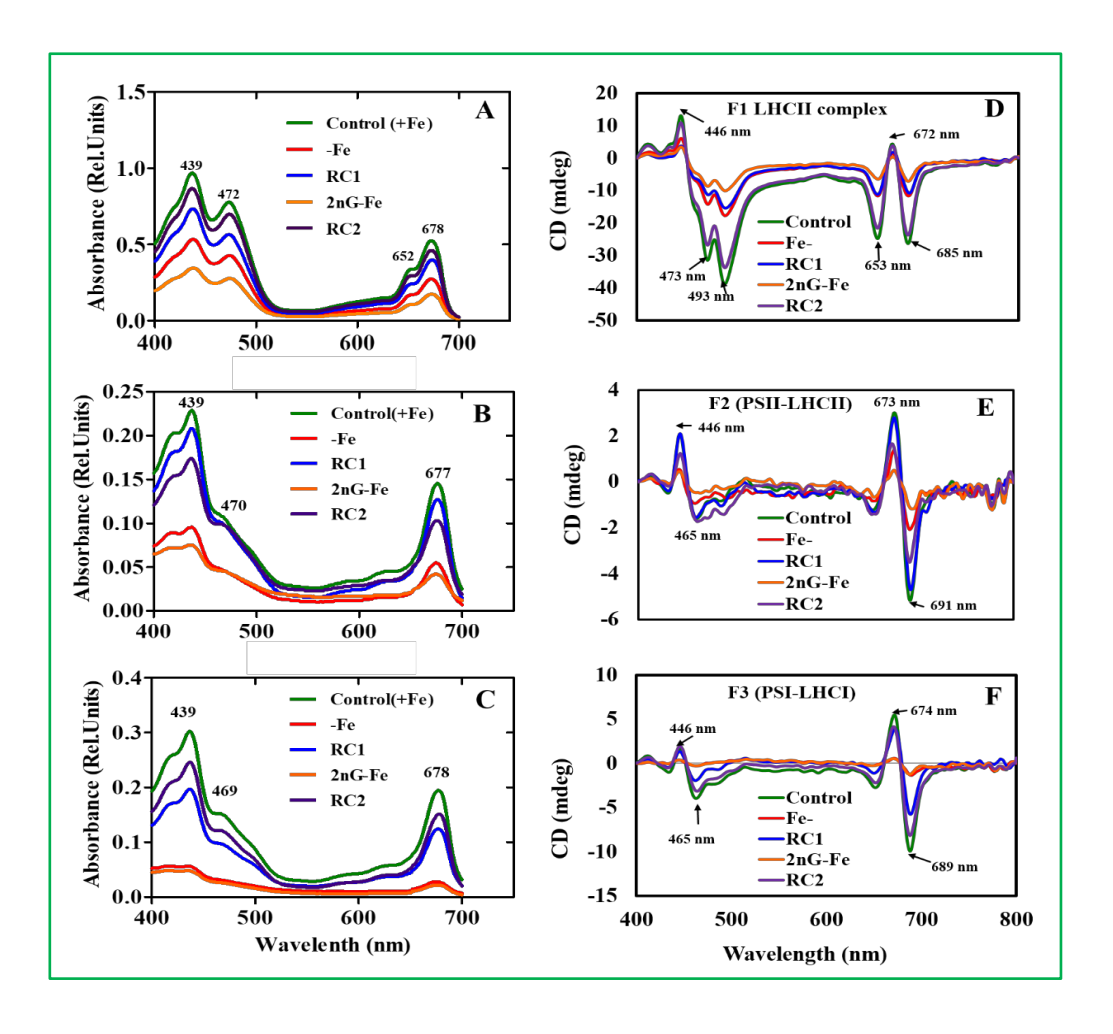


Fig. 4.6 An equal volume (200 μ L) was collected from each fraction (F1, F2 & F3) for analys is of absorption and CD spectra. (A) F1 fractions from all the tubes were taken for the absorption cross-section of their pigments (B) F2 fractions were used for the study of pigments associated with PSII-LHCII supercomplexes, (C) F3 fraction for PSI-LHCI complexes. The CD spectra of each fraction from (F1, F2 & F3) was taken and labelled as (D), (E) and, (F) respectively. Three individual measurements were done from three independent SDG separations.

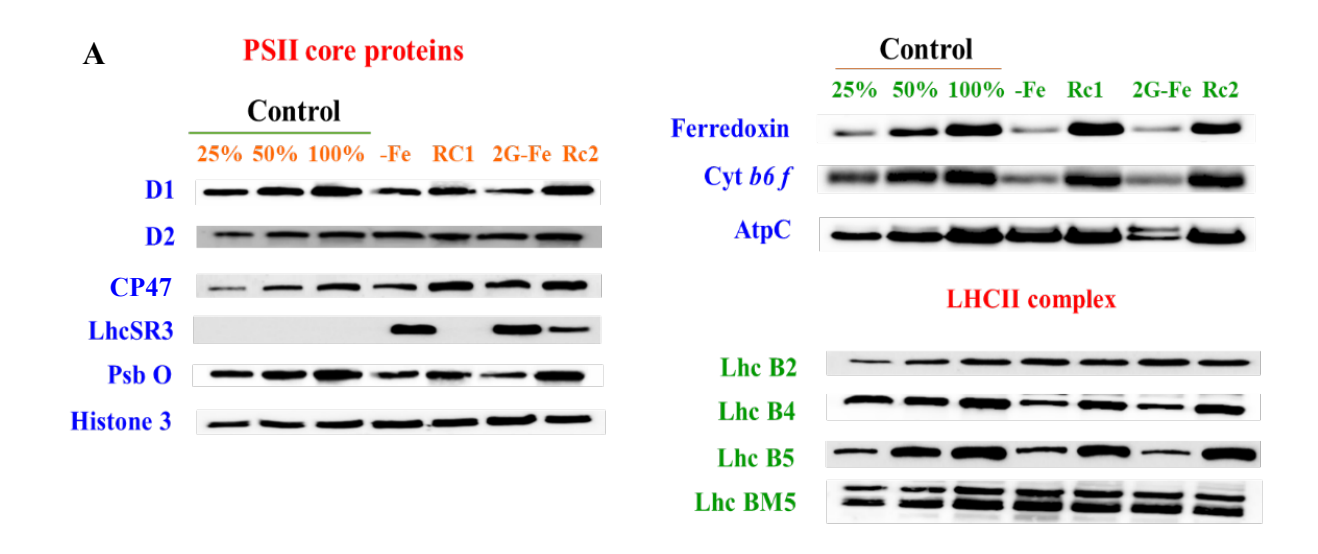
4.1.6 Immunoblots of PSII-LHCII protein polypeptides

The abundance of photosynthetic proteins was analyzed by immunoblot analysis. The polypeptides were separated using Bis-Tris gel and immunoblots were carried out by probing with respective antibodies to examine the protein content of PSII core as well as LHCII complex. PSII core complex has two intrinsic core proteins, D1, and D2 along with CP43 and CP47, which are chlorophyll containing inner antenna subunits (Zouni et al., 2001). Under severe as well as the first stage of iron stress, D1 and D2 were

marginally reduced while no significant change in the protein content of CP43 and CP47 (Fig. 4.7). The OEC complex protein content was reduced in both iron limiting conditions which is in agreement with decreased Fo values from handy pea data. These antenna proteins majorly transfer the energy via chlorophyll molecules to the reaction centre and thereby the total energy was hampered, due to lack of iron in the cells. These result indicates that iron stress show more impact on D1 and not on the D2 core protein, as reported with previous studies (Yadavalli et al., 2012).

When comes to LHC complex, there are six trimers per one dimeric core in the thylakoid membrane of C. reinhardtii cells. Lhcb4 (CP29) and Lhcb5 (CP26) are two minor antenna proteins that present as monomers, while CP24 gene is not found in the algal genome (Drop et al., 2014). The light harvesting complexes, Lhcb4, and Lhcb5 content were affected in iron stress whereas there was no change in Lhcb2 and LhcBM5 proteins. The CP29 and CP26 proteins are the minor subunits which are drastically reduced under iron deficiency condition (Fig. 4.7B). Interestingly, the Lhcb2 is not changed significantly this is due to peripherally arrangement. Thus, it could be expected that the generation of ROS during stress conditions would damage the inner LHCII subunits, which is an agreement of our ROS measurement results (Fig. 4.8B). It is well known that 10² play a major role in the damage of the D1 protein at the acceptor side of PSII during the stress conditions and also in high light condition (Nishiyama & Murata, 2014). The previous reports show that 10² produced via lipid peroxidation which may damage core protein D1 as well as the LHCII subunits. Hence, our results are in corroboration with our earlier published reports (Yadavalli et al., 2012). The iron containing photosynthetic proteins were investigated and their protein content was lower, in response to iron-deficient cells when compared to control cells. This is in agreement with our photosynthetic activity measurements. While the iron-containing

photosynthetic protein Cyt *b6f* was decreased 75% in severe iron-deficient conditions, it could be maintained in the iron-recovery condition. The atpc subunit of ATP synthase was also reduced in the second generation of Fe deficiency, however, it was restored in Fe added cultures. To demonstrate the decrease in abundance of iron-containing proteins in response to iron deficiency condition, we have monitored the abundance of a non-iron containing protein known as LhcSR3. This protein expression was increased in iron-deficient conditions which are necessary for NPQ, increased concerning iron limitation condition (Naumann et al., 2007; Peers et al., 2009). Like Pet B, one of the polypeptide of ferredoxin and PSII core protein, D1 and PSI core protein, PsaD were also decreased by 65% in severe iron-limited cells (Fig. 4.7B). It is interesting to know that the LhcSR3 expression still appeared in RC2 and this could be due to the cells being in stress condition. This shows that in recovery 2 the photosynthetic activity, supercomplexes, and protein contents were not restored to the level of control, this may be due to the presence of NPQ (Fig. 4.1-4.4).





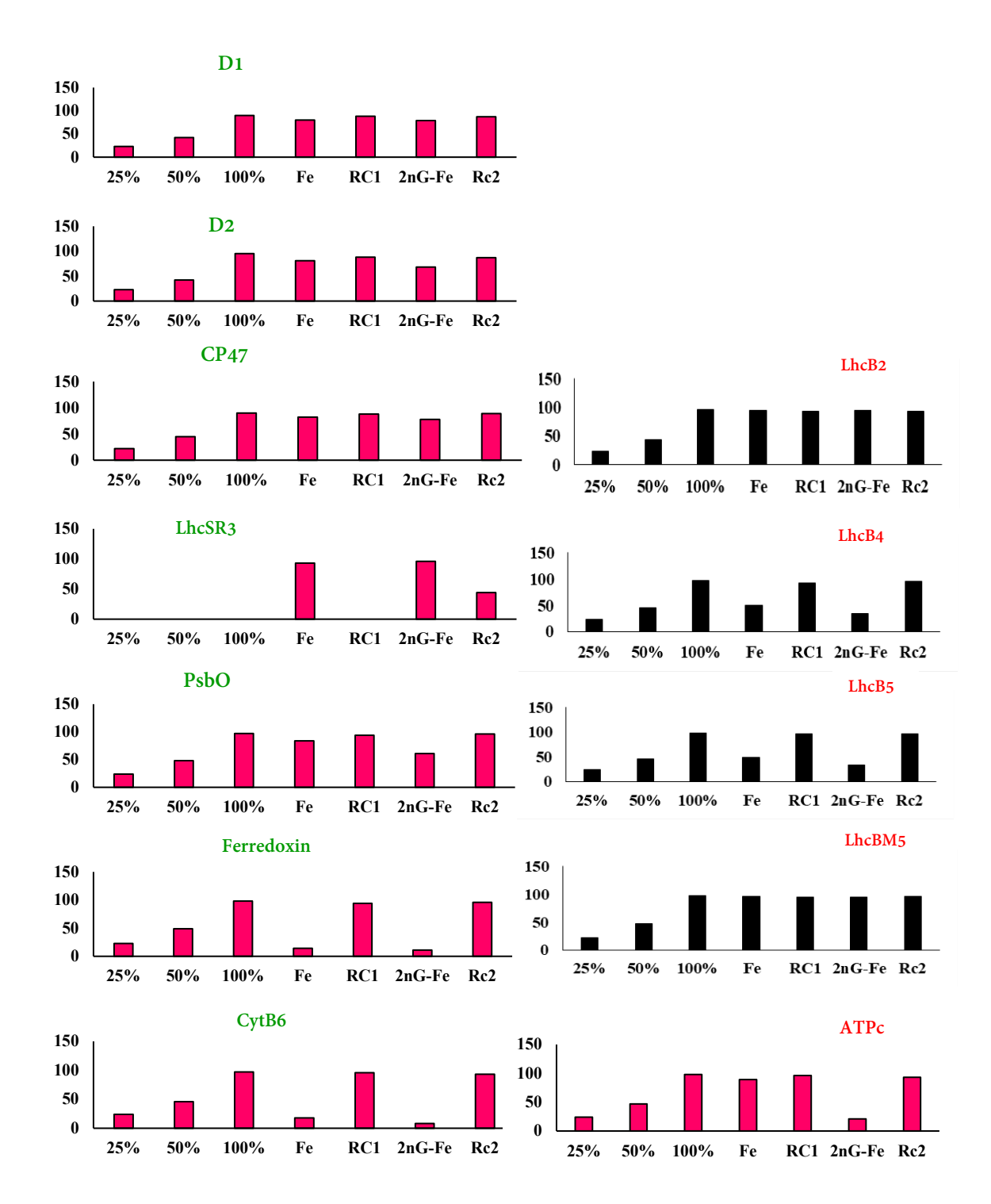
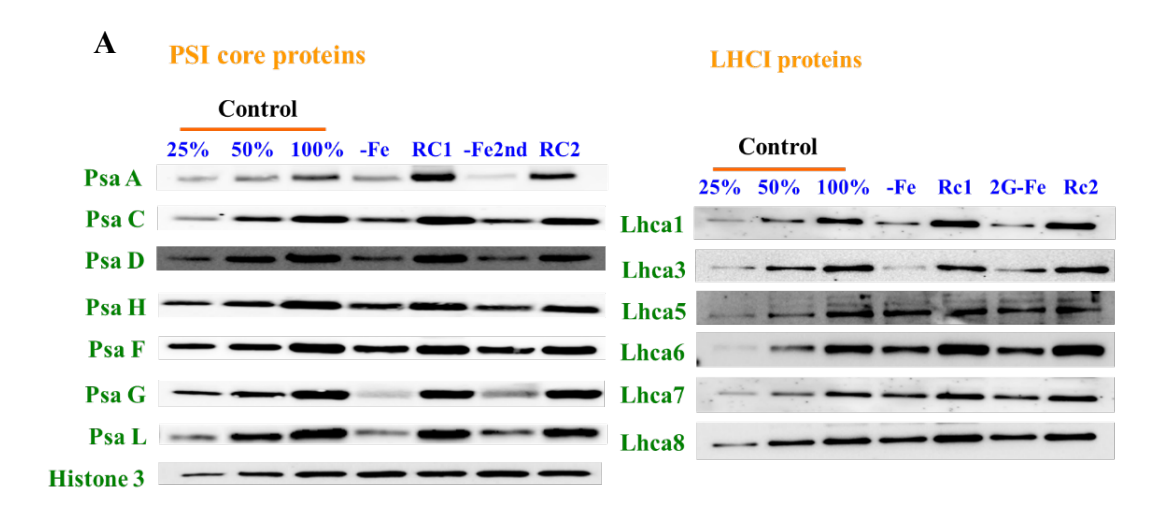


Fig. 4.7 (A) Immunoblots of PSII core proteins (D1, D2, and Cp47), OEC complex, PsbP and LHCII polypeptides (Lhcb2, Lhcb3, Lhcb4, Lhcb5, and LchBM5) from control, -Fe, RC1, 2nd Generation -Fe and RC2 conditions. The polypeptides were loaded with an equal concentration of protein (5 μg) per lane and the dilutions were made from the control sample in 25, 50 and 100% as a positive control and for equal with loading was represented with Histone 3 (H3) antibody. (B) Quantification of each protein by using Image J software for easy compression (n=3).

4.1.7 Protein profile of PSI and LHCI complex

It is a well-known fact that the PSI complex is more prone to iron limiting conditions in higher plants, green algae and cyanobacteria. During evolution, the PSI core proteins were conserved from cyanobacteria to plant. Photosynthetic organisms have developed the supramolecular organization of PSI consisting of PSI core with a peripheral antenna system to adapt the different environmental conditions (Blankenship, 1992). The cyanobacterial PSI core is in trimeric form whereas plant and green algal PSI are in monomeric form and which is associated with LHCI complex resulted in the formation of PSI-LHCI supercomplex (Jordan et al., 2001). In *C. reinhardtii* there are more Lhc gene copies present than in higher plants or cyanobacteria (Stauber et al., 2003; Takahashi et al., 2004; Yadavalli et al., 2011). In iron deficient conditions, major changes were observed in the core subunits of PSI (Fig. 4.8A) The PsaA protein is the core protein of PSI which binds all cofactors of the electron transport. The PsaC, RC of PSI was decreased by 50% and 50% in the first and second phases of respective iron deficient conditions whereas the PsaD content was reduced to 25% in both iron deficient conditions (Fig. 4.8B).



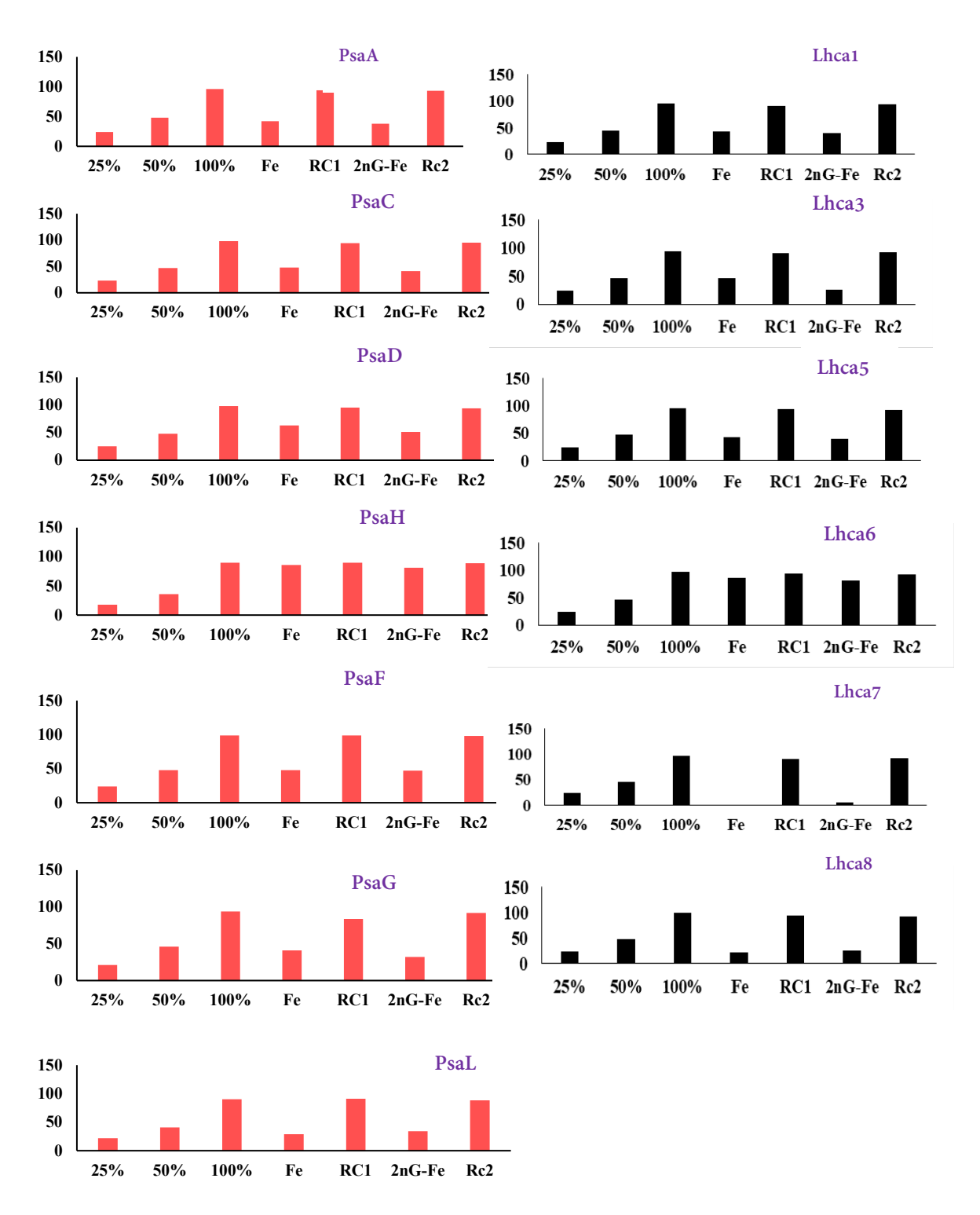


Fig. 4.8 (A) Immunoblots of PSI core proteins (PsaA, PsaC, PsaD, PsaF, PsaG, PsaH and PsaL) and LHC1proteins were extracted from control, -Fe, RC1, and 2nd Generation –Fe and RC2 conditions. An equal amount of protein was loaded in to (5 μ g) each lane. The control protein loaded with different dilutions (25, 50 and 100%) for easy comparison and Histone-3 was used as a loading control.

The extrinsic protein subunits PsaG, PsaL were significantly decreased due to severe iron deficiency after 72 h of growth. Previous reports about the effect of iron deficiency on the PSI stromal ridge, clearly explains the loss of PsaE protein in *C.reinhardtii* (Yadavalli et al., 2012). The proteins, PsaD and PsaE are involved in stabilization of PsaC and the stromal hump which in turn forms the ferredoxin docking site (Chitnis et al., 1995; Rochaix, 2002). The loss of PsaC deviates the electron transport, as it binds to electron acceptors F_A and F_B of ferredoxin and it is essential for the proper functioning of PSI (Oh-oka, et al., 1988). Ferredoxin, which is an iron-containing photosynthetic protein was reduced by 80% in iron-deficient than iron-recovery cells.

In chloroplasts, the photosynthetic subunits-PSI and the Cyt b6/f complex are Fe-S containing clusters that are involved in the operation of electron transfer reactions. The Fd complex is involved in the electron flux from PSI to the dark reactions of photosynthesis. It is expected the Fe complexes would change significantly under Fe starvation leading to alteration of electron transport. The decreased PsaG also lead to the dissociation of a large part of the PSI antenna (Ozawa et al., 2018). The LHCI subunits show different susceptibility to severe iron stress conditions. Interestingly, no significant change in polypeptides of Lhca7, and Lhca8 from the PSI-LHCI supercomplexes was observed. However, Lhca1, Lhca3, Lhca5, and Lhca6 subunits were marginally reduced in all deficient samples (Fig. 4.8B). The arrangement of LHCI subunits from the PSI complex has been revealed through crystal structure from C.reinhardtii (Suga et al., 2019). The detachment of each LHCI protein from the PSI-LHCI supercomplex leads to a loss of 10-14 chlorophylls; which in turn leads to a decrease in the absorption cross-section of PSI and this cause stress-induced chlorosis. The LHCI complex is arranged in a shape of semicircle which includes Lhca5, 6, 8, 7, and Lhca3 present in the inner half ring and Lhca1, 4, 2, and Lhca9 are located in the

outer half-ring (Suga et al., 2019). Interestingly, the inner LHCI subunits got affected, as one can expect the peripheral subunits to be more susceptible to any kind of stress. The blue native gel also suggested that PSI complexes including LHC complex and PSI core proteins are decreased under the severe iron deficient condition which is also correlated with our ROS vs Fv/Fm data (Fig. 4.9B). Hence, we reported that PSI is more sensitive than PSII which is marginally decreased even in severe iron deficient conditions. The above results show that the Fe containing proteins are severely affected, whereas Fe independent proteins weren't severely affected.

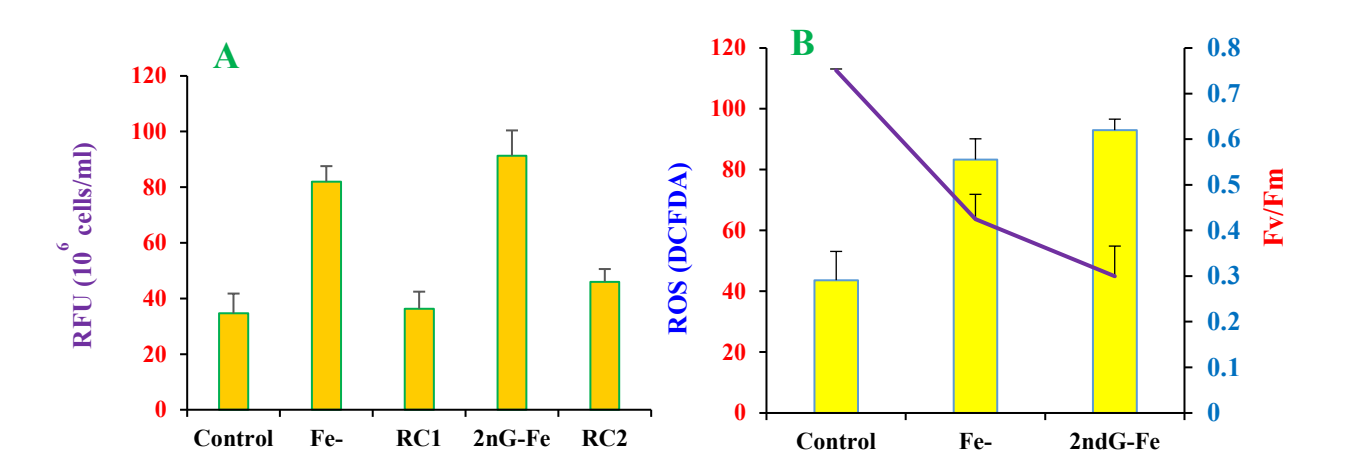


Fig. 4.9 Total reactive oxygen species (ROS) were measured with H_2DCFDA , concentration of 5 μ m/ml. (A) ROS were quantified from the cells at 24 h, 48 h and 72 h of control, -Fe, RC1, 2nd Generation-Fe and RC2 condition. (B) Graph showing compression of total photosynthetic activity (Fv/Fm) with ROS. Fv/Fm activity has decreased with increased ROS in *C. reinhardtii* cells.

However, most of the proteins were still degraded. Since the cells were grown in Fe deficiency the biogenesis of all these proteins was affected. Moreover, the biosynthesis of pigments was severely affected, which is evidence of the change in photosynthetic activity and pigment-protein complexes. All these were proved that when Fe is added to the iron deficient cells, the photosynthetic activity, protein-pigment protein interactions and proteins were restored. Though Fe is a trace element, it is an important cofactor to several complexes in both PSI and PSII. Hence, Fe is a vital trace element to perform photosynthesis.

4.1.8 Observation of aggregated proteins

Less expression of proteins may cause disassemble of the supercomplexes as well as a change in the inefficiency of photosynthesis. The results show that PSI and PSII core protein abundance have been reduced, if that is the case, the stoichiometric change in thylakoids would occur. However, still, some proteins are intact (Lhcs and few PSI proteins) despite a change in core proteins (D1 and PsaA) and less abundance in proteins could be aggregated, hence they could not separate in gels (Fig. 4.10).

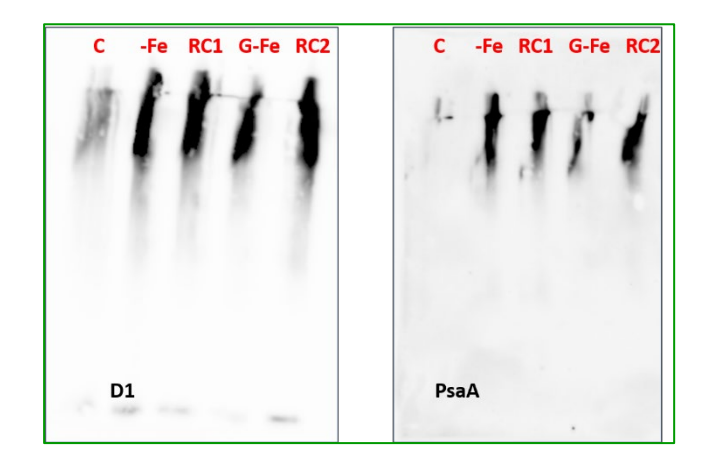


Fig. 4.10 Protein aggregation analysis from *C.reinhardtii* cells grown under control, -Fe, RC1, 2nd generation of –Fe and, RC2 conditions. 5 µg of protein was run the gel for the first dimension and cut the gel piece from stacking region of each sample and incubated with 2% Mercaptoethanol for 3 hours and then placed on to 8% acrylamide gel to see the aggregation in the all the samples.

This was again run on SDS-PAGE to see the aggregated products. To our surprise, the core proteins D1 and PsaA were present in Fe deficiency conditions after the denaturation (Fig. 4.10). Interestingly, we also found these proteins in Fe recovery samples. Usually, the protein undergoes a change in confirmations and misfolded whey they aggregate. Since the core proteins are misfolded, the cell cannot perform regular photosynthesis. Since the aggregated core proteins seem to be irreversible, that might be the reason the cells were not completely reversible after adding iron to cells. As a result, the photosynthesis yield is less in severe Fe deficiency and also in recovery cells. Our results are in agreement with an earlier report that high light induced aggregation of core protein (D1) which was irreversible whereas the LHCII was reversible (Yamamoto et al., 2013). The irreversible aggregation of proteins could have caused because of the generation of ROS. Thus, the irreversibly misfolded proteins ascribed to cross link with the surrounding proteins, hence their abundance has been diminished (Fig. 6&7). Consequently, protein aggregation is one of the main processes to indulge the photochemical reactions, as a result, change in energy transfer and thylakoid organization was observed in Fe deficiency.

4.2 CONCLUSIONS

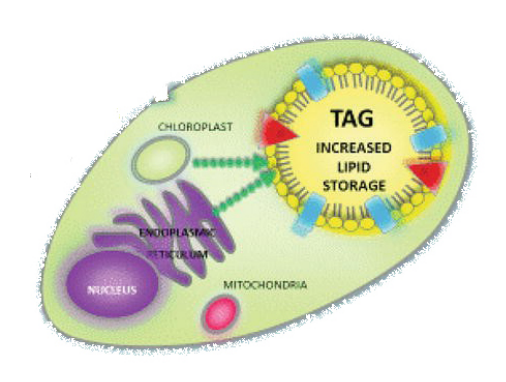
These results demonstrated that photochemical yield is significantly decreased in severe iron deficiency conditions because of irreversible aggregation. However, the recovery conditions RC1 explains that both photochemical yield and photosynthetic activity were recovered equals control whereas RC2 has recovered up to 75% which is not equal to the control level. The photosynthetic activity has been decreased due to an increment with inactive RCs, the reduction of Q_A, impairment of electron transport between Q_A to Q_B of PSII. The regulation of electron transport activity of PSII (SM, N, ETO/RC,

Chapter 4

ETO/CSm), and significant increment of energy dissipation around PSII (KN, DIO/RC, DIO/CSm). Structural integrity and stability of PSII were majorly affected, which is explained by the L and K-bands. The significant difference in the peak intensities from CD spectra indicates the decreased in the interactions of pigment-pigment, namely the dissociation of LHC complexes with PSII due to lack of iron. Up-regulation of reactive oxygen species was harmful and damage the core proteins of PSII and PSI complexes under both stages of iron stress conditions. From the blue native gel two LHCII heterotrimers, monomeric LHC, RC dimer of PSII and PSI were decreased with severe iron deficiency and these complexes were recovered like control. Furthermore, the sucrose density gradient fractions reveals that LHCII, PSII-LHCII and PSI-LHCI complexes were significantly decreased in Fe deficiency condition. The Ferredoxin and Cytb6 were decreased in both iron deficient conditions whereas they were recovered from iron supplemented cells. However, the impact of iron limitation shows a decrease in PsaA and PsaC protein content which are essential for the proper function of PSI complex. The core protein of PSI and PSII have been misfolded due to reversible aggregation, thus change in photochemical activities. The recovery conditions show the restoration of PSII-LHCII complex and PSI-LHCI supercomplexes from iron starvation. Overall, the present study explains about effective in the way of dynamics of total photosynthetic activity from iron stress and their recovery conditions.

Alteration of membrane lipids and triacylglycerol accumulation in *C.reinhardtii* under iron starvation

Chapter 5



5.1 INTRODUCTION

Microalgae are identified as promising and suitable live feedstocks for biofuel production due to their high photosynthetic efficiency. They can adapt to different environmental stress conditions such as high light, salinity, heat and nutrient deprivation. They are known to accumulate valuable products such as lipids, starch, carotenoids in response to horse environmental conditions (Chisti, 2007; Minhas et al., 2016). Algae have become essential strategies for enhancing commercial production of microalgal metabolites under nutrient deprivation, high salinity, extreme temperatures, or high irradiance (Cho et al., 2007; Kakarla et al., 2018). Inducing high lipid content in microalgae for biodiesel production is recognized as a promising strategy for future resources. Many algae are performing the photosynthesis by capturing the solar energy and store it as chemical energy such as starch and lipids, in the particularly high level of TAG. Biodiesel production can be obtained by transesterification of TAG with methanol under the presence of a suitable catalyst (e.g. H₂SO₄).

However, most of the microalgae accumulate the abundance of TAG under only nutrient stress conditions such as nitrogen starvation. Generally, stress conditions were lead to decreases the growth rates and economic production of biodiesel will depend on the algal growth and its lipid composition. Various stress conditions like nitrogen starvation (Rios et al., 2015; Lin, 2018) iron starvation (Gorain et al., 2013), copper stress (Hamed et al., 2017), heat stress (Ördög et al., 2016), pH (Abinandan et al., 2019) and, high-light stress (Fan and Zheng, 2017) have been reported effectively to induce the lipid accumulation in microalgae. Further studies on nutritional requirements for growth of *Dunaliella tertiolecta* has accumulated the TAGs (Chen et al., 2011). The micronutrient, iron is essential in biochemical pathways as a cofactor in plants as well as in microalgae. The limitation of micron nutrients (e.g. zinc and iron) resulting in the

conversion of membrane lipids into individual fatty acids which leads to lipid droplets (LDs) formation (Chen et al., 2011). Impacts of absences elements such as N, S, P and Mg on the microalgal metabolism have been studied in *C.reinhardtii* (Çakmak et al., 2014). Nitrogen starvation is severely inhibited the algal growth and induce more TAG accumulation in *C.reinhardtii* (James et al., 2011). Due to its potential influence on TAG accumulation, iron stress is likely to have wide-ranging effects on ER and membrane structures. Therefore, we hypothesize that two stages of iron starvation conditions (iron deficient (-Fe) cells further culturing into iron-deficient medium-called as severe iron starvation (2nd –Fe)) would be effective for inducing the lipid accumulation in *C.reinhardtii*. This hypothesis may offer an important way to induce more lipid content in microalgae. No studies are showing the potential to induce lipid accumulation of microalgae by two stages of iron stresses.

The present study focused on *C.reinhardtii* cultured in two stages of the iron starvation culturing system consisting of growth rate and subsequent their recovery conditions (RC1 and RC2) (supplementation of iron). Here, we focused on lipid content and TAG accumulation as above mentioned iron-deficient conditions. Fourier transform infrared spectroscopy was used to measure the carbon partitioning into carbohydrate and lipid. Further, liquid chromatography-mass spectrometry (LC/MS) was used to study the fatty acid composition of cells cultivated from two stages of iron deficient and their recovery conditions.

5.2 RESULTS AND DISCUSSION

5.2.1 Growth and biomass analysis in iron-deficient C. reinhardtii

The standard growth medium contains the iron concentration up to $18-20 \mu M$ iron (Fe²⁺) which will be good for the growth of *C.reinhardtii* (Kropat et al., 2011). To test the iron deficient for cell growth, cells were washed twice with iron-free medium and

then transfer into medium containing the iron sufficient (TAP +Fe as a control) as well as iron deficient medium (Fig. 4.1A, Chapter 4). The growth was monitored for four days at 750nm. In the iron-sufficient conditions, the absorbance value increased in doubled the OD value after 2 days and then reached to maximum growth (1.11 ± 0.18) after 72 h. Initially, in iron deficient medium have traces of iron molecules in original inoculated cells and these iron molecules were utilised by the cell for first multiplication. So the real iron stress to *C.reinhardtii* starts after the first cell division. Similarly, the absorbance of the iron-deprived culture decreased (0.23 ± 0.02) over the first 2 days in culture but then it was increased (0.42 ± 0.04) to half-fold value over the following 4 days. Moreover, iron is present as a cofactor in several enzymes such as hydrogen dehydrogenase, nitrite reductase and superoxide dismutase (Marschner, 1995). Thus microalgae grown with iron supplemented media may enhance the iron containing enzymes which ultimately enhance the rate of cell metabolism.

Thus, the iron deficient culture was transferred into iron sufficient medium (\pm Fe) to check the recovery of growth and called it as recovery1 and the RC1 growth has been increased (0.361 \pm 0.12) within one day and it reached to maximum (0.91 \pm 0.17) growth. This indicates that iron element acts as a cofactor in many proteins and that reform the normal cellular metabolism to maintain the necessity of ATP production in the cell. Further, the iron limitation culture was transferred again into the same iron-free medium which is called as severe iron starvation for *C. reinhardtii* where the Fe content is almost zero. Hence, in order see to the real Fe deficiency on *C.reinhardtii* cells, the severe cells will give more insights of Fe importance in these cells in terms of photosynthesis and metabolism. In this severe Fe deficiency condition, the growth has been hampered (0.313 \pm 0.03). During the RC2 the growth was increased to 0.636 \pm

0.13. When Fe was supplemented to cells, the activation of enzymatic antioxidants was increased to protect the reactive oxygen species.

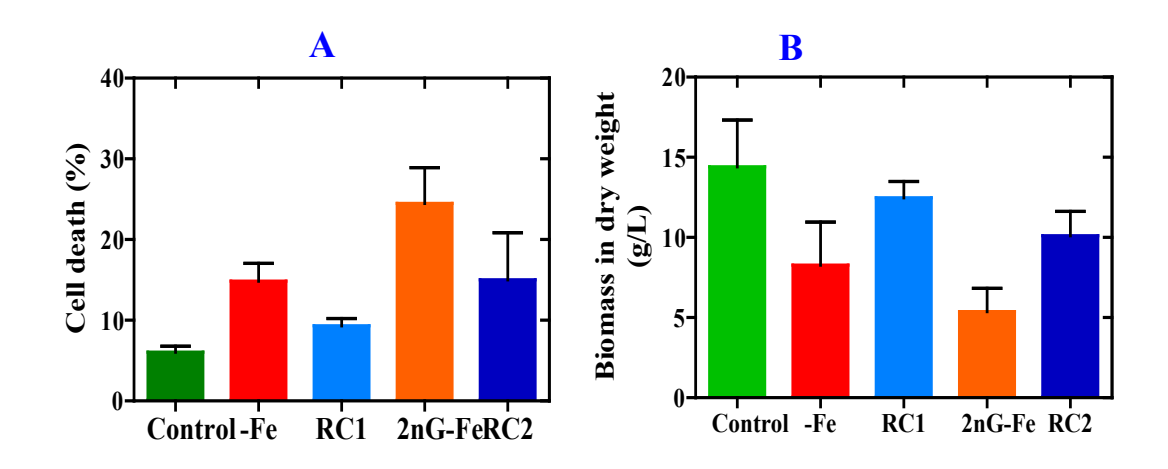


Fig. 5.1 (A) Biomass and Cell death measurements of *C.reinhardtii* cells from iron sufficient (+Fe) and iron deficiency (-Fe) conditions. (A) Biomass quantification from control, 1^{st} stage of iron deficiency, recovery 1 (RC1), 2^{nd} stage of iron deficiency and, recovery 2 (RC2) conditions. Control, RC1 and RC2 culture conditions were maintained in TAP containing 20 μ m of iron and TAP-Fe medium containing no iron. Total biomass from all the conditions and cultures were collected after 4 days of their growth. (C) Showing cell death from all the conditions and is expressed in (%). All the experiments were done with three individual and data was shown with \pm SD.

In severe iron limitation, the cell growth was slow and it has taken a long time for recovery in iron sufficient medium. The decreased growth is due to maybe cell death, so we have done the cell viability assay for all the conditions and it reveals that cell death has been found at the first stage of iron deficiency up to (14%) whereas in severe iron starvation condition was at (26%) (Fig. 5.1B). When comes to recovery conditions with 11% for RC2 and 13% for RC2. This difference in growth rate indicates the importance of iron nutrition to Chlamydomonas cell growth. Further total biomass in terms of dry cell weight has been measured after four days of cell growth (Fig. 5.1B). The total biomass from the cells grown under TAP +Fe medium containing iron was up

to 14 g/L, whereas it was decreased in the biomass (8 g/L) in the first generation of Fe deficiency (Fig. 5.1A). We noticed that increased biomass (12 g/L) in their RC1 reached to the level of control. On the other hand severe iron-deficient condition, the biomass has been decreased (5 g/L) but it was increased up to (10 g/L) in the RC2. The reports on nitrogen starvation in *C.reinhardtii* shows that cell growth has severely decreased which leads to a decrease in total biomass (James et al., 2011). There are two major problems for obtaining maximal biodiesel from microalgae which are low cellular lipid content and poor cell density. Stress conditions promote neutral lipid content while decreasing cell biomass in the medium (Davis et al., 2011).

Our results also show that the decreased dry weights of microalgae under iron starvation while increased in the total lipid levels under severe iron starvation. This decrease in biomass due to cell death, since continuous exposure of cells to iron limitation, which causes the stress on plastids and ER, hence it results in degradation of cells and which we observed the decreased in biomass. Such degradation might involve apoptosis. Recently it has been demonstrated that because severe ER stress leads to apoptosis in many organisms like Chlamydomonas (Howell, 2013).

5.2.2 Identification of Lipid droplets from confocal microscopy

The accumulation of lipid bodies was examined using confocal microscopy (Fig. 5.2). The microscopy results are shows that the first stage of iron limitation cells decreased in size and displayed abnormal cell morphology (Fig. 5.2). Cells were grown under iron sufficient (control) TAP medium did not show any accumulation of lipid bodies (Fig. 5.2). Lipid body production was majorly induced in iron less medium for both first stage and severe iron deficient conditions. Recently we reported that in the first generation of Fe deficiency the lipid droplets were accumulated.

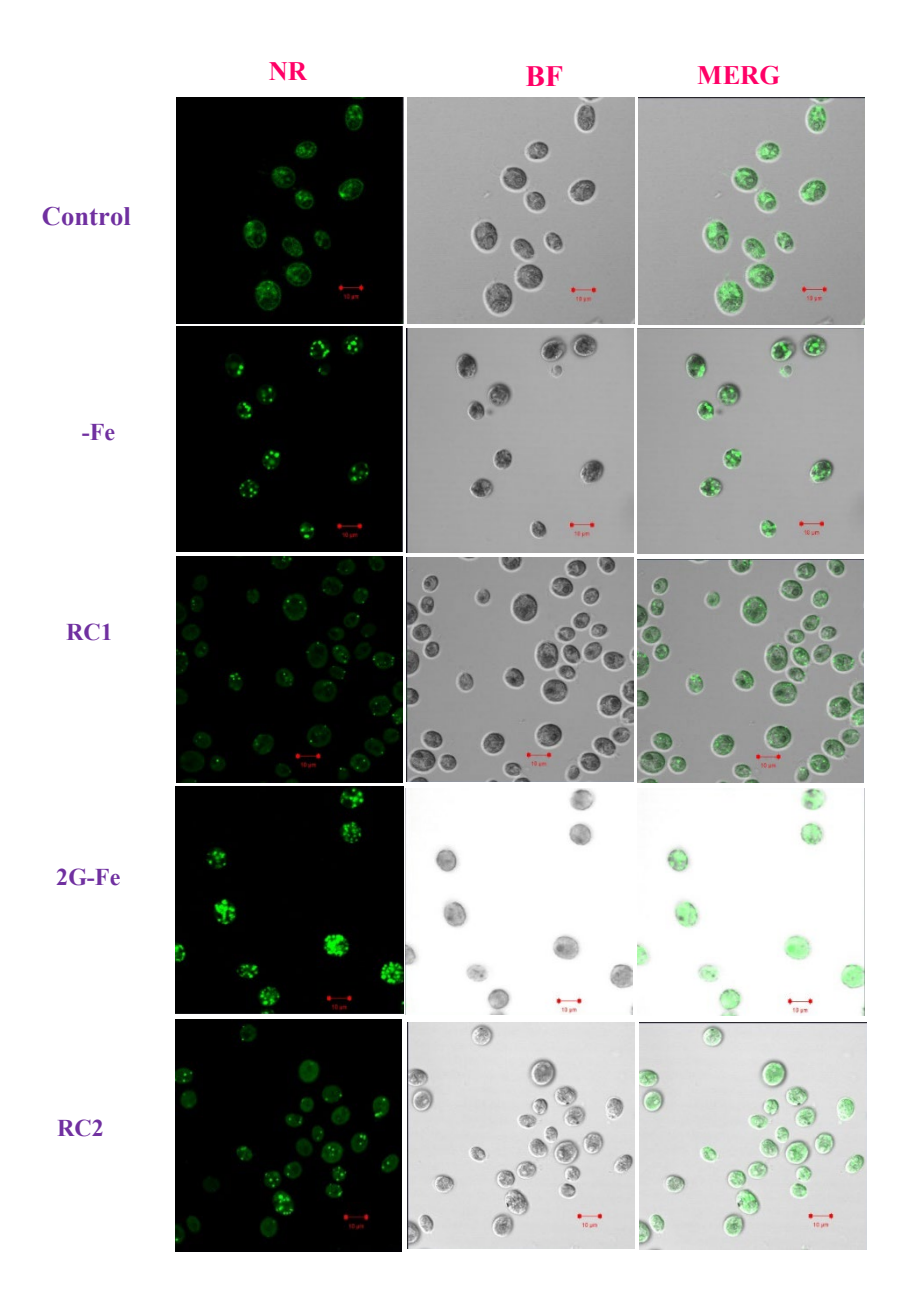


Fig. 5.2 *C. reinhardtii* cells stained with Nile Red over four days under confocal bright field (BF) and fluorescence (NR) images. Fluorescence and bright-field images of wild-type cc- 125 cells grown in (control) TAP medium and with TAP-Fe medium (iron deficiency and RC1 recovery cells from iron deficiency) (2nd G-Fe deficiency and RC2 is the recovery cells from the 2G-Fe condition). (10 μm scale bar).

Interestingly, the severe iron deficiency accumulated more and larger lipid bodies compared to the first stage of iron deficient conditions. The earlier studies under nitrogen starvation the lipid bodies accumulation was observed in Chlamydomonas (Wang et al., 2009). Further, the recovery cells from severe deficiency are showing some lipid bodies when compare to both iron deficient conditions. During the nitrogen starvation course, *C.reinhardtii* has accumulated the lipids up to 45% to 50% (Moellering and Benning, 2010; James et al., 2011). We have observed 65% of lipid accumulation in the 48 h of the severe iron starvation condition than the first stage of the iron deficient condition (40%). This indicates that severe iron starved culture was more appropriate with consisting of high content of lipid and it may be advantageous for lipid extraction for biofuels.

5.2.3 Nile Red fluorescence for neutral lipid study

To study the effect of iron deficiency in the cell population level after 48 h, we analysed the Nile Red fluorescence measurements of 10,000 cells from each group (i.e., iron deficient and control) by using flow cytometry. Nutrient limitation causes decreased cell multiplication and most of the microalgae divert the individual fatty acids into TAG accumulation (Sharma et al., 2012). Many of cells with 3-fold fluorescence levels were observed in the iron deficient whereas the severe iron deprived culture show the fluorescence up to 4-fold than in the control cells. The fluorescence in RC1 was almost similar to the control (Fig. 5.3A), indicating that severe iron deficient treatment induced significant lipid accumulation. The severe iron deficiency cells undergo more stress thereby accumulating the more lipids. Thus, the iron deficient-induced pathway is similar from nitrogen starvation which induces the LD accumulation and it involves degradation of chloroplast membranes lipids, which in turn remodelling of their lipids leads to the formation of TAGs in *C.reinhardtii* cells (Siaut et al., 2011). The neutral

lipids from severe iron limiting cells may useful for the production of biodiesel. The biomass was decreased while the Nile red fluorescence was increased when the cells were grown in Fe deficiency up to 48-72h (Fig. 5.1A). Interestingly, the effect of iron limitation on lipid accumulation was observed from the beginning of the cell growth, however, the accumulation of lipids was high in mid-log phase (Fig. 5.3B). These results revealed that the metabolism of iron and carbon in *C. reinhardtii* is interlinked, under iron deficiency which is a major proportion of carbon fixed by photosynthesis via, Calvin–Benson cycle that linked to produce neutral lipids (Velmurugan et al., 2014). When compared to the biomass with total lipid content, the decreased biomass and increased in lipid content was observed in both stages of iron starvation, however, it escalated in severe Fe stress (Fig. 5.3C).

The Nile Red fluorescence from neutral lipid content was measured *in vitro* over the time-course (12-72h) measurements under iron sufficient and deficient conditions (Fig. 5.2). When an equal number of cells were normalised for comparative measurements and NR fluorescence determines the level of neutral lipid content in *C.reinhardtii* cells. NR dye enabled to bind to neutral lipids in the lipid bodies and to be selectively measured from the cells. Recently James et al., (2014) reported that N deficiency decreases the growth in the medium and stimulates the neutral lipid level in *C.reinhardtii*. The first iron deficient cells exhibited a relative 4-fold increase in neutral lipid content than the iron sufficient cells after 48 h of growth. We have been observed that the severe iron deficiency cells exhibited the NR fluorescence in a 4-fold increase in neutral lipid content. However, the second RC2 cells show a 2-fold increase in the NR fluorescence. Previous reports on N, S, and P limitation were shows that an increased amount of neutral lipid content has been observed in *C.reinahrdtii* cells (Cakmak et al., 2014). Our recent report on Fe limitation, neutral lipid content was

increased in *C.reinhardtii*. We have transferred the 1st stage of iron deficient cells into TAP-Fe medium to see the neutral lipid content. It should be noted that the severe iron-limited cells accumulating the higher content of lipids when to compare to first iron limiting cells within 48 h. So the results from total lipid content were concerting with data from Nile Red staining (Figs. 5.2 & 5.3B). Our results on severe iron starvation condition could be advantageous to produce more neutral lipids in microalgae.

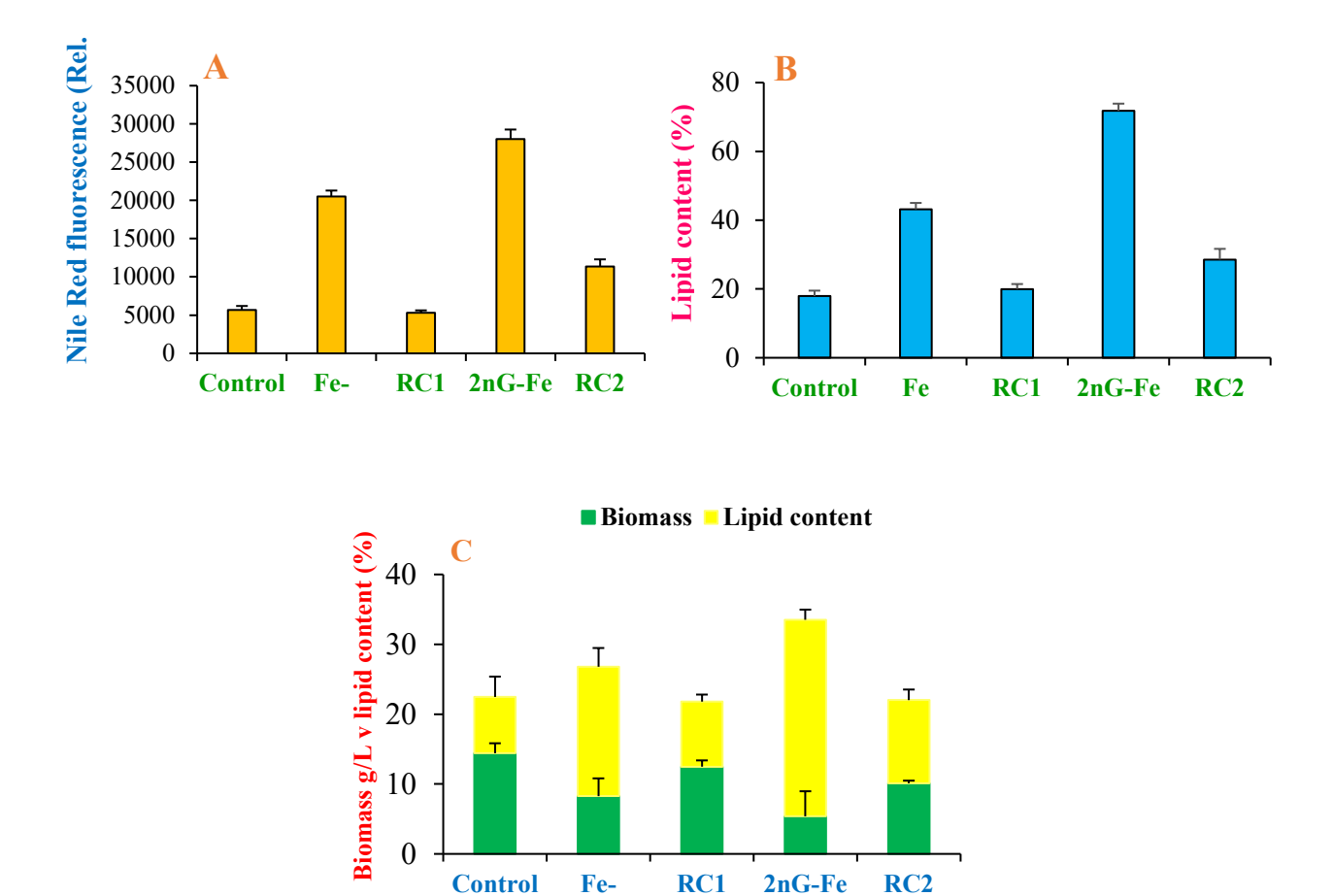


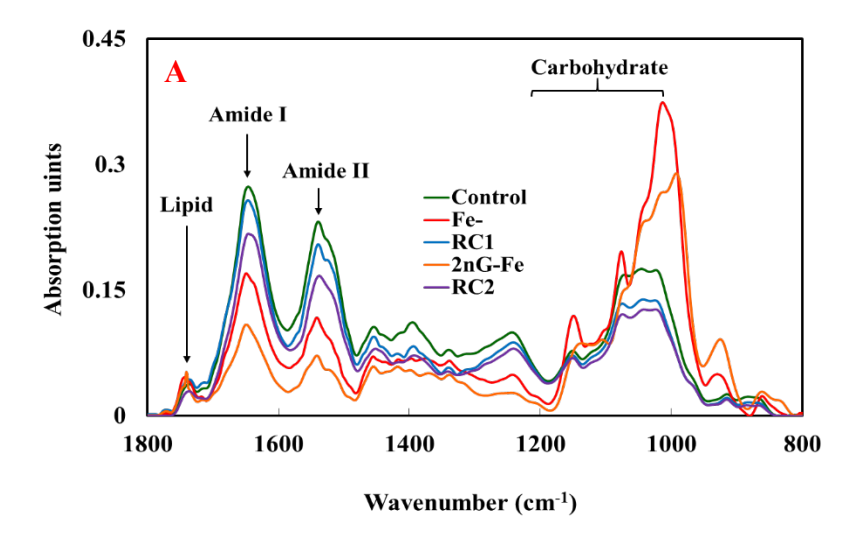
Fig. 5.3. (A) Fluorescence spectroscopy and total lipid content analysis of *C. reinhardtii*. (A) Neutral lipid content was measured by FACS measurements. (B) Total lipid content quantified in control (TAP), iron deficiency, RC1, 2G-Fe and, RC2 cells over four days of growth. (C) Comparison between fluorescence from Nile Red with a total biomass of all the culture conditions.

5.2.4 Lipid and carbohydrate measurements by FTIR

Based on the total lipid content and NR fluorescence results, we have monitored the carbon partition between lipid and carbohydrate by FTIR spectroscopy studies (Fig. 5.4). FTIR spectra were measured in the range from 1800 to 800 cm⁻¹. The protein amide bond I arise at 1642 cm⁻¹ and amide bond II was at 1541 cm⁻¹. Based on vibrational stretches due to peptide bond, carbohydrate and, lipid molecules, we have plotted in their spectral ratios of lipid: amide I and carbohydrate: amide I as described (Dean et al., 2010). Previous reports demonstrated that a decrease in the protein content has been observed with many microalgae grown under N, S and P deprivation (Kilham et al., 1997; Cakmak et al., 2012). Our results also showed the drastic decreasing the protein content under severe iron starvation than the first stage of iron limitation in *C.reinhardtii* (Fig. 5.4). The FTIR study (Fig. 5.4A) shows strong absorption peak for the carbohydrate region (C–O–C) compared with weaker absorptions for the protein amide I and amide II bands with the first stage of iron deficiency as well as severe iron starvation.

However, it should be noted that their correlations with intensity with different FTIR bands have different extinction coefficients in all the conditions. Decreases in protein content by different elemental deprivations (Fig. 5.4A) suggesting that photosynthetic energy is used to synthesize the more lipids and carbohydrates as energy storage which is correlating with our data from neutral lipid and carbohydrate measurements (Figs. 5.3 & 5.4). Carbon storage as a lipid and carbohydrate was measured in all conditions after 48 hours of iron limitation. In the 1st stage of iron deficient condition which is normally storing excess carbon as starch due to more operation of Calvin-Benson cycle towards fixation of carbon as a starch, Therefore, an increased ratio of carbohydrate: amide I was observed (6 fold) whereas the severe iron

limiting cells show gradual decreasing (4 fold) in the carbohydrate: amide ratio after 3 days of growth (Fig. 5.4C). Hence, this decreased carbohydrate content may be due to fixation of carbon into lipids. The lipid content has been increased when first-generation and severe iron deprived cells over 3 days of the growth (Fig. 5.4B).



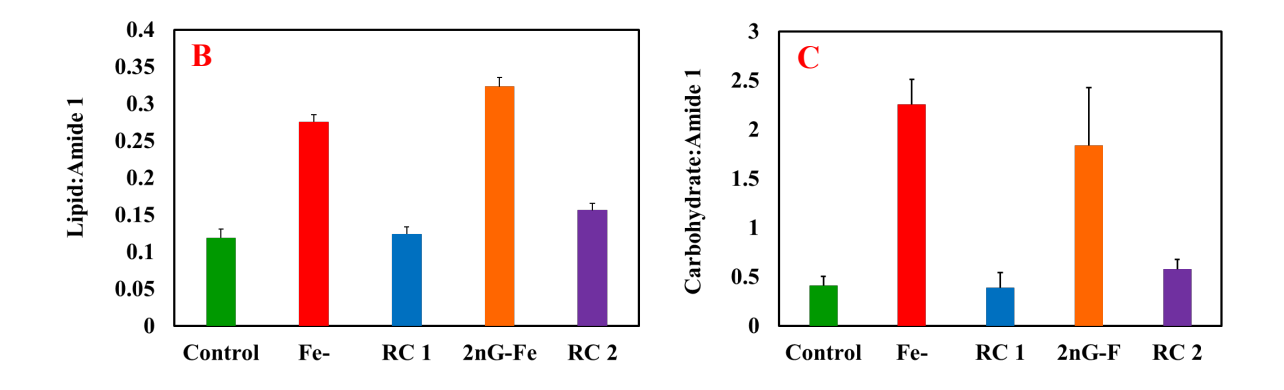


Fig. 5.4 FTIR analysis of carbon storage in *C. reinhardtii* under iron deprivation. (A) Control (green), -Fe (red), RC1 (blue), 2G-Fe (orange), and RC2 (purple) in colour. (B) Lipid: amide I ratio for all conditions over the 4 days. (C) Carbohydrate: amide I ratio for the culture under iron deprived conditions.

The lipid: amide I ratio increased up to 2-fold for first iron deficiency and 4-fold in the severe iron deprived cells (Fig. 5.4b). Previous results are also suggested that the recycling of membrane lipids, MGDG and DGDG into TAG accumulation in *C.reinhardtii* (Urzica et al., 2013). We have tested the polar lipids extracted from above conditions and this data was suggested that polar lipids especially MGDG and DGDG were degraded faster in Fe deficiency, hence our results confirm that these two major lipids were diverted to participate in the formation of TAGs in *C.reinhardtii* (Fig. 5.3). From other reports on N supplementation to growth media has been shown it enhances the cell growth and decreases the lipid content (Huang et al., 2013).

Similarly, iron supplementation (RC1 & RC2) causes increased cell growth and protein content (peptide bond-1600 to 1500 cm⁻¹) (Fig. 5.4). However, the first RC1 cells show the lipid: amide I ration is equal to the control cells whereas the RC2 cells show up to increase in one-fold level. Iron-stress induced TAG accumulation was observed after an alteration chlorophyll content which indicates that iron deficiency affects majorly with the chloroplast membranes without affecting the lipid accumulation. FTIR measurements appear in more authentic and snap short approach to compare the NR fluorescence for detection of biodiesel in microalgae. Ours is the first report to indicate the 2nd stage of iron deficiency condition to enhance the lipid productivity of *C.reinhardtii* under photo-heterotrophic condition.

5.2.5 TAG accumulation studies using TLC

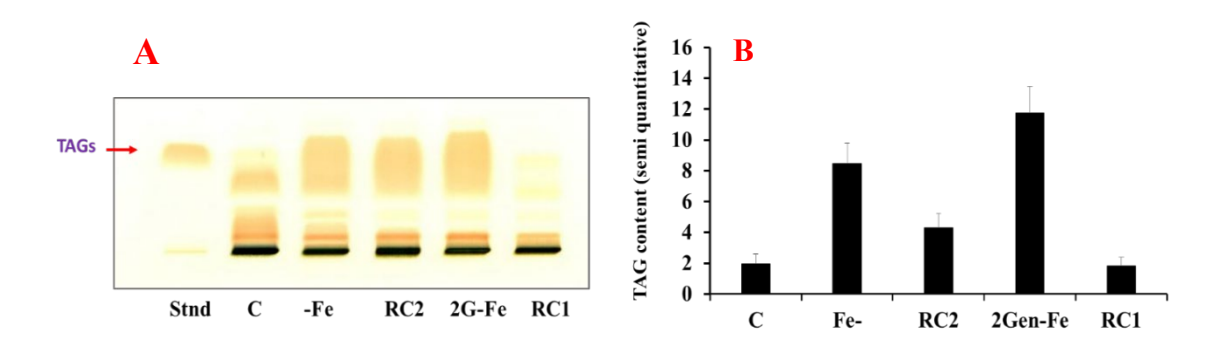


Fig. 5.5 (A) TAG content from thin layer chromatography and semi-quantitative measurement of fatty acid content from (B) TLC bands of *C. reinhardtii* cells grown in TAP and TAP-Fe medium after four days of growth. Data expressed as a percentage of dry cell weight. Means n = 3 replicates.

Further, the effect of severe iron starvation on lipid content and productivity as compared with the first stage of iron deficiency and control conditions. To examine the TAGs accumulation induced by iron deficiency, we have extracted the total lipids from the cells grown under first and severe iron deficiency as well as their recovery conditions after 48 h (Fig. 5.5). In *C.reinhardtii*, TAG accumulation upon nitrogen starvation contains (45%) mainly TAGs after 48 h of cell growth (Nguyen et al., 2011). The TAG analysis on TLC plate stained with brief iodine which revealed that more TAGs accumulation was observed during the iron starvation (Fig. 5.5A). *C.reinhardtii* cells grown under control have one fold of lipid content. Here we have found that severe iron deficiency has the lipid content up to 4 folds than the first stage of iron deficiency condition. Thus treatment with two-stage of iron stress is a promising method to induce the lipid accumulation in microalgae.

5.2.6 Identification of lipids from LC/MS analysis

The fatty acid composition of algal cells cultivated under normal TAP and iron starvation medium. Our recent report shows that saturated fatty acids have increased in the first generation of Fe deficiency, however, it is interesting to understand the second generation of Fe deficiency and their recovery as it accumulated more TAG. Here, the extracted total fatty acids were analysed by transesterification and the resultant fatty acid methyl esters (FAMEs) were analysed by LC/MS method. *C. reinhardtii* cells contain up to 24% mono unsaturated fatty acids per dew from the severe iron starvation than the first stage of iron starvation (Table 5). More saturated FA up to 26% was found in *C. reinhardtii* cells when severely iron deprived condition than the first stage of iron deprived condition (21%). Naturally, TAGs are consist of saturated FA (16:0, 18:0) and accumulation of TAG under iron starvation might be due to an increased saturated FA in *C.reinhardtii*. Similarly, recovery conditions, (RC1 & 2) contains nearly similar level of saturated FA (18% & 16%) respectively than iron sufficient condition (control) (15%). The earlier report shows that the saturated FA was up to 20% under nitrogen deficiency in *C. reinhardtii* cells (James et al., 2011).

Interestingly the saturated FA is more in Fe deficiency than other nutrient deficiency. Thus, the more saturated FA is useful to the production of biofuels. However, the major fatty acids, C16:0, C16:3, C18:0, C18:3 and C18:4 were found in *C. reinhardtii* cells and they have significantly increased upon both stages of iron starvation. Other essential fatty acids identified which include omega-3, α-linolenic acid (18:3), linoleic acid (18:2), and the omega-9 fatty acids, oleic acid (18:1). The mono saturated fatty acids from all the conditions were analysed (Fig. 5.6). Total mono saturated fatty acids composition was major in severe iron starvation than 1st stage of iron deficiency conditions however, other control and their Rc1 and Rc2 have the low

amount in their cells. Cells have the more mono saturation and they are useful for the production of biofuels (James et al., 2011). So severe iron starvation have the more mono saturation in their cells and these cells may use for biofuel production. The reports on changes in fatty acid composition have been studied previously under different environmental changes including temperature, pH, and nitrogen deficiency in Chlamydomonas *sp.* (Poerschmann et al., 2004; James et al., 2011; Çakmak et al., 2014). Further, short-chain fatty acids C14 were detected and they were more in all conditions expect from control (Table 5). These results suggesting that severe iron starved cells more favourable to produce the TAGs than the first stage of iron starvation. So this kind of strategies is may be useful for biofuel production from green algae.

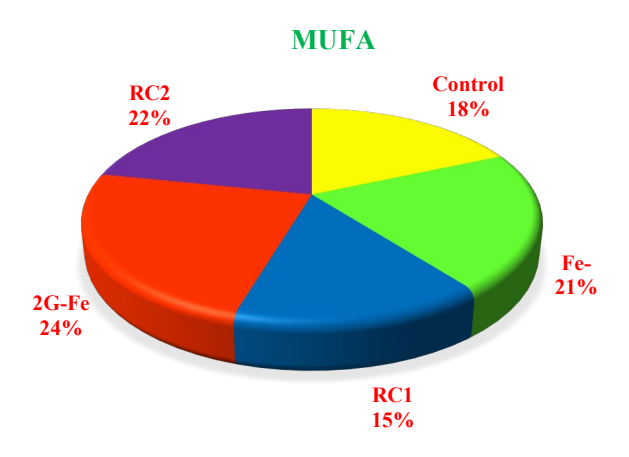


Fig. 5.6 Mono saturated fatty acid composition from C, -Fe, Rc1, 2G-Fe and, Rc2 conditions. The total MSF was more in the 2G-Fe conditions than the other conditions. All the conditions were showed with pi-chart with each percentage.

5.2.7 Iron starvation induces the DGAT2A expression

We have tested the expression of Diacylglycerol acyl-transferase activity with cells collected only from severe iron limiting condition in the time course of 0-72 hours (Fig. 5.7). Algae and plants can synthesize TAGs that can serve as storage lipids.

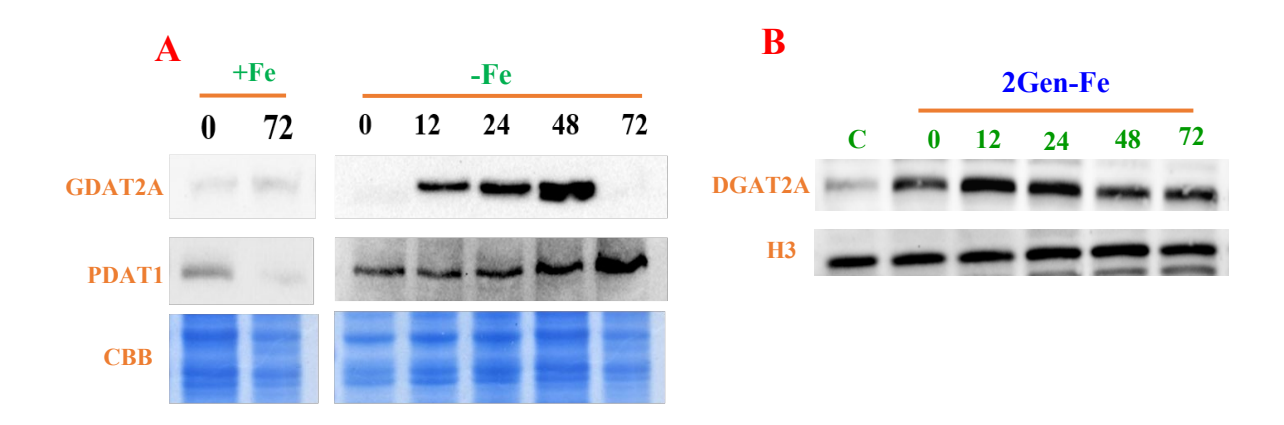


Fig. 5.7 (A) 1st stage of iron deficiency from 0-72 h time course and expression studies of DGAT2A and PDAT1. The expression of Acyl-CoA: Diacylglycerol acyltransferase protein under 2G-Fe starvation in *C.reinhardtii* cells. 5 μg of protein was loaded for each lane and protein was collected from the cells grown from 0-72 h with severe iron starvation. CBB gels showed as a loading control for panel A and Histrone3 (H3) protein was used as a loading control for panel B.

We examined levels of two key enzymes involved in lipid synthesis in *C. reinhardtii*. Phospholipid:diacylglycerol acyltransferase (PDAT1) (Boyle et al., 2012) is an enzyme that catalyses TAG synthesis via two pathways: transacylation of diacylglycerol with acyl groups from phospholipids and galactolipids, and DAG:DAG transacylation (Yoon et al., 2012; Kobayashi et al., 2013). Another enzyme, DGAT2A (Boyle et al., 2012), contributes to the incorporation of hydroxylated fatty acids into TAG (Zhang et al., 2009). There are six genes encoding DGAT in Chlamydomonas and previous

studies have shown that the expression of DGAT2A is increased in nitrogen-starved cells (Boyle et al., 2012). We analysed DGAT2A and PDAT1 protein levels by western blotting using histone H3 as a control. After 72 h of growth in iron-deprived conditions the level of both enzymes was increased, although the expression of DGAT was lower than that of PDAT1. This enzyme is required to contribute to the incorporation of hydroxylated fatty acids into TAG (Zhang et al., 2009). Iron starvation affects the expression of PDAT1 and DGAT2A in a similar manner to nitrogen starvation with the abundance of both enzymes increasing considerably after 48–72 h of iron deficiency condition (Fig. 5.7A). Iron deficiency-induced TAG synthesis pathway is dependent on both acyl-CoA-dependent and -independent acyltransferases (Yoon et al., 2012).

Our data corroborate a previous report that PDAT1 from *C. reinhardtii* mediates lipid turnover by using its hydrolase activity to catabolize galactolipids and phospholipids for TAG synthesis. In cyanobacteria, *Synechococcus* sp. PCC7942, the thylakoids lipids which are PG, MGDG and DGDG were reduced in order to maintain the dynamics of membrane (Ivanov et al., 2007). However, little is known about the TAG accumulation during iron starvation. Free fatty acids from glycerol lipid of MGDG were incorporated into TAG with help of DGAT2A enzyme. Here, we are showing the DGAT2A protein expression from severe iron starvation.

Since severe iron starvation induces the lipid accumulation, we found that the DGAT2A protein expression was also increased. As shown in Fig. 5.7B with increased expression of DGAT2A during the severe iron starvation. However, at the first stage of iron deficient condition, DGAT expression was lower than what we observed in the severe iron starved Chlamydomonas cells.

Table 5: Total fatty acids were identified through direct LC/MS and data expressed in $\mu mol/mg$.

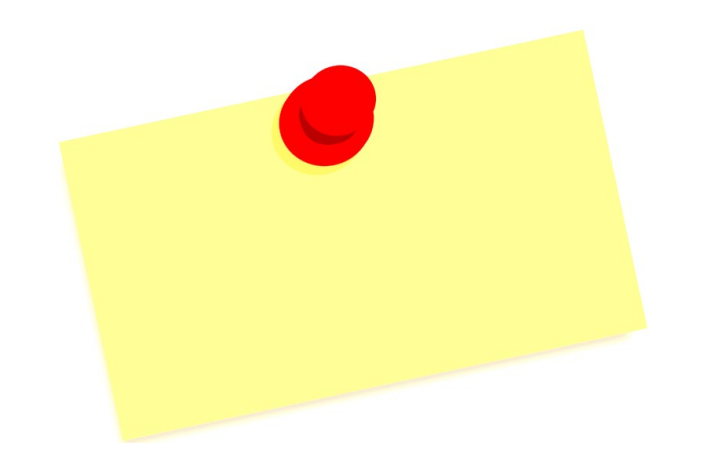
	Control	-Fe	RC1	2G-Fe	RC2
C14:0	0.26 ± 0.11	3.50 ± 0.36	1.84 ± 0.08	2.14 ± 0.91	1.20 ± 0.88
C14:1	0.26 ± 0.06	1.47 ± 0.73	2.60 ± 1.02	1.12 ± 0.22	2.28 ± 0.57
C14:2	0.50 ± 0.27	3.22 ± 0.66	3.32 ± 1.34	4.82 ± 0.99	4.72 ± 1.22
C14:3	1.35 ± 0.31	1.48 ± 0.62	0.83 ± 0.17	1.96 ± 0.53	2.37 ± 0.50
C16:0	0.61 ± 0.06	3.07 ± 1.63	2.32 ± 0.88	3.90 ± 0.47	3.20 ± 0.53
C16:1	1.28 ± 0.26	5.53 ± 1.15	1.06 ± 0.79	7.55 ± 0.81	4.17 ± 0.77
C16:2	1.94 ± 1.37	3.21 ± 0.55	1.98 ± 1.30	3.16 ± 0.62	1.68 ± 0.89
C16:3	1.06 ± 0.24	6.33 ± 0.77	4.47 ± 0.51	6.18 ± 0.95	4.21 ± 0.59
C18:0	0.53 ± 0.21	8.20 ± 0.84	5.43 ± 1.18	8.86 ± 0.85	7.18 ± 0.56
C18:1	2.29 ± 1.17	2.48 ± 0.43	2.85 ± 0.97	0.96 ± 0.41	2.32 ± 0.36
C18:2	1.59 ± 1.00	1.11 ± 0.60	3.81 ± 0.84	1.81 ± 0.83	3.22 ± 1.12
C18:3	1.58 ± 0.24	9.38 ± 1.09	10.83 ± 0.21	13.01 ± 0.21	9.22 ± 0.98
C18:4	1.95 ± 1.01	5.49 ± 1.29	8.33 ± 1.52	9.73 ± 0.79	7.99 ± 0.72
Total	15.23	54.47	49.67	65.19	53.78
ΣSF	1.40	14.78	9.59	14.90	11.58
ΣMSF	3.83	9.48	6.52	9.62	8.78
ΣPUFA	9.99	30.22	33.56	40.67	33.42

5.3 CONCLUSIONS

Iron is an important cofactor for photosynthetic function as most of the complexes are comprises of Fe. If the Fe is removed from the medium, the photosynthesis efficiency reduced, however, still the cells were able to survive. In order to endure cells from Fe, it accumulates significant amount of lipids. Here, the cells were grown in two different generations in Fe deficiency where we observed significant accumulation of lipids about 4 folds higher than the control, specifically in the second generation of Fe deficiency. The electron micrographs show that the large lipid droplets were deposited in severe Fe deficiency.

Further, we detected an enormous amount of triacylglycerol (9.87 mg/g dw) accumulation in severe Fe deficiency which is about 6 folds higher when compared to the control (1.75 mg/g dw). As par, the literature the accumulation of TAG from Fe depleted cells are higher than any other nutritional deficiency. Interestingly, the accumulated TAG would have originated from the degraded lipids from the chloroplast. Further, we also analysed the fatty acid contents from the cells, which indicates that Fe depleted cells have accumulated more saturated fatty acids than unsaturated fatty acids which could be more useful for the biofuel production. From our study, we are sure that the obtained results, where the highest accumulation of TAGs can be used as feedstocks for biofuel production.

Summary and conclusions



SUMMARY

Nutrients, Cu, Fe, S, Mn, Mg, and, Zn are major nutrients for all living photosynthetic organisms and they act as a co-factor in several proteins. The limitation of these nutrients creates a major problem for photosynthetic organisms. Predominantly iron is in insoluble form as Fe(III) ferric oxides. The major content of iron is associated with PSI and it has 12 iron atoms per PSI monomer (Straus, 2004). In higher plants, iron deficiency leads to decreased electron transport chain and thereby decreased abundance of photosynthetic proteins (Andaluz et al., 2006) which ultimately leads to a decrease in the total PSII quantum yield.

In the first objective, was to have focused mainly on photochemistry and organization of PSII-LHCII supercomplexes under iron deficiency. Results from growth analysis suggest that cell growth has decreased by 55% when compared to control cells and the maximum growth was observed after 4 days. The cell size has reduced to 6 μm with iron deficient condition from control cells which are in 10-12 μm in size. The impairment of energy transfer from PSII to PSI was confirmed by the maximum fluorescence peak at 680 nm in iron deficient cells which is due to the accumulation of electrons at QA site of PSII. Interestingly, the recovery cells have the fluorescence maxima equals to control cells. It explains that the iron is required for the proper function of electron transfer reactions around PSII complex. In control cells, the three OJIP phases have attained maximum fluorescence (P=Max) indicating the efficient electron transport which constitutes from PSII, via Cyt b6/f, and PSI. The initial fluorescence, Fo decreased at 72 h with iron starvation. It recovered to the control level during the iron supplementation. The onset of Fe deficiency caused the Fv/Fo and Fv/Fm values were decreased under Fe deficiency. Results from inhibitor, DCMUtreated control cells have maximum fluorescence and the P level due to accumulation

of all the electrons at Q_A sit there by active reaction centers were closed at PSII. However, DCMU-treated Fe-deficient cells show the reduced P phase and it suggests that all PSII reaction centers were closed due to lack of iron and their Fv/Fm and Fv/Fo were low in Fe-deficient cells. Further membrane complexes were separated with BN-PAGE results suggest the PSII–LHCII, and PSI–LHCI supercomplexes were destabilized in Fe-deprived conditions. Apart from supercomplexes, the other PSII reaction center dimer, ATP synthase complex, RUBISCO subunit, and Cyt *b6f* complex were not assembled in iron deficient condition. 2 LHCII trimers were separated in control, one of the trimer (LHC 3a) content was increased and LHC 3b content was decreased in iron deficient condition.

The supercomplexes of recovery cells depicted like control cells (+Fe), suggests that Fe is very important for the stabilization and proper formation of supercomplexes in the chloroplast. Immunoblot data explains that the CP43, CP47, D1, and D2 proteins were decreased. PsbO is the protein of OEC subunit and it was reduced significantly whereas the PsbP subunit is not changed under Fe-deficiency. The Lhcb1 and Lhcb2 are the major LHCII trimer subunits which were reduced whereas CP26 and LhcBm5 minor subunits were not significantly changed. However, CP29 and other minor subunits have significantly reduced (50%) under Fe deficiency. These results suggesting that reduced efficiency of light-harvesting capacity and reduction in the energy transfer to the reaction center. In the second objective, we have studied the severe Fe deficiency, which is the first set of Fe deficiency cells were again inoculated to Fe deficiency medium to understand the role of Fe in *C. reinhardtii*. The second generation of Fe deficiency cells would be completely absent from Fe. We have focused on how the photochemical reactions and thylakoid organization are restored in the recovery cells. Chl *a* fluorescence results suggest that the PSII photosynthetic activity

was decreased due to inactive RCs, the reduction of Q_A, impairment of electron transport between Q_A to Q_B. The regulation of electron transport activity parameters has decreased (SM, N, ETO/RC, ETO/CSm) under both stages of iron deficient conditions. Normalization data from Chl fluorescence, K, and L-bands reveal that the significantly increased energy dissipation constant (K_N, DIO/RC, DIO/CSm) has been observed in severe iron deficient condition. The CD data suggest that changes from macro-domain organization of thylakoid membranes, pigment–pigment interactions, dissociation of LHC complexes with PSII core complex due to the significant difference at peak intensities from iron and severe iron limiting conditions. From the blue native gel, the two LHCII monomeric complexes, PSII dimers and, PSI were decreased with severe iron deficiency whereas these complexes were restored in the recovery conditions. Furthermore, the sucrose density gradient fractions, LHCII, PSII-LHCII, and PSI-LHCI complexes were significantly destabilized in Fe deficiency conditions and supercomplexes have been restored in the recovery conditions.

However, results from total ROS measurements formation of reactive oxygen species were explained that these ROS species creates the damage to core proteins of PSII and PSI complexes under both iron stress conditions. The Ferredoxin and Cyt *b6f* were decreased in both iron deficient conditions whereas these proteins were also recovered from iron supplemented cells. However, the impact of iron limitation shows a decrease in PsaA and PsaC protein content which are essential for the proper function of PSI complex. The core proteins of PSI and II have been misfolded due to aggregation, thus change in photochemical activities was observed. The photochemical yield was significantly decreased in severe iron deficiency conditions because of the aggregation of proteins. The recovery conditions show the restoration of PSII-LHCII complex and PSI-LHCI supercomplexes from iron starvation. Overall, the present study

explains about effective in the line of dynamics of total photosynthetic from severe iron stress and their recovery conditions. Further, disassociation and restoration of thylakoid membranes during the iron starvation in the chloroplast are due to the remodeling of glycolipids like MGDG, DGDG, DGTS, and PG. These chloroplast membrane lipids are important in proper maintenance of the thylakoid membrane and function of photochemical reactions in the chloroplast. In the third objective, we have focused on the role of membrane lipids, recycling of membrane lipids into TAG accumulation during the iron starvation. The growth analysis suggested that it has decreased (40%) in the first stage of iron starvation whereas for severe iron starvation showing the 65% and also the recovery conditions RC1 and RC2 were regained their growth, RC1 was reached up to equals to control level but RC2 showed with slow growth. Cell death assay results were also indicating that cell death was 25% and 13% in severe and 1st stage of iron starvation conditions, respectively. Iron stress conditions may induce cell apoptosis and thereby it leads to cell death in *C.reinhardtii*.

Further, NR fluorescence results for relative lipid quantification from plate reader assay and FACS analysis revealed that severe iron starvation condition accumulates the more lipid than the 1st stage of iron starvation but recovery 2 conditions were also accumulating the lipid with minor level. However, TAG accumulation or synthesis has occurred at ER and the pathway is known as the Kennedy pathway which is regulated by many enzymes. The major regulatory enzymes are DGAT2A and PADT1 which are involved in the TAG biosynthesis. The expression results from these two enzymes were indicates that 1st stage of iron starvation condition induces the DGTA2A and PDAT1 expression.

It suggests that these two enzymes involved in the conversion of DAT to TAGs. When comes to severe iron starvation condition, we have observed that DGAT2A protein expression. The expression studies confirm that during the iron starvation *C.reinhardtii* cells accumulating more TAG than control cells. TLC analysis confirms that TAG accumulation was observed in the 1st stage as well as in severe iron starvation conditions. Enhanced lipid accumulation was observed under severe iron starvation in *C.reinhardtii*. This is our first report on severe iron starvation induces the more lipid content in the Chlamydomonas. However, the individual fatty acids from LC/MS measurements show that saturated fatty acids C16:0, C18:0 were increased in the iron stress conditions. Overall the microalgae induce more lipids and it is suitable for the production of biofuels.

CONCLUSIONS

Finally, we conclude that iron starvation decreases the total photosynthetic activity (Fv/Fm), impairs the energy transfer from Q_A to Q_B region at PSII, decreased the protein content of PSII, PSI and, LHCII complexes. Iron starvation induces the disorganization of thylakoid membranes lipids, MGDG, DGDG, SQDG and, PI and they degraded in to their individual fatty acids which are distributed in throughout the cell.

So these fatty acids involved in the Kennedy pathway and also ER stress due to iron starvation and it synthesise the energy storage molecules like carbohydrates and TAGs. The enzymes, PDAT1 and DGAT2A were expressed to synthesise the TAG molecules and stored in the form of lipid droplets during the iron starvation. Normal cell having the more protein content but less lipid in their cells. Nutrient limiting conditions are the useful strategies for the getting the more lipid content in the algal cells. Our study is shows more TAG content in the iron starved *C.reinhardtii* cells. So, these nutrient limiting conditions from algae may be useful for the production of live feedstock and future fuels.

Bibliography



REFERENCES

- Akhtar, P., Dorogi, M., Pawlak, K., Kovacs, L., Bota, A., Kiss, T., Lambrev, P.H. (2015) Pigment interactions in light-harvesting complex II in different molecular environments. J. Biol. Chem. 290: 4877-4886.
- Alados, I., Foyo-Moreno, I., and Alados-Arboledas, L. (1996) Photosynthetically active radiation; measurements and modelling. Agric. Meteorol. 78: 121–131.
- Amunts, A., Drory, O., and Nelson, N. (2007) The structure of a plant photosystem I supercomplex at 3.4 Å resolution. Nature 447: 58–63.
- Andaluz, S., Lopez-Millan, A.F., De las Rivas, J., Aro, E.M., Abadia, J., Abadia, A. (2006) Proteomic profiles of thylakoid membranes and changes in response to iron deficiency. Photosynth. Res. 89: 141-155.
- Anderson, J.M., and Andersson, B. (1988) The dynamic photosynthetic membrane and regulation of solar energy conversion. Trends. Biochem. Sci. 13: 351-355.
- Antal, T.K., Volgusheva, A.A., Kukarskih, G.P., Bulychev, A.A., Krendeleva, T.E., Rubin, A.B. (2006) Effects of sulfur limitation on photosystem II functioning in *Chlamydomonas reinhardtii* as probed by chlorophyll *a* fluorescence. Physiol. Plantarum. 128: 360-367.
- Awai, K., Maréchal, E., and Block, M.A. (2001) Two types of MGDG synthase genes, found widely in both 16:3 and 18:3 plants, differentially mediate galactolipid syntheses in photosynthetic and nonphotosynthetic tissues in *Arabidopsis thaliana*. Proc. Natl. Acad. Sci. USA 98:10960–10965.
- Baniulis, D., Yamashita, E., Whitelegge, J.P., Zatsman, A.I., Hendrich, M.P., Hasan, S.S., ryan, C.M., and Cramer, W.A. (2009) Strucutre-Function, Stability, and Chemical modification of the Cyanobacterial cytochrome b6f complex from Nostoc sp. PCC 7120. J. Biol. Chem. 284: 9861-9869.
- Barber, J., Nield, J., Morris, E., Zheleva, D., Hankamer, B. (1997) The structure, function and dynamics of photosystem two. Physiol. Plant. 100: 817–827.
- Barber, J. (2003) Photosystem II: the engine of life. Q. Rev. Biophys. 36: 71–89.
- Berg, J.M. Tymoczko, J.L., Stryer, L., Stryer, L., Biochemistry (2007) W.H. Freeman, New York. Springer, Dordrecht. pp. 129-139.

- Ben-Shem, A., Frolow, F., and Nelson, N. (2003) Crystal structure of plant photosystem I. Nature 426: 630–635.
- Bibby, T.S., Nield, J., and Barber, J. (2001) Iron deficiency induces the formation of an antenna ring around trimeric photosystem I in cyanobacteria. Nature 412: 743-745.
- Blaby-Haas, C.E. and Merchant, S.S. (2013) "Sparing and salvaging metals in chloroplasts," in Encyclopedia of In organic and Bioinorganic Chemistry. Metals in. Cells. Eds. pp.1-13.
- Blankenship, R.E. (1992) Origin and early evolution of photosynthesis. Photosynth. Res. 33, 91-111.
- Boekema E. (2001) A giant chlorophyll–protein complex induced by iron deficiency in cyanobacteria. Nature 412: 745-748.
- Boekema, E.J., Hifney, A., Yakushevska, A.E., Piotrowski, M., Keegstra, W., Berry, S., Kruip, J. (2001) A giant chlorophyll-protein complex induced by iron deficiency in cyanobacteria. Nature 412: 745-748.
- Bograh, A., Gingras, Y., Tajmir Riahi, H.A., Carpentier, R. (1997) The effects of spermine and spermidine on the structure of photosystem II proteins in relation to inhibition of electron transport. FEBS lett. 402: 41-44.
- Bolton, J.R. (1977) Photochemical conversion and storage of solar energy. J. Solid. State. Chem. 22: 3-8.
- Boudière, L., Michaud, M., Petroutsos, D., Rébeillé, F., Falconet, D., Bastien, O., Roy, S., Finazzi, G., Rolland, N., Jouhet, J. and Block, M.A. (2014) Glycerolipids in photosynthesis: composition, synthesis and trafficking. Biochim. Biophy. Acta. 1837: 470-480.
- Bradford, M.M. (1976) A rapid and sensitive method for the quantitation of microgram quantities of protein utilizing the principle of protein-dye binding. Anal. Biochem. 72: 248-254.
- Breton, J. (1984) Orientation of Photosynthetic Pigments in vivo: Structural and Functional Aspects. In C. Sybesma (Ed.), Advances in Photosynthesis Research: Proceedings of the VIth International Congress on Photosynthesis,

- Brussels, Belgium, August 1–6, (1983) 3; 11-17., Dordrecht: Springer Netherlands.
- Briat, J.F. and Curie, C. (2007) Iron utilization and metabolism in plants, Curr. Opin. Plant. Biol. 10: 276-282.
- Caffarri, S., Kouril, R., Kereiche, S., Boekema, E.J., and Croce, R. (2009) Functional architecture of higher plant photosystem II supercomplexes. EMBO J. 17: 868-876.
- Caspy, I. and Nelson, N. (2018) Structure of the plant photosystem I. Biochem. Soci. Transact. 46: 285-294.
- Chauhan, D. (2011) A novel photosynthetic strategy for adaptation to low-iron aquatic environments. Biochemistry 50: 686-692.
- Chauhan, D., Folea, I.M., Jolley, C.C., Kouřil, R., Lubner, C.E., Lin, S., Fromme, P. (2011) A Novel Photosynthetic Strategy for Adaptation to Low-Iron Aquatic Environments. Biochemistry 50: 686-692.
- Chen, H.C., Newton, A.J., and Melis, A. (2005) Role of SulP, a nuclear-encoded chloroplast sulfate permease, in sulfate transport and H₂ evolution in *Chlamydomonas reinhardtii*. Photosynth. Res. 84: 289-296.
- Chen, Y. and Barak, P. (1982) Iron Nutrition of Plants in Calcareous Soils. In N. C. Brady (Ed.), Advan. Agron. 35: 217-240.
- Chitnis, P.R., Xu, Q., Chitnis, V.P., Nechushtai, R. (1995) Function and organization of Photosystem I polypeptides. Photosynth. Res. 44: 23-40.
- Clemens, S., Naumann, B., Hippler, M. (2009) Proteomics of metal mediated protein dynamics in plants iron and cadmium in the focus. Front. Biosci. (Landmark Ed), 14: 1955-1969.
- Cramer, W.A. (2019) Structure–function of the cytochrome *b6f* lipoprotein complex: a scientific odyssey and personal perspective. Photosynth. Res. 139: 53-65.
- Curie, C., Panaviene, Z., Loulergue, C., Dellaporta, S.L., Briat, J.F., and Walker, E.L. (2001) Maize yellow stripe1 encodes a membrane protein directly involved in Fe (III) uptake. Nature 409: 346–349.

- Dall'Osto, L., Lico, C., Alric, J., Giuliano, G., Havaux, M., Bassi, R. (2006) Lutein is needed for efficient chlorophyll triplet quenching in the major LHCII antenna complex of higher plants and effective photoprotection in vivo under strong light. BMC Plant. Biol. 6: 32.
- Debus, R. J., Barry, B. A., Sithole, I., Babcoek, G. T., McIntosh, L. (1988) Biochemistry 27: 9071-9074.
- Debus, R.J. (1992) The manganese and calcium ions of photosynthetic oxygen evolution. Biochim. Biophy. Act. Bioenerg. 1102; 269-352.
- Dean, A.P., Sigee, D.C., Estrada, B., and Pittman, J.K. (2010) Using FTIR spectroscopy for rapid determination of lipid accumulation in response to nitrogen limitation in freshwater microalgae. Bioresour. Technol. 101: 4499–4507.
- Dix, DR., Bridgham, J.T., Broderius, M.A., Byersdorfer, C.A., Eide, D.J. (1994) The FET4 geneen codes the low affinity Fe(II) transport protein of *Saccharomyce scerevisiae*. J. Biol. Chem. 269: 26092–26099.
- Dobrikova, A.G., Varkonyi, Z., Krumova, S.B., Kovacs, L., Kostov, G.K., Todinova, S.J., Garab, G. (2003) Structural rearrangements in chloroplast thylakoid membranes revealed by differential scanning calorimetry and circular dichroism spectroscopy. Thermo-optic effect. Biochemistry 42: 11272-11280.
- Domonkos, I., Malec, P., Sallai, A., Kovács, L., Itoh, K., Shen, G., ...and Strzalka, K. (2004) Phosphatidylglycerol is essential for oligomerization of photosystem I reaction center. Plant physiology, 134: 1471-1478.
- Dong, L., Tu, W., Liu, K., Sun, R., Liu, C., Wang, K., and Yang, C. (2015) The PsbS protein plays important roles in photosystem II supercomplex remodeling under elevated light conditions. J. Plant. Physiol. 172: 33-41.
- Dorne, A., Joyard, J., and Douce, R. (1990) Do thylakoids really contain phosphatidylcholine?. Proc. Natl. Acad. Sci. USA 87: 71–74.

- Drop, B., Webber-Birungi, M., Yadav, S.K., Filipowicz-Szymanska, A., Fusetti, F., Boekema, E. J., and Croce, R. (2014) Light-harvesting complex II (LHCII) and its supramolecular organization in *Chlamydomonas reinhardtii*. Biochim. Biophys. Acta. 1837: 63-72.
- Droppa, M., Horváth, G., Hideg, É., Farkas, T. (1995) The role of phospholipids in regulating photosynthetic electron transport activities: treatment of thylakoids with phospholipase C. Photosynth. Res. 46: 287–293.
- Dubertret, G., Mirshahi, A., Mirshahi, M., Gerard-Hirne, C., Trémolieres, A. (1994) Evidence from in vivo manipulations of lipid composition in mutants that the Δ3-trans-hexadecenoic acid-containing phosphatidylglycerol is involved in the biogenesis of the light-harvesting chlorophyll *a/b*-protein complex of *Chlamydomonas reinhardtii*. Europ. J. Biochem. 226: 473-482.
- El Maanni, A., Dubertret, G., Delrieu, M.J. (1998) Mutants of *Chlamydomonas* reinhardtii affected in phosphatidylglycerol metabolism and thylakoid biogenesis. Plant. Physiol. Biochem. 36: 609–619.
- Esperanza, M., Cid, Á., Herrero, C., Rioboo, C. (2015a) Acute effects of a prooxidant herbicide on the microalga *Chlamydomonas reinhardtii*: Screening cytotoxicity and genotoxicity endpoints. Aquat. Toxicol. 165: 210-221.
- Esperanza, M., Seoane, M., Rioboo, C., Herrero, C., Cid, A. (2015b) *Chlamydomonas reinhardtii* cells adjust the metabolism to maintain viability in response to atrazine stress. Aquat. Toxicol. 165: 64-72.
- Falkowski, P.G., and Raven, J. (1997) Aquatic Photosynthesis. Freshw. Biol. 69: 375.
- Ferreira, K.N., Iverson, T.M., Maghlaoui, K., Barber, J., and Iwata, S. (2004)

 Architecture of the photosynthetic oxygen-evolving centre. Science 303: 1831–
 1839.
- Ferroni, L., Baldisserotto, C., Giovanardi, M., Pantaleoni, L., Morosinotto, T., Pancaldi, S. (2011) Revised assignment of room-temperature chlorophyll fluorescence emission bands in single living cells of *Chlamydomonas reinhardtii*. J. Bioener. Biomem. 43: 163-173.

- Fischer, N, Sétif, P., and Rochaix, J.D. (1997) Targeted mutations in the psaC gene of *Chlamydomonas reinhardtii*: preferential reduction of FB at low temperature is not accompanied by altered electron flow from photosystem I to ferredoxin. Biochemistry 36: 93-102.
- Froehlich, J,E., Benning, C., and Dörmann, P. (2001) The digalactosyldiacylglycerol (DGDG) synthase DGD1 is inserted into the outer envelope membrane of chloroplasts in a manner independent of the general import pathway and does not depend on direct interaction with monogalactosyldiacylglycerol synthase for DGDG biosynthesis. J. Biol. Chem. 276: 31806–31812.
- Fromme, P., Jordan, P., and Krauss, N. (2001) Structure of photosystem I. Biochim. Biophys. Acta. 1507: 5–31.
- Fujii, S., Kobayashi, K., Nakamura, Y., Wada, H. (2014) Inducible knockdown of monogalactosyldiacylglycerol synthase1 reveals roles of galactolipids in organelle differentiation in Arabidopsis cotyledons. Plant. Physiol. 166: 1436– 1449.
- Garab, G., Ughy, B., De Waard, P., Akhtar, P., Javornik, U., Kotakis, C., ... and Plavec, J. (2017) Lipid polymorphism in chloroplast thylakoid membranes—as revealed by 31 P-NMR and time-resolved merocyanine fluorescence spectroscopy. Scient. Report, 7: 1-11.
- Garab, G. and Van Amerongen, H. (2009) Linear dichroism and circular dichroism in photosynthesis research. Photosynth. Res. 101: 135-146.
- Garab, G., Kieleczawa, J., Sutherland, J.C., Bustamante, C., Hind, G. (1991) organization of pigment-protein complexes into macrodomains in the thylakoid membranes of wild type and chlorophyll *f* less mutant of barley as revealed by circular dichroism. Photochem. Photobio. 54: 273-281.
- Garab, G., Wells, S., Finzi, L., and Bustamante, C. (1988) Helically organized macroaggregates of pigment-protein complexes in chloroplasts: evidence from circular intensity differential scattering. Biochemistry 27: 5839-5843.
- Giehl, R.F.H., Lima, J.E., and von Wirén, N. (2012) Localized iron supply triggers lateral root elongation in Arabidopsis by altering the AUX1 mediated Auxin distribution. Plant. Cell. 24: 33–49.

- Glaesener, A.G., Merchant, S.S., and Blaby-Haas, C.E. (2013) Iron economy in *Chlamydomonas reinhardtii*. Front. Plant. Sci, 4: 337.
- Goussi, R., Manaa, A., Derbali, W., Ghnaya, T., Abdelly, C., Barbato, R. (2018) Combined effects of NaCl and Cd²⁺ stress on the photosynthetic apparatus of *Thellungiella salsuginea*. Biochim. Biophy. Acta. 1859: 1274-1287.
- Govindjee, Shevela, D. and Björn, L.O. (2017) Evolution of the Z-scheme of photosynthesis: a perspective. Photosynth. Res. 133: 5–15.
- Green, B.R. and Parson, W.W. (2003) Light-harvesting antennas in photosynthesis. Adv. Photosynth. Resp. pp. 513.
- Griffiths, H. (2006) Plant biology: designs on rubisco. Nature 441: 940–941.
- Griffiths, M.J., and Harrison, S.T.L. (2009) Lipid productivity as a key characteristic for choosing algal species for biodiesel production. J. Appl. Phycol. 21: 493–507.
- Guerinot, M.L. and Yi, Y. (1994) Iron: nutritious, noxious, and not readily available. Plant Physiol. 104: 815–820.
- Harris, E.H. (2001) Chlamydomonas as a model organism. Annu. Rev. Plant Physiol. Plant. Mol. Biol. 52: 363–406.
- Hasan, S.S., and Cramer, W.A. (2014) Internal lipid architecture of the heterooligomeric cytochrome *b6f* complex. Structure 22: 1008–1015.
- Herbik, A., Bölling, C., and Buckhout, T. J. (2002) The involvement of a multi copper oxidase in iron uptake by the green algae *Chlamydomonas reinhardtii*. Plant. Physiol. 130: 2039-2048.
- Hill, R. (1937) Oxygen evolved by isolated chloroplasts. Nature 139: 881–882.
- Hoham, R.W., Bonome, T.A., Martin, C.W., Leebens-Mack, J.H. (2002) A combined 18s rdna and rbcL phylogenetic analysis of Chloromonas and Chlamydomonas (chlorophyceae, volvocales) emphasizing snow and other cold-temperature habitats. J. Phycol. 38: 1051-1064.
- Höhner, R., Barth, J., Magneschi, L., Jaeger, D., Niehues, A., Bald, T., Grossman, A., Fufezan, C. and Hippler, M. (2013) The metabolic status drives acclimation of iron deficiency responses in *Chlamydomonas reinhardtii* as revealed by

- proteomics based hierarchical clustering and reverse genetics. Mol. Cell. Proteom. 12: 2774-2790.
- Hölzl, G., Witt, S., and Gaude, N. (2009) The role of diglycosyl lipids in photosynthesis and membrane lipid homeostasis in Arabidopsis. Plant. Physiol. 150: 1147–1159.
- Imramovsky, A., Pesko, M., Ferriz, J.M., Kralova, K., Vinsova, J., and Jampilek, J. (2011) Photosynthesis Inhibiting efficiency of 4-chloro-2-(chlorophenylcarbamoyl)phenyl alkylcarbamates. Bioorganic. Med. Chem. Lett. 21: 4564–4567.
- Jahns, P., Latowski, D., and Strzalka, K. (2009) Mechanism and regulation of the violaxanthin cycle: the role of antenna proteins and membrane lipids. Biochim. Biophys. Acta. 1787: 3–14.
- James, G.O., Hocart, C.H., Hillier, W., Chen, H., Kordbacheh, F., Price, G.D., Djordjevic, M.A. (2011) Fatty acid profiling of *Chlamydomonas reinhardtii* under nitrogen deprivation. Bioresour. Technol. 102: 3343-3351.
- Jansson, S. (1999) A guid to the Lhc genes and their relatives in Arabidopsis. Trends. Plant. Sci. 4: 236-240.
- Jo, W. J., Kim, J. H., Oh, E., Jaramillo, D., Holman, P., Loguinov, A.V. (2009) Novel insights into iron metabolism by integrating deletome and transcriptome analysis in an iron deficiency model of the yeast *Saccharomycescerevisiae*. BMC Genomics. 10: 130.
- Jolley, C., Ben-Shem, A., Neslon, N., and Fromme, P. (2005) Structure of plant photosystem I revealed by theretical modeling. J. Biol. Chem. 280: 33627-33636.
- Jordan, P., Fromme, P., Witt, H.T., Klukas, O., Saenger, W., Krauss, N. (2001) Threedimensional structure of cyanobacterial photosystem I at 2.5 Å resolution. Nature 411: 909-917.
- Junge, W., and Nelson, N. (2015) ATP synthase. Annu. Rev. Biochem. 84: 631–657.

- Kansy, M., Wilhelm, C., and Goss, R. (2014) Influence of thylakoid membrane lipids on the structure and function of the plant photosystem II core complex. Planta. 240: 781–796.
- Kelly, A.A., Froehlich, J.E., and Dörmann, P. (2003) Disruption of the two digalactosyldiacylglycerol synthase genes DGD1 and DGD2 in Arabidopsis reveals the existence of an additional enzyme of galactolipid synthesis. The Plant Cell, 15: 2694-2706.
- Kobayashi, K., Kondo M, and Fukuda, H. (2007) Galactolipid synthesis in chloroplast inner envelope is essential for proper thylakoid biogenesis, photosynthesis, and embryogenesis. Proc. Natl. Acad. Sci. USA 104: 17216–17221.
- Kobayashi, K., Narise, T., and Sonoike, K. (2013) Role of galactolipid biosynthesis in coordinated development of photosynthetic complexes and thylakoid membranes during chloroplast biogenesis in Arabidopsis. J. Plant. 73: 250–261.
- Kobayashi, K., Endo, K., and Wada, H. (2016) Multiple impacts of loss of plastidic phosphatidylglycerol biosynthesis on photosynthesis during seedling growth of *Arabidopsis*. Front. Plant. Sci. 7: 336.
- Kodru, S., Malavath, T., Devadasu, E., Nellaepalli, S., Stirbet, A., Subramanyam, R., Govindjee. (2015) The slow S to M rise of chlorophyll *a* fluorescence reflects transition from state 2 to state 1 in the green alga *Chlamydomonas reinhardtii*. Photosynth. Res. 125: 219-231.
- Kolli, B.K., Tiwari, S., and Mohanty, P.K. (1998) Ultraviolet-B Induced Damage to Photosystem II in Intact Filaments of Spirulina platensis. Zeitschrift. Für. Naturforschung. C. 53: 369 - 377.
- Kroll, H., Knell, M., Powers, J., Simonian, J. (1957) Aphenolic analog of ethylenediamine- tetraaceticacid. J. Am. Chem. Soc. 79: 2024–2025.
- Kubota-Kawai, H., Mutoh, R., Shinmura, K., Sétif, P., Nowaczyk, M.M., Rögner, M., Ikegami, T., Tanaka, H. and Kurisu, G. (2018) X-ray structure of an asymmetrical trimeric ferredoxin–photosystem I complex. Nat. Plants. 4: 218-224.

- La Fontaine, S., Quinn, J.M., Nakamoto, S.S., Page, M. D., Göhre, V., Moseley, J.L. (2002) Copper-dependent iron assimilation pathway in the model photosynthetic eukaryote *Chlamydomonas reinhardtii*. Eukaryot. Cell. 1: 736–757.
- Lanquar, V., Lelièvre, F., Bolte, S., Hamès, C., Alcon, C., Neumann, D. (2005) Mobilization of vacuolariron by AtNRAMP3 and AtNRAMP4 is essential for seed germination on low iron. EMBO J. 24: 4041–4051.
- Li, M., Calteau, A., Semchonok, D.A., Witt, T.A., Nguyen, J.T., Sassoon, N., Boekema, E.J., Whitelegge, J., Gugger, M., Bruce, B.D. (2019) Physiological and evolutionary implications of tetrameric photosystem I in cyanobacteria. Nat. Plants. 5: 1309-19.
- Lürling, M., and Beekman, W. (2006) Growth of Daphnia magna males and females fed with the cyanobacterium *Microcystis aeruginosa* and the green alga *Scenedesmus obliquus* in different proportions. Hydrochim. Hydrobiol. 34: 375-382.
- Loll, B., Kern, J., Saenger, W., Zouni, A., Biesiadka, J. (2005) Towards complete cofactor arrangement in the 3.0 Å resolution structure of photosystem II. Nature 438, 1040-1044.
- Madireddi, S.K., Nama, S., Devadasu, E.R., Subramanyam, R. (2014) Photosynthetic membrane organization and role of state transition in *cyt*, *cpII*, *stt7* and npq mutants of *Chlamydomonas reinhardtii*. J. Photochem. Photobiol. B 137:77-83.
- Malone, L.A., Qian, P., Mayneord, G.E. (2019) Cryo-EM structure of the spinach cytochrome b6 f complex at 3.6 Å resolution. Nature 575: 535–539.
- Mazor, Y., Borovikova, A., Caspy, I., and Nelson, N. (2017) Structure of the plant photosystem I supercomplex at 2.6 Å resolution. Nat. Plants. 3: 17014.
- Melis, A. (2009) Solar energy conversion efficiencies in photosynthesis: minimizing the chlorophyll antennae to maximize efficiency. Plant Sci. 177: 272–280.
- Merchant, S. S., Prochnik, S. E., Vallon, O., Harris, E. H., et al., (2007) The Chlamydomonas genome reveals the evolution of key animal and plant functions. Science 318: 245-250.

- Michel, K.P. and Pistorius, E.K. (2004) Adaptation of the photosynthetic electron transport chain in cyanobacteria to iron deficiency: The function of IdiA and IsiA. Physiol. Plant, 120: 36-50.
- Michel, K. P., Thole, H. H., and Pistorius, E.K. (1996) IdiA, a 34 kDa protein in the cyanobacteria *Synechococcus sp.* strains PCC 6301 and PCC 7942, is required for growth under iron and manganese limitations. Microbiology 142: 2635-2645.
- Minagawa, J., and Takahashi, T. (2004) Structure, Function and Assembly of Photosystem II and Its Light-Harvesting Proteins. Photosynth. Res. 82: 241-63.
- Moore, A. (2008) Biofuels are dead: long live biofuels part two. N. Biotechnol. 25: 96-100.
- Moore, J.K., Doney, S.C., Glover, D.M., Fung, I.Y. (2002) Iron cycling and nutrient-limitation patterns in surface waters of the World Ocean. Deep Sea Research Part II: Topic. Stud. Oceanog. 49: 463-507.
- Moore, T.S., Du, Z., and Chen, Z. (2001) Membrane lipid biosynthesis in *Chlamydomonas reinhardtii*. In vitro biosynthesis of diacylglyceryltrimethylhomoserine. Plant Physiol. 125: 423–429.
- Moellering, E.R., Miller, R., and Benning, C. (2009) Molecular genetics of lipid metabolism in the model green alga *Chlamydomonas reinhardtii*. In: Wada H, Murata N eds. Lipids in Photosynthesis. Springer, Dordrecht. pp. 139-155.
- Moseley, J.L., Allinger, T., Herzog, S., Hoerth, P., Wehinger, E., Merchant, S., Hippler, M. (2002) Adaptation to Fe-deficiency requires remodeling of the photosynthetic apparatus. EMBO J. 21: 6709-6720.
- Msilini, N., Essemine, J., Zaghdoudi, M., Harnois, J., Lachaal, M., Ouerghi, Z., Carpentier, R. (2013a) How does iron deficiency disrupt the electron flow in photosystem I of lettuce leaves?. J. Plant. Physiol. 170: 1400-1406.
- Msilini, N., Oueslati, S., Amdouni, T., Chebbi, M., Ksouri, R., Lachaâl, M., Ouerghi, Z. (2013b) Variability of phenolic content and antioxidant activity of two lettuce varieties under Fe deficiency. J. Sci. Food. Agri. 93: 2016-2021.

- Msilini, N., Zaghdoudi, M., Govindachary, S., Lachaa,l M., Ouerghi, Z., Carpentier, R. (2011) Inhibition of photosynthetic oxygen evolution and electron transfer from the quinone acceptor Q_A to Q_B by iron deficiency. Photosynth. Res. 107: 247-256.
- Murdock, J.N. and Wetzel, D.L. (2009) FTIR microspectroscopy enhances biological and ecological analysis of algae. Appl. Spectrosc. Rev. 44: 335–361.
- Nagy, G., Unnep, R., Zsiros, O., Tokutsu, R., Takizawa, K., Porcar, L., Minagawa, J. (2014) Chloroplast remodeling during state transitions in *Chlamydomonas reinhardtii* as revealed by noninvasive techniques in vivo. Proc. Natl. Acad. Sci. USA 111: 5042-5047.
- Naumann, B., Busch, A., Allmer, J., Ostendorf, E., Zeller, M., Kirchhoff, H., Hippler,
 M. (2007) Comparative quantitative proteomics to investigate the remodeling of bioenergetic pathways under iron deficiency in *Chlamydomonas reinhardtii*.
 Proteomics, 7: 3964-3979.
- Naumann, B., Stauber, E.J., Busch, A., Sommer, F., Hippler, M. (2005) N-terminal processing of Lhca3 Is a key step in remodeling of the photosystem I-light-harvesting complex under iron deficiency in *Chlamydomonas reinhardtii*. J. Biol. Chem. 280: 20431-20441.
- Neelam, S., and Subramanyam, R. (2013) Alteration of photochemistry and protein degradation of photosystem II from *Chlamydomonas reinhardtii* under high salt grown cells. J. Photochem. Photobiol. B 124: 63-70.
- Nelson, N., and Yocum, C.F. (2006) Structure and function of Photosystems I and II. Annu. Rev. Plant. Biol. 57: 521–565.
- Nelson, N., and Junge, W. (2015) Structure and energy transfer in photosystems of oxygenic photosynthesis. Annual. Rev. Biochem, 84: 659-683.
- Nishiyama, Y., and Murata, N. (2014) Revised scheme for the mechanism of photoinhibition and its application to enhance the abiotic stress tolerance of the photosynthetic machinery. Appl. Microbiol. Biotechnol. 9: 8777-8796.
- Oh-oka, H., Takahashi, Y., Kuriyama, K., Saeki, K., & Matsubara, H. (1988) The protein responsible for center A/B in spinach photosystem I: isolation with iron-sulfur cluster(s) and complete sequence analysis. J. Biochem. 103: 962-968.

- Ossenbühl, F., Göhre, V., Meurer, J., Krieger-Liszkay, A., Rochaix, J.D., Eichacker, L.A. (2004) Efficient Assembly of Photosystem II in *Chlamydomonas* reinhardtii Requires Alb3.1p, a Homolog of Arabidopsis ALBINO3. Plant Cell 16: 1790-1800.
- Ozawa, S.I., and Bald, T. (2018) Configuration of Ten Light-Harvesting Chlorophyll *a/b* Complex I Subunits in *Chlamydomonas reinhardtii* Photosystem I. Plant Physiol. 178: 583-595.
- Papageorgiou, G.C., Tsimilli-Michael, M., and Stamatakis, K. (2007) The fast and slow kinetics of chlorophyll *a* fluorescence induction in plants, algae and cyanobacteria: a viewpoint. Photosynth. Res. 94: 275-290.
- Parson, W.W., and Nagarajan, V. (2003) Optical Spectroscopy in Photosynthetic Antennas. In B. R. Green & W. W. Parson (Eds.), Light-Harvesting Antennas in Photosynthesis (pp. 83-127). Dordrecht: Springer Netherlands.
- Peers, G., Truong, T.B., Ostendorf, E., Busch, A., Elrad, D., Grossman, A.R., Hippler, M., Niyogi, K.K. (2009) An ancient light-harvesting protein is critical for the regulation of algal photosynthesis. Nature 462: 518-521.
- Pineau, B., Girard-bascou, J., and Eberhard, S. (2004) A single mutation that causes phosphatidylglycerol deficiency impairs synthesis of photosystem II cores in *Chlamydomonas reinhardtii*. Eur. J. Biochem. 271: 329–338.
- Pistorius, A.M.A., DeGrip, W.J., and Egorova-Zachernyuk, T.A. (2009) Monitoring of biomass composition from microbiological sources by means of FTIR spectroscopy. Biotechnol. Bioeng. 103: 123–129.
- Porra, R.J., Thompson, W.A., and Kriedemann, P.E. (1989) Determination of accurate extinction coefficients and simultaneous equations for assaying chlorophylls *a* and *b* extracted with four different solvents: verification of the concentration of chlorophyll standards by atomic absorption spectroscopy. Biochim. Biophys. Acta. 975: 384–394.
- Price, C.A., (1968) Iron Compounds and Plant Nutrition. Ann. Rev. Plant Physiol. 19: 239-248.

- Qin, X., Pi, X., and Wang, W. (2019) Structure of a green algal photosystem I in complex with a large number of light-harvesting complex I subunits. Nat. Plants 5: 263–272.
- Rees, D., Noctor, G., and Ruban, A.V. (1992) pH dependent chlorophyll fluorescence quenching in spinach thylakoids from light treated or dark adapted leaves. Photosynth. Res. 31: 11–19.
- Riekhof, W.R., Sears, B.B., and Benning, C. (2005) Annotation of genes involved in glycerolipid biosynthesis in *Chlamydomonas reinhardtii*: discovery of the betaine lipid synthase BTA1Cr. Eukaryotic cell 4: 242-252.
- Rochaix, J.D. (2002) Chlamydomonas, a model system for studying the assembly and dynamics of photosynthetic complexes. FEBS lett. 529: 34-38.
- Rubinelli, P., Siripornadulsil, S., Gao Rubinelli, F., Sayre, R.T. (2002) Cadmium and iron stress-inducible gene expression in the green alga *Chlamydomonas reinhardtii*: evidence for H43 protein function in iron assimilation. Planta 215: 1–13.
- Rutherford, A.W. and Faller, P. (2003) Photosystem II: evolutionary perspectives. Philos. Trans. R. Soc. B. Biol. Sci. 358: 245–253.
- Sakurai, I., Mizusawa, N., and Ohashi, S. (2007) Effects of the lack of phosphatidylglycerol on the donor side of photosystem II. Plant. Physiol, 144: 1336–1346.
- Schägger, H., and von Jagow, G. (1991) Blue native electrophoresis for isolation of membrane protein complexes in enzymatically active form. Anal. Bioch, 199: 223-231.
- Schaller, S., Latowski, D., Jemioła-Rzemin'ska, M. (2011) Regulation of LHCII aggregation by different thylakoid membrane lipids. Biochim. Biophys. Acta. 1807: 326–335.
- Schansker, G., Tóth, S.Z., and Strasser, R.J. (2005) Methylviologen and dibromothymoquinone treatments of pea leaves reveal the role of photosystem I in the Chl *a* fluorescence rise OJIP. Bioch. Bioph. Acta. Bioeng. 1706: 250-261.

- Schansker, G., and Strasser, R.J. (2005) Quantification of non-Q_B reducing centers in leaves using a far red pre-illumination. Photosynth. Res. 84: 145-151.
- Schmid, V.H.R. (2008) Light harvesting complexes of vascular plants. Cell. Mol. Life Sci. 65: 3619-3639.
- Senge, M.O., Ryan, A.A., Letchford, K.A., Mac Gowan, S.A., Mielke, T. (2014) Chlorophylls, symmetry, chirality, and photosynthesis. Symmetry. 6: 781–843.
- Setif, P., Fischer, N., Lagoutte, B., Bottin, H., Rochaix, J.D. (2002) The ferredoxin docking site of photosystem I. Biochim. Biophy. Acta. 1555: 204-209.
- Sheng, X., Watanabe, A., Li, A., Kim, E., Song, C., Murata, K., Liu, Z. (2019) Structural insight into light harvesting for photosystem II in green algae. Nat. Plants. 5: 1320-1330.
- Shevela, D., and Björn, L. O. (2018) Photosynthesis: solar energy for life. Singapore: World Scientific, pp. 188.
- Smith, J.L., Zhang, H., Yan, J., Kurisu, G., and Cramer, W.A. (2004) Cytochrome *bc* complexes: a common core of structure and function sourrounded by diversity in the outlying provinces. Curr. Opin. Struct. Biol. 14: 432-439.
- Soares, M.C.S., Marinho, M.M., Huszar, V.L.M., Branco, C.W.C., and Azevedo, S.M.F.O. (2008) The effects of water retention time and watershed features on the limnology of two tropical reservoirs in Brazil. Lakes Reserv. Res. Manag. 13: 257–269.
- Spiller, S., and Terry, N. (1980) Limiting Factors in Photosynthesis: II. iron stress diminishes photochemical capacity by reducing the number of photosynthetic units. Plant. Physiol. 65: 121-125.
- Srivastava, A., Guissé, B., Greppin, H., Strasser, R.J. (1997) Regulation of antenna structure and electron transport in Photosystem II of Pisum sativum under elevated temperature probed by the fast polyphasic chlorophyll a fluorescence transient: OKJIP. Bioch. Biophy. Acta. Bioenerg. 1320: 95-106.
- Starckx., V and Senne. (2012) A place in the sun algae is the crop of the future. Geel Flanders Today 7: 703–705.

- Stauber, E.J., Fink, A., Markert, C., Kruse, O., Johanningmeier, U., Hippler, M. (2003) Proteomics of *Chlamydomonas reinhardtii* light-harvesting proteins. Eukaryot. Cell. 2: 978-994.
- Stehfest, K., Toepel, J., and Wilhelm, C. (2005) The application of micro-FTIR spectroscopy to analyze nutrient stress-related changes in biomass composition of phytoplankton algae. Plant Physiol. Biochem. 43: 717–726.
- Stookey, L.L. (1970) Ferrozine a new spectrophotometric reagent for iron. Anal.Chem, 42: 779–781.
- Strasser, B.J. (1997) Donor side capacity of Photosystem II probed by chlorophyll *a* fluorescence transients. Photosynth. Res. 52: 147-155.
- Strasser, R.J., and D. Stirbet, A. (1998) Heterogeneity of photosystem II probed by the numerically simulated chlorophyll *a* fluorescence rise (O–J–I–P). Math. Comput. Simul. 48: 3-9.
- Strasser, R., and Nedbal, L. (2004) Chlorophyll fluorescence. Photosynthetica. 37: 214-228.
- Strasser, R., Srivastava, A., and Tsimilli-Michael, M. (2000) The fluorescence transient as a tool to characterize and screen photosynthetic samples. Prob. Photosynth: Mechanism, regulation and adaptation. 48: 3-9.
- Straus, N. (2004) Iron Deprivation: Physiology and Gene Regulation. In: Bryant D (ed)
 The Molecular Biology of Cyanobacteria, vol 1. Advan. Photo. Resp. Springer
 Netherlands, 731-750.
- Steffen, R., Kelly, A.A., and Huyer, J. (2005) Investigations on the reaction pattern of photosystem II in leaves from *Arabidopsis thaliana* wild type plants and mutants with genetically modified lipid content. Biochemistry, 44: 3134–3142.
- Stroebel, D., Choquet, Y., Popot, J.L., Picot, D. (2003) An atypical heam in the cyto hrome *b*(*6*)*f* complex. Nature 426: 413-421.
- Styring, S., Sjöholm, J., and Mamedov, F. (2012) Two tyrosines that changed the world: Interfacing the oxidizing power of photochemistry to water splitting in photosystem II. Biochim. Biophys. Acta. Bioenerg. 1817: 76-87.

- Strzepek, R.F., and Harrison, P.J. (2004) Photosynthetic architecture differs in coastal and oceanic diatoms. Nature 431: 689-692.
- Su, X., Ma, J., Pan, X., Zhao, X., Chang, W., Liu, Z., et al., (2019) Antenna arrangement and energy transfer pathways of a green algal photosystem-I–LHCI supercomplex. Nat. plants, 5: 273.
- Subramanyam, R., Jolley, C., Brune, D.C., Fromme, P., Webber, A.N. (2006) Characterization of a novel Photosystem I–LHCI supercomplex isolated from *Chlamydomonas reinhardtii* under anaerobic (State II) conditions. FEBS Lett. 580: 233-238.
- Subramanyam, R., Jolley, C., Thangaraj, B., Nellaepalli, S., Webber, A., Fromme, P. (2010) Structural and functional changes of PSI-LHCI supercomplexes of *Chlamydomonas reinhardtii* cells grown under high salt conditions. Planta 231: 913-922.
- Suga, M., Ozawa, S.-I., Yoshida-Motomura, K., Akita, F., Miyazaki, N., Takahashi, Y. (2019) Structure of the green algal photosystem I supercomplex with a decameric light-harvesting complex I. Nat. Plants 5: 626-636.
- Takahashi, Y., Yasui, T., Stauber, E.J., Hippler, M. (2004) Comparison of the Subunit Compositions of the PSI–LHCI Supercomplex and the LHCI in the Green Alga *Chlamydomonas reinhardtii*. Biochemistry 43: 7816-7823.
- Terauchi, A.M., Peers, G., Kobayashi, M.C., Niyogi, K.K., Merchant, S.S. (2010) Trophic status of *Chlamydomonas reinhardtii* influences the impact of iron deficiency on photosynthesis. Photosynth. Res. 105: 39-49.
- Terzulli, A., and Kosman, D.J. (2010) Analysis of the high-affinity iron up take systemat the *Chlamydomonas reinhardtii* plasma membrane. Eukaryot. Cell. 9: 815–826.
- Tikhonov, A.N. (2014) The cytochrome *b6f* complex at the crossroad of photosynthetic electron transport pathways. Plant. Physiol. Biochem. 81:163–183.
- Timperio, A.M., D'Amici, G.M., Barta, C., Loreto, F., Zolla, L. (2007) Proteomics, pigment composition, and organization of thylakoid membranes in iron deficient spinach leaves. J. Exp. Bot. 58: 3695-3710.

- Toporik, H., Li, J., Williams, D., Chiu, P.L., Mazor, Y. (2019) The structure of the stress-induced photosystem I-IsiA antenna supercomplex. Nat. Struct. Mol. Biol, 26: 443-449.
- Toth, T.N., Rai, N., Solymosi, K., Zsiros, O., Schroder, W.P., Garab, G., Kovacs, L. (2016) Fingerprinting the macro-organisation of pigment-protein complexes in plant thylakoid membranes in vivo by circular-dichroism spectroscopy. Biochim. Biophys. Acta. 1857: 1479-1489.
- Towbin, H., Staehelin, T., and Gordon, J. (1979) Electrophoretic transfer of proteins from polyacrylamide gels to nitrocellulose sheets: procedure and some applications. Proc. Natl. Acad. Sci. USA 76: 4350-4354.
- Umena, Y., Kawakami, K., Shen, J.R., Kamiya, N. (2011) Crystal structure of oxygen evolving photosystem II at a resolution of 1.9 Å. Nature 473: 55–60.
- Van Heerden, P.D.R., Swanepoel, J. W., Krüger, G.H.J. (2007).Modulation of photosynthesis by drought in two desert scrub species exhibiting C3-mode CO₂ assimilation. Environ. Exper. Bot. 61: 124-136.
- Varsano, T., Wolf, S.G., and Pick, U. (2006) A chlorophyll *a/b*-binding protein homolog that is induced by iron deficiency is associated with enlarged photosystem I units in the eucaryotic alga *Dunaliella salina*. J. Bio. Chem. 281: 10305-10315.
- Visviki I, and Santikul D. (2000) The pH tolerance of *Chlamydomonas applanata* (Volvocales, Chlorophyta). Arch. Environ. Cont. Toxicol. 38:147-151.
- Vredenberg, W.J. and Duysens, L.N.M. (1963) Transfer of energy from bacteriochlorophyll to a reaction centre during bacterial photosynthesis. Nature 197: 355–357.
- Wada, H., and Murata, N. (1998) Membrane lipids in cyanobacteria. In: SiegenthalerP-A, Murata N (eds) Lipids in Photosynthesis: Structure, Function and Genetics.Springer, Dordrecht, pp 65–81.
- Walker, E.L., and Connolly, E.L. (2008) Time to pump iron: iron-deficiency-signaling mechanisms of higher plants. Curr. opin. Plant Bio. 11: 530-535.
- Wallin, I.E. (1993) Symbionticism in the light of recent cytological investigations Ivan E. Wallin, 1969. Bio. Systems. 31: 181–183.

- Wang, H. Y., Klatte, M., Jakoby, M., Bäumlein, H., Weisshaar, B., Bauer, P. (2007) Iron deficiency mediated stress regulation of four sub group Ib BHLH genes in *Arabidopsis thaliana*. Planta 226: 897–908.
- Watanabe, M., Kubota, H., Wada, H., Narikawa, R., and Ikeuchi, M. (2011) Novel supercomplex organization of photosystem I in *Anabaena* and *Cyanophora paradoxa*. Plant Cell Physiol. 52: 162–168.
- Whitelegge, J., Zhang, H., and Aguilera, R. (2002) Full subunit coverage liquid chromatography electrospray ionization mass spectrometry (LCMS⁺) of an oligomeric membrane protein cytochrome *b6f* Complex. Mol. Cell. Proteom. 1: 816–827.
- Wu, W., Ping, W., and Wu, H. (2013) Monogalactosyldiacylglycerol deficiency in tobacco inhibits the cytochrome b6f-mediated intersystem electron transport process and affects the photostability of the photosystem II apparatus. Biochim. Biophys. Acta. 1827: 709–722.
- Xiaodong, S., Jun, M., Xiaowe, P., Xuelin, Z., Wenrui, Ch., Zhenfeng, L., Xinzheng, Z., and Mei, Li. (2019) Antenna arrangement and energy transfer pathways of a green algal photosystem-I–LHCI supercomplex. Nat. Plants, 5: 273-281.
- Yadavalli, V., Malleda, C., and Subramanyam, R. (2011) Protein-protein interactions by molecular modeling and biochemical characterization of PSI-LHCI supercomplexes from *Chlamydomonas reinhardtii*. Mol. Biosyst. 7: 3143-3151.
- Yadavalli, V., Jolley, C.C., Malleda, C., Thangaraj, B., Fromme, P., Subramanyam, R. (2012a) Alteration of proteins and pigments influence the function of photosystem I under iron deficiency from *Chlamydomonas reinhardtii*. PloS one 7: e35084.
- Yadavalli, V., Neelam, S., Rao, A.S., Reddy, A.R., Subramanyam, R. (2012b)Differential degradation of photosystem I subunits under iron deficiency in rice.J. Plant. Physiol. 169: 753-759.
- Yamamoto, Y., Hori, H., Kai, S., Ishikawa, T., Ohnishi, A., Tsumura, N., Morita, N. (2013) Quality control of Photosystem II: reversible and irreversible protein aggregation decides the fate of Photosystem II under excessive illumination. Front. Plant. Sci. 4: (433).

- Yamashita, E., Zhang, H., and Cramer, W.A. (2007) Strucutre of the cytochrome b6f complex: quinone analogue inhibitors as ligands of heam. J. Mol. Biol. 370: 39-45.
- Yang, T.J.W., Lin, W. D., and Schmidt, W. (2010) Transcriptional profiling of the Arabidopsis iron deficiency response reveals conserved transition metal homeostasis networks. Plant. Physiol. 152: 2130–2141.
- Yang, W., Wittkopp, T.M., Li, X., Warakanont, J., Dubini, A., Catalanotti, C., Kim, R.G., Nowack, E.C., Mackinder, L.C., Aksoy, M. and Page, M.D. (2015) Critical role of *Chlamydomonas reinhardtii* ferredoxin-5 in maintaining membrane structure and dark metabolism. Proc. Nat. Acad. Sci, USA 112: 14978-14983.
- Yu, B., and Benning, C. (2003) Anionic lipids are required for chloroplast structure and function in Arabidopsis. Plant. J. 36: 762–770.
- Zheng, L., Li, Y., Li, X., Zhong, Q., Li, N., Zhang, K., Zhang, Y., Chu, H., Ma, C., Li, G., Zhao, J. (2019) Structural and functional insights into the tetrameric photosystem I from heterocyst-forming *cyanobacteria*. Nat. Plants 5: 1087-97.
- Zouni, A., Witt, H.T., Kern, J., Fromme, P., Krauss, N., Saenger, W., & Orth, P. (2001) Crystal structure of photosystem II from *Synechococcus elongatus* at 3.8 Å resolution. Nature 409: 739-743.

Publications

- 1. Chouhan. N, ER. Devadasu and, Subramanyam. R (2020). Autophagy induced accumulation of lipids in prgl1 and pgr5 of Chlamydomonas reinhardtii under high light. (submitted to BBA-Molecular and Cell Biology of Lipids).
- 2. **ER**. **Devadasu**, and Subramanyam R. (2020). Enhanced lipid productivity and TAG accumulation in *Chlamydomonas reinhardtii* casued by severe iron starvation. (Submitted to Algal Research).
- 3. **ER**. **Devadasu**, K. Dhokne, J. Pandya, Subramanyam R. (2020). Recovery of photosynthetic activity and supercomplexes from severe iron starvation in *Chlamydomonas reinhardtii*. (submitted to BBA-Bioenergetics).
- S. Neelam, ER. Devadasu, S. D. Kanna, S. Nama, P. Akhtar, B. Ughy, Győző Garab, P. H. Lambrev, R. Subramanyam (2020). Long- and short-term acclimation of the photosynthetic apparatus to salinity in *Chlamydomonas reinhardtii*. The role of *Stt7* protein kinase. (submitted to Plant Journal).
- H. Parapatla, R. Gudla, GV. Kondru, ER. Devadasu, HA. Nagarajaram, M. Sritharan, R. Subramanyam, D. Siddavattam (2020). Organophosphate Hydrolase interacts with ferric-enterobactin and promotes iron uptake in association with TonB dependent transport system. Biochem. J. 1-20.
- 6. E. Devadasu, Dinesh kumar C, N. Chauhan, S. Madireddi, Girish kumar R, Subramanyam R. (2019). Changes in the photosynthetic apparatus and lipid droplet formation in *Chlamydomonas reinhardtii* under iron deficiency. Photosynth. Res. 139: 253-266.
- 7. S. Madireddi, S. Nama, ER. Devadasu, R. Subramanyam (2019). Thylakoid membrane dynamics and state transitions in *Chlamydomonas reinhardtii* under elevated temperature. Photosynth. Res. 139: 215-226.
- 8. YS Alagar, D Pushparaju Yeggoni, E. Devadasu (2017). Molecular Binding Mechanism of 5-hydroxy-1-methylpiperidin-2-one with Human Serum Albumin. J. Biomol. Struct. Dyn. 36: 810-817.
- 9. E. Devadasu, S. Madireddi, S. Nama, Subramanyam R. (2016). Iron deficiency causes changes in Photochemistry, Thylakoid organization and accumulation of Photosystem II proteins in *Chlamydomonas* reinhardtii. Photosynth. Res. 130: 469-478.

- 10. S. Nama, S. Madireddi, **ER Devadasu**, R. Subramanyam (2015). High light induced changes in organization, Protein profile and function of Photosynthetic machenary in *Chlamydomonas reinhardtii*. J. Photochem. Photobiol. (Biol), 152: 367-376.
- 11. S. Kodru, T. Malavath, **ER**. **Devadasu**, S. Nellaepalli, A. Stirbet, R. Subramanyam, Govindjee (2015). The slow S to M rise of chlorophyll a fluorescence induction reflects transition from state 2 to state 1 in the green alga *Chlamydomonas reinhardtii*. Photosynth. Res. 125: 219-31.
- 12. S. Madireddi, S. Nama, **ER Devadasu**, Subramanyam R. (2014). Photosynthetic membrane organization and role of state transition in cyt, cpII, stt7 and npq mutants of *Chlamydomonas reinhardtii*. J. Photochem. Photobiol. (Biol). 137: 77-83.

Conferences presentations

- 1. Elsinraju Devadasu, and Subramanyam Rajagopal. "Recovery of photosynthetic activity and supercomplexes from sever iron starvation in *Chlamydomonas reinhardtii*" on Algal biomass to solar energy held at Porto, Portugal during February 11-14 (2020).
- 2. Elsinraju Devadasu, and Subramanyam R. "Changes in the photosynthetic apparatus and lipid droplet formation in Chlamydomonas reinhardtii under iron deficiency". Andhra Pradesh Science Congress held at Yogi Vemana University, Kadapa during November 9-11 (2018).
- 3. **Elsinraju Devadasu**, Sai Kiran Madireddi, Srilatha Nama, and Subramanyam Rajagopal. "Unravelling of photosynthesis and accumulation of lipids in *Chlamydomonas reinhardtii* under Iron deficiency". International conference on Photosynthesis and hydrogen energy research for sustainability-2017, held at School of Life Sciences, University of Hyderabad, India during October 30th-November 3rd (2017).

PORTLAND PRESS

11

12

Q1

15

16

17 18

19 20 21

22

23

24

25

27

28

29

30

31

32

34

37

38 39

41

Research Article

Organophosphate hydrolase interacts with ferric-enterobactin and promotes iron uptake in association with TonB dependent transport system

Hari Parapatla¹, Ramurthy Gudla¹, Guruprasad Varma Konduru^{2,3}, Elsin Raju Devadasu⁴, Hampapathula Adimurthy Nagarajaram⁵, Manjula Sritharan¹, Rajagopal Subramanyam⁴ and Dayananda Siddayattam¹

¹Department of Animal Biology, School of Life Sciences, University of Hyderabad, Hyderabad 500046, India; ²Laboratory of Computational Biology, Centre for DNA Fingerprinting and Diagnostics, Uppal, Hyderabad 500039, India; ³Graduate Studies, Manipal Academy of Higher Education, Manipal, Karnataka 576104, India; ⁴Department of Plant Sciences, School of Life Sciences, University of Hyderabad, Hyderabad 500046, India; ⁵Department of Systems and Computational Biology, School of Life Sciences, University of Hyderabad, Hyderabad 500046, India

Correspondence: Dayananda Siddavattam (sdsl@uohyd.ernet.in or siddavattam@gmail.com)

Our previous studies have shown the existence of organophosphate hydrolase (OPH) as a part of the inner membrane associated TonB complex (ExbB/ExbD and TonB) of Sphingobium fuliginis. We now show its involvement in iron uptake by establishing direct interactions with ferric-enterobactin. The interactions between OPH and ferric-enterobactin were not affected even when the active site architecture is altered by substituting active site aspartate with either alanine or asparagine. Protein docking studies further substantiated these findings and predicted the existence of ferric-enterobactin binding site that is different from the catalytic site of OPH. A lysine residue (82K) found at the predicted ferric-enterobactin binding site facilitated interactions between OPH and ferricenterobactin. Substitution of lysine with alanine did not affect triesterase activity, but it abrogated OPH ability to interact with both ferric-enterobactin and ExbD, strengthening further the fact that the catalytic site is not the site for binding of these ligands. In the absence of interactions between OPH^{K82A} and ExbD, OPH^{K82A} failed to target membrane in E. coli cells. The Sphingobium fuliginis TonB dependent transport (St TonBDT) system was reconstituted in E. coli GS027 cells generated by deleting the exbD and tonB genes. The E. coli GS030 cells having SfTonBDT system with OPH showed increased iron uptake. Such an increase was not seen in *E. coli* GS029, cells having _{Sf}TonBDT system generated either by omitting OPH or by including its variants, OPH^{D301A}, OPH^{D301N} suggesting a role for OPH in enhanced iron uptake.

Introduction

Phosphotriesterases (PTEs), also known as organophosphate hydrolases (OPH), are present in a number of soil bacteria. These binuclear metallo-enzymes hydrolyze P-O, P-S and P-C bonds found in a variety of organophosphate insecticides and nerve agents [1]. The inner membrane associated OPH contains a 23 amino acid long signal peptide with unique characteristic features. It contains a Twin Arginine Transport (TAT) motif (MQTRRVVLK) at the N-terminus and a lipobox motif (LAGC) at the signal peptidase cleavage site [2]. OPH is targeted to the inner membrane in a prefolded conformation and remains anchored to it through a diacyl glycerol moiety linked to an invariant cysteine residue present at the junction of signal peptidase cleavage site [2,3]. There are no transmembrane domains in OPH and the entire protein exists in the periplasmic space [3]. Recent studies have shown the existence of OPH as part of a multi-protein complex [3,4]. The TonB dependent transport system components, TonB, ExbB/ExbD were co-eluted when the membrane associated

Received: 16 April 2020 Revised: 14 July 2020 Accepted: 20 July 2020

Accepted Manuscript online: 20 July 2020 Version of Record published: 0 Month 2020

ORIGINAL ARTICLE



Changes in the photosynthetic apparatus and lipid droplet formation in *Chlamydomonas reinhardtii* under iron deficiency

Elsinraju Devadasu¹ · Dinesh Kumar Chinthapalli^{1,3} · Nisha Chouhan¹ · Sai Kiran Madireddi¹ · Girish Kumar Rasineni² · Prabhakar Sripadi³ · Rajagopal Subramanyam¹

Received: 22 April 2018 / Accepted: 28 August 2018 © Springer Nature B.V. 2018

Abstract

The unicellular photosynthetic alga *Chlamydomonas reinhardtii* was propagated in iron deficiency medium and patterns of growth, photosynthetic efficiency, lipid accumulation, as well as the expression of lipid biosynthetic and photosynthesis-related proteins were analysed and compared with iron-sufficient growth conditions. As expected, the photosynthetic rate was reduced (maximally after 4 days of growth) as a result of increased non-photochemical quenching (NPQ). Surprisingly, the stress-response protein LHCSR3 was expressed in conditions of iron deficiency that cause NPQ induction. In addition, the protein contents of both the PSI and PSII reaction centres were gradually reduced during growth in iron deficiency medium. Interestingly, the two generations of Fe deficiency cells could be able to recover the photosynthesis but the second generation cells recovered much slower as these cells were severely in shock. Analysis by flow cytometry with fluorescence-activated cell sorting and thin layer chromatography showed that iron deficiency also induced the accumulation of triacylglycerides (TAG), which resulted in the formation of lipid droplets. This was most significant between 48 and 72 h of growth. Dramatic increases in DGAT2A and PDAT1 levels were caused by iron starvation, which indicated that the biosynthesis of TAG had been increased. Analysis using gas chromatography mass spectrometry showed that levels of 16:0, 18:0, 18:2 and 18:3^{Δ9,12,15} fatty acids were significantly elevated. The results of this study highlight the genes/enzymes of *Chlamydomonas* that affect lipid synthesis through their influence on photosynthesis, and these represent potential targets of metabolic engineering to develop strains for biofuel production.

 $\textbf{Keywords} \ \ Electron \ transport \cdot Iron \ deficiency \cdot LHCSR3 \cdot Major \ lipid \ droplet \ protein \cdot Photosystems \cdot Triacylglycerol$

Electronic supplementary material The online version of this article (https://doi.org/10.1007/s11120-018-0580-2) contains supplementary material, which is available to authorized users.

☐ Rajagopal Subramanyam srgsl@uohyd.ernet.in

Published online: 14 September 2018

- Department of Plant Sciences, School of Life Sciences, University of Hyderabad, Hyderabad, Telangana 500046, India
- Center for Excellence in Medical Services Pvt. Ltd., Kineta Towers, Road No. 3, Banjara Hills, Hyderabad, Telangana 500034, India
- ³ Analytical Chemistry and Mass Spectrometry, CSIR-Indian Institute of Chemical Technology, Hyderabad, Telangana 500 007, India

Introduction

The microalgae, a diverse group of eukaryotic photosynthetic organisms, occupy diverse habitats including freshwater, marine and more extreme environments such as hot springs and frozen regions (Li et al. 2012a, b). This ability to adapt to different environmental conditions is due to the plasticity of algal physiology. Microalgae have been used as a source of biodiesel (Chisti et al. 2007) and they are considered promising candidates for large-scale biofuel production due to their high photosynthetic efficiency and oil accumulation ability (Borowitzka and Moheimani 2013; Moody et al. 2014).

Abiotic stress leads to a variety of cellular responses in eukaryotic photosynthetic algae, including changes to the photosynthetic apparatus (Glaesener et al. 2013). In addition, stress leads to increased accumulation of lipids, particularly triacylglycerides (TAG) (Juergens et al. 2015).



ORIGINAL ARTICLE



Thylakoid membrane dynamics and state transitions in *Chlamydomonas reinhardtii* under elevated temperature

Sai Kiran Madireddi¹ · Srilatha Nama¹ · Elsinraju Devadasu¹ · Rajagopal Subramanyam¹

Received: 17 March 2018 / Accepted: 16 July 2018 © Springer Nature B.V. 2018

Abstract

Moderately elevated temperatures can induce state transitions in higher plants by phosphorylation of light-harvesting complex II (LHCII). In this study, we exposed unicellular algae *Chlamydomonas reinhardtii* to moderately elevated temperatures (38 °C) for short period of time in the dark to understand the thylakoid membrane dynamics and state transition mechanism. Here we report that under elevated temperatures (1) LHCII gets phosphorylated similar to higher plants and (2) there is decreased absorption cross section of photosystem II (PSII), whereas (3) there is no change in absorption cross section of photosystem I (PSI) indicating that LHCII trimers are largely disconnected with both photosystems under moderately elevated temperatures and (4) on return to room temperature after elevated temperature treatment there is a formation of state transition complex comprising of PSII–LHCII–PSI. The temperature-induced state transition mechanism also depends on stt7 kinase-like in light-induced state transition. The protein content was stable at the moderately elevated temperature treatment of 40 °C; however, at 45 °C severe downregulation in photosynthetic performance and protein content was observed. In addition to the known changes to photosynthetic apparatus, elevated temperatures can destabilize the PSII–LHCII complex that can result in decreased photosynthetic efficiency in *C. reinhardtii*. We concluded that the membrane dynamics of light-induced state transitions differs considerably from temperature-induced state transition mechanisms in *C. reinhardtii*.

 $\textbf{Keywords} \ \ Chlamydomonas \cdot Elevated \ temperature \cdot LHCII \ phosphorylation \cdot Non-photochemical \ quenching \cdot State \ transition \cdot Thylakoids \ organization$

Introduction

Temperature is one of the abiotic stress factors that influences the photosynthetic apparatus. According to the Intergovernmental Panel on Climate Change (IPCC) report 2013, global temperatures due to elevated CO₂ emissions and other human practices are predicted to increase by between 0.5 and 8.6 °F by the year 2100. Elevated temperature has an adverse effect on crop productivity. Thus in this scenario of increasing global temperatures, there is an immediate need to more intricately explore its effect on the photosynthetic

Electronic supplementary material The online version of this article (https://doi.org/10.1007/s11120-018-0562-4) contains supplementary material, which is available to authorized users.

Published online: 20 July 2018

apparatus: an important source for the primary assimilation of biological material on the planet.

Photosynthesis is very sensitive to heat stress (Berry and Bjorkman 1980). Many components of photosynthesis are sensitive to elevated temperature stress such as PSII, ATP synthesis, and carbon fixation process (Nishiyama et al. 2001). Early events of elevated temperature stress include reduced Rubisco activity, changes in macro-organization of the chloroplast, compromised thylakoid structure by decreased grana stacking, ion leakage, and changes in energy distribution between photosystems (Law and Crafts-Brandner 1999; Mohanty et al. 2002; Salvucci and Crafts-Brandner 2004).

Mild heat stress enhances non-photochemical reduction of plastoquinone pool (Bukhov and Carpentier 2004) by simulation of cyclic electron flow around PSI. This adaptation is required to compensate for ATP demand required for carbon fixation, photorespiration (Osmond 1981), and Rubisco activation. Severe heat stress impairs PSII activity, whereas PSI is relatively resistant to it (Havaux



Rajagopal Subramanyam srgsl@uohyd.ernet.in; rajagopal98@gmail.com

Department of Plant Sciences, School of Life Sciences, University of Hyderabad, Hyderabad 500046, India



Journal

Journal of Biomolecular Structure and Dynamics

Volume 36, 2018 - Issue 3

Letter to the Editor

Molecular binding mechanism of 5-hydroxy-1methylpiperidin-2-one with human serum albumin

Pages 810-817 | Received 14 Oct 2016, Accepted 20 Feb 2017, Accepted author version posted online: 01 Mar 2017, Published online: 22 Mar 2017

66 Download citation

▶ https://doi.org/10.1080/07391102.2017.1300106



ORIGINAL ARTICLE



Iron deficiency cause changes in photochemistry, thylakoid organization, and accumulation of photosystem II proteins in *Chlamydomonas reinhardtii*

Elsin Raju Devadasu¹ · Sai Kiran Madireddi¹ · Srilatha Nama¹ · Rajagopal Subramanyam¹

Received: 25 January 2016/Accepted: 13 June 2016/Published online: 21 June 2016 © Springer Science+Business Media Dordrecht 2016

Abstract A trace element, iron (Fe) plays a pivotal role in photosynthesis process which in turn mediates the plant growth and productivity. Here, we have focused majorly on the photochemistry of photosystem (PS) II, abundance of proteins, and organization of supercomplexes of thylakoids from Fe-depleted cells in Chlamydomonas reinhardtii. Confocal pictures show that the cell's size has been reduced and formed rosette-shaped palmelloids; however, there is no cell death. Further, the PSII photochemistry was reduced remarkably. Further, the photosynthetic efficiency analyzer data revealed that both donor and acceptor side of PSII were equally damaged. Additionally, the room-temperature emission spectra showed the fluorescence emission maxima increased due to impaired energy transfer from PSII to PSI. Furthermore, the protein data reveal that most of the proteins of reaction center and light-harvesting antenna were reduced in Fe-depleted cells. Additionally, the supercomplexes of PSI and PSII were destabilized from thylakoids under Fe-deficient condition showing that Fe is an important element in photosynthesis mechanism.

Keywords Blue native gel electrophoresis · Fe deficiency · Light-harvesting complexes · Photochemistry · Photosystem II · Thylakoid organization

Electronic supplementary material The online version of this article (doi:10.1007/s11120-016-0284-4) contains supplementary material, which is available to authorized users.

Introduction

Iron is a relatively abundant micronutrient in the earth's crust, which often chronically limits to photosynthesis in the ocean and on land also. Iron is present predominantly in the poor form of insoluble complexes, such as Fe(III) ferric oxides in oxygen-rich surface water and neutral to alkaline soil. The soluble form of Fe(II) is very limited in soil, and the low bioavailability of iron complexes creates a major obstacle for photosynthetic organisms (Glaesener et al. 2013). Fe deficiency in photosynthetic organisms is evident by the development of chlorosis (loss of chlorophyll), which is accompanied by loss of photosynthetic machinery and inhibition of photosynthetic electron transport reactions (Spiller and Terry 1980).

It is well known that Fe is a cofactor in photosystem (PS) II, PSI, the cytochrome (Cyt) b6/f complex, and Cyt c6 (Yadavalli et al. 2011, 2012a). Since PSI is the prime target because of its relatively high Fe content (12 Fe per PSI) and for instance, changes from 4:1 ratio of PSI:PSII to 1:1 under Fe deficiency in cyanobacteria (Straus 2004). Further, Fe deficiency causes a decrease in the number of PSI complex, resulting in a bottleneck in the photosynthetic electron flow (Strzepek and Harrison 2004). Most of the cyanobacteria species express the auxiliary light-harvesting proteins which increase the cross section of PSI to balance a similar level of electron throughput with a smaller Fe investment to avoid the oxidative stress in the cell (Chauhan et al. 2011). In cyanobacteria, the alteration in the pigment-protein complex and appearance of an additional pigment-protein complex around PSII (IdiA: Iron deficiency induced protein) protect PSII at the acceptor side against damage (Michel et al. 1996; Michel and Pistorius 2004) and formation of an iron stress-induced protein A (IsiA) (Boekema et al. 2001; Chauhan et al. 2011). Fe



Rajagopal Subramanyam srgsl@uohyd.ernet.in

Department of Plant Sciences, School of Life Sciences, University of Hyderabad, Hyderabad 500046, India

REGULAR PAPER

The slow S to M rise of chlorophyll a fluorescence reflects transition from state 2 to state 1 in the green alga Chlamydomonas reinhardtii

Sireesha Kodru · Tirupathi Malavath · Elsinraju Devadasu · Sreedhar Nellaepalli · Alexandrina Stirbet · Rajagopal Subramanyam · Govindjee

Received: 16 November 2014 / Accepted: 8 January 2015 © Springer Science+Business Media Dordrecht 2015

Abstract The green alga *Chlamydomonas* (C.) reinhardtii is a model organism for photosynthesis research. State transitions regulate redistribution of excitation energy between photosystem I (PS I) and photosystem II (PS II) to provide balanced photosynthesis. Chlorophyll (Chl) a fluorescence induction (the so-called OJIPSMT transient) is a signature of several photosynthetic reactions. Here, we show that the slow (seconds to minutes) S to M fluorescence rise is reduced or absent in the stt7 mutant (which is locked in state 1) in C. reinhardtii. This suggests that the

In earlier publications, Sireesha Kodru and Sreedhar Nellaepalli have used their names as Kodru Sireesha and Nellaepalli Sreedhar, respectively.

Rajagopal Subramanyam—in earlier publications, has used his name as Subramanyam Rajagopal.

Electronic supplementary material The online version of this article (doi:10.1007/s11120-015-0084-2) contains supplementary material, which is available to authorized users.

S. Kodru · T. Malavath · E. Devadasu · R. Subramanyam (🖂) Department of Plant Sciences, School of Life Sciences, University of Hyderabad, Hyderabad 500 046, India e-mail: srgsl@uohyd.ernet.in

S. Nellaepalli

Department of Biochemistry, School of Life Sciences, University of Hyderabad, Hyderabad 500 046, India

A Stirbet

204 Anne Burras Lane, Newport News, VA 23606, USA

Govindjee (⋈)

Departments of Biochemistry and Plant Biology, and Center of Biophysics & Quantitative Biology, University of Illinois at Urbana-Champaign, Urbana, IL 61801-3707, USA

e-mail: gov@illinois.edu

Published online: 08 February 2015

SM rise in wild type C. reinhardtii may be due to state 2 (low fluorescence state; larger antenna in PS I) to state 1 (high fluorescence state; larger antenna in PS II) transition, and thus, it can be used as an efficient and quick method to monitor state transitions in algae, as has already been shown in cyanobacteria (Papageorgiou et al. 1999, 2007; Kaňa et al. 2012). We also discuss our results on the effects of (1) 3-(3,4-dichlorophenyl)-1,4-dimethyl urea, an inhibitor of electron transport; (2) n-propyl gallate, an inhibitor of alternative oxidase (AOX) in mitochondria and of plastid terminal oxidase in chloroplasts; (3) salicylhydroxamic acid, an inhibitor of AOX in mitochondria; and (4) carbonyl cyanide *p*-trifluoromethoxyphenylhydrazone, an uncoupler of phosphorylation, which dissipates proton gradient across membranes. Based on the data presented in this paper, we conclude that the slow PSMT fluorescence transient in C. reinhardtii is due to the superimposition of, at least, two phenomena: qE dependent non-photochemical quenching of the excited state of Chl, and state transitions.

Keywords Chlorophyll fluorescence · Light-harvesting complex · Photosystem I · Photosystem II · State transitions

Abbreviations

AOX Alternative oxidase **CEF** Cyclic electron flow Chl Chlorophyll Cytochrome Cyt

DCMU 3-(3,4-Dichlorophenyl)-1,4-dimethyl urea;

also known as Diuron

FCCP Carbonyl cyanide

p-trifluoromethoxyphenylhydrazone

LEF Linear electron flow

NADP Nicotinamide adenine dinucleotide phosphate

Ndh NAD(P)H dehydrogenase





Contents lists available at ScienceDirect

Journal of Photochemistry & Photobiology, B: Biology

journal homepage: www.elsevier.com/locate/jpb



High light induced changes in organization, protein profile and function of photosynthetic machinery in *Chlamydomonas reinhardtii*



Srilatha Nama, Sai Kiran Madireddi, Elsin Raju Devadasu, Rajagopal Subramanyam *

Department of Plant Sciences, School of Life Sciences, University of Hyderabad, Hyderabad 500046, India

ARTICLE INFO

Article history:
Received 29 June 2015
Received in revised form 26 August 2015
Accepted 27 August 2015
Available online 30 August 2015

Keywords: Chlamydomonas reinhardtii Chlorophyll a fluorescence High light intensity Light harvesting complexes Pigment–pigment interactions Supercomplexes Thylakoids

ABSTRACT

The green alga *Chlamydomonas (C.) reinhardtii* is used as a model organism to understand the efficiency of photosynthesis along with the organization and protein profile of photosynthetic apparatus under various intensities of high light exposure for 1 h. Chlorophyll (Chl) a fluorescence induction, OJIPSMT transient was decreased with increase in light intensity indicating the reduction in photochemical efficiency. Further, circular dichroism studies of isolated thylakoids from high light exposed cells showed considerable change in the pigment–pigment interactions and pigment–proteins interactions. Furthermore, the organization of supercomplexes from thylakoids is studied, in which, one of the hetero-trimer of light harvesting complex (LHC) II is affected significantly in comparison to other complexes of LHC's monomers. Also, other supercomplexes, photosystem (PS)II reaction center dimer and PSI complexes are reduced. Additionally, immunoblot analysis of thylakoid proteins revealed that PSII core proteins D1 and D2 were significantly decreased during high light treatment. Similarly, the PSI core proteins PsaC, PsaD and PsaG were drastically changed. Further, the LHC antenna proteins of PSI and PSII were differentially affected. From our results it is clear that LHCs are damaged significantly, consequently the excitation energy is not efficiently transferred to the reaction center. Thus, the photochemical energy transfer from PSII to PSI is reduced. The inference of the study deciphers the structural and functional changes driven by light may therefore provide plants/alga to regulate the light harvesting capacity in excess light conditions.

© 2015 Elsevier B.V. All rights reserved.

1. Introduction

Photosynthesis is a primary process that provides energy source to the biosphere in the form of reduced carbon. The oxygenic photosynthetic organisms like cyanobacteria, algae and plants are often exposed to various abiotic stress factors, majorly by high light. Optimum light intensity is essential for photosynthesis to convert solar energy into chemical energy. As the environment is changing fast, hence, plants/ algae are forced to deal with sudden high light conditions, which leads to damage of photosystems, particularly photosystem (PS)II [1]. These conditions are characterized by those light intensities, where the additional energy cannot be used for increased carbon fixation and oxygen production and thus are potentially harmful. These high light intensities cause photoinhibition resulting in reduction of photosynthetic quantum yield [2]. During evolution, green plants and photosynthetic organisms have adapted different approaches to develop and survive in various environmental conditions characterized by high light, low light response [3] and intense fluctuating light conditions or the incoming light which is spectrally altered due to certain types of different stress conditions [4]. On the other hand, there have been reports about influence of different quality and quantity of light conditions for their acclimation and photoprotective mechanisms such as, in diatoms for acclimation to high light require perception of blue light [5]. Under surplus light condition beyond threshold limit for photosynthetic efficiency, oxidative damage to photosynthetic apparatus frequently occurs by impart of singlet oxygen radicals in the proximity of PSII which can attack and cause irreversible damage to D1 protein, whereas superoxide and hydroxyl radical formation at the acceptor side of PSI leads to oxidative damage of chloroplast proteins and lipids [6]. It has been reported that PSII photodamage is associated with light absorption by manganese cluster of oxygen evolving complex [7]. To restore the function of PSII by repair cycle process which includes selective degradation of the damaged D1 protein and regeneration of complex by de novo synthesized D1 protein [8,9]. It is well known that repair process of damaged PSII can be inhibited by reactive oxygen species (ROS) which disseminates from oxidative stress [10,11]. Different photoprotection mechanisms have been studied to avoid photodamage of PSII and thus maintaining repair of damaged PSII [12]. Excess light absorbed is dissipated as heat through a mechanism called non-photochemical quenching [13]. Various types of quenching processes have been reported based on their time scale of induction and relaxation i.e., high energy excitation quenching which is the main component of non-photochemical quenching (NPQ) and is triggered by the formation of a ΔpH across the thylakoid membrane [14], zeaxanthin dependent quenching through xanthophyll cycle [15]. Further, quenching due to state transitions, which is a process

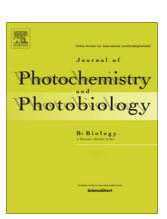
^{*} Corresponding author. Tel.: +91 40 2313 4572; fax: +91 40 2301 0120. E-mail address: srgsl@uohyd.ernet.in (R. Subramanyam).

ELSEVIER

Contents lists available at ScienceDirect

Journal of Photochemistry and Photobiology B: Biology

journal homepage: www.elsevier.com/locate/jphotobiol



Photosynthetic membrane organization and role of state transition in cyt, cpII, stt7 and npq mutants of Chlamydomonas reinhardtii



Sai Kiran Madireddi, Srilatha Nama, Elsin Raju Devadasu, Rajagopal Subramanyam*

Department of Plant Sciences, School of Life Sciences, University of Hyderabad, Hyderabad 500046, India

ARTICLE INFO

Article history: Received 28 November 2013 Received in revised form 13 March 2014 Accepted 31 March 2014 Available online 24 April 2014

Keywords: Chl a fluorescence Cyt b₆/f Light harvesting complex Non photochemical quenching Photosystems State transitions

ABSTRACT

In Chlamydomonas reinhardtii, cytochrome b_6/f and chlorophyll b binding proteins are important in energy distribution between photosystem (PS)II and PSI. In this study, we have used C. reinhardtii mutants deficient in cytochrome b_6/f complex (cyt), chlorophyll b binding protein (cpII), non-photochemical quenching (npq) and LHC II kinase (stt7) to study the importance of these proteins in electron transport, phosphorylation, and structural organization of thylakoid supercomplexes under optimum growth conditions. Fast ChI a fluorescence studies have shown that lack of CpII and Cyt b_6/f caused reduced photochemical yield (F_v/F_m) . The disappearance of I phase in cyt mutant showed that electron transfer from Cyt b_6/f to PSI is reduced due to un availability of Q_0 site for docking of PQH2 therefore LHC II kinase was unable to phosphorylate LHCII in cyt mutant. Further, blue native gel electrophoresis revealed the differential organization of photosynthetic membrane protein complexes in different mutants. Particularly, LHCII trimerization is more in cyt mutant, however, all other mutants were similar to that of wild type. Based on our results, we propose that the LHCII trimer accumulation and its organization with other complexes are very important in state transitions.

© 2014 Elsevier B.V. All rights reserved.

1. Introduction

Photosynthesis is the process in which light energy is converted into chemical energy in terms of ATP and NADPH which can be used up by light independent reactions. The photosynthesis process in both higher plants and green algae triggers when light is absorbed by light harvesting antennae complexes (LHC) of photosystem (PSI) and PSII. Crystallographic studies revealed that the LHCI complex of higher plants contains 4–5 subunits [1]. However, LHCI complex of *Chlamydomonas reinhardtii* is larger and contains 9–14 subunits per reaction centre [2,3]. In which, the LHCII complex consists of type I (Lhcbm3, Lhcbm4, Lhcbm6, Lhcbm8, and Lhcbm9), type II (Lhcbm5), type III (Lhcbm2 and Lhcbm7), and type IV (Lhcbm1) and also comprizes two minor antennas (CP26 and CP29) [4].

Imbalanced light energy causes change in the redox state of intersystem electron transport chain in both PSI and PSII. In order to balance the excitation energy between PSII and PSI, the PQ pool triggers state transition [5–7]. During this process, the peripheral LHCII proteins can shuttle between PSI in the stroma and PSII in

the grana in order to optimize overall electron transport [8]. In this process Stt7 (Stn7 is an orthologue present in Arabidopsis thaliana) is the key kinase enzyme involved in phosphorylation of LHCII leads state transitions in C. reinhardtii [9]. In electron flow chain the kinase is activated in response to redox change in the thylakoid membrane. Also, reduction of the PQ pool, either by unbalanced PSII/PSI activity (in favor of the former) or by the chlororespiratory chain, activates the kinase through a mechanism that requires plastoquinol binding to the Cyt b₆/f complex [10]. The loss or modification of Stt7 or Stn7 blocks the state transitions and LHCII phosphorylation [9,11]. The phosphorylated Pi-LHCII disconnects from PSII and migrates to PSI to balance the energy. This process is reversible when the LHCII kinase is inactivated by oxidation of the plastoquinol where Pi-LHCII gets dephosphorylated by a thylakoid associated phosphatase (TAP38) [12,13], which seems to have constitutive but low activity. Dephosphorylated LHCII moves back to PSII, leading to state I.

PQ pool and Cyt b_6/f plays a crucial role in functional coordination of PSI and PSII during redox mechanism. It is well known that Cyt b_6/f is a membrane bound complex that transfers electrons from lipophilic quinones to hydrophilic plastocyanine. In this process proton are transfered across the thylakoid membrane, consequently develops proton gradient, thereby controlling electron transport. It is now known that Cyt b_6/f also plays a key role in

^{*} Corresponding author. Tel.: +91 40 2313 4572; fax: +91 40 2301 0120. E-mail address: srgsl@uohyd.ernet.in (R. Subramanyam).

Change in photochemistry, thylakoid organization and lipid accumulation in Chlamydomonas reinhardtii

ORIGINALITY REPORT

16%

13%

26%

SIMILARITY INDEX

INTERNET SOURCES

PUBLICATIONS

STUDENT PAPERS

PRIMARY SOURCES

Submitted to University of Hyderabad, Hyderabad

Student Paper

24%

eprints.soton.ac.uk

Internet Source

Prof. S. RAJAGOPAL Dept. of Plant Sciences School of Life Sciences University of Hyderabad Hyderabad-500 046.

6%

3

link.springer.com

Internet Source

6%

Elsin Raju Devadasu, Sai Kiran Madireddi, Srilatha Nama, Rajagopal Subramanyam, "Iron deficiency cause changes in photochemistry, thylakoid organization, and accumulation of photosystem II proteins in Chlamydomonas reinhardtii", Photosynthesis Research, 2016 Publication

5

Elsinraju Devadasu, Dinesh Kumar Chinthapalli, Nisha Chouhan, Sai Kiran Madireddi et al. "Changes in the photosynthetic apparatus and lipid droplet formation in Chlamydomonas

reinhardtii under iron deficiency",

The enclosed plagiarism report (34%) includes three papers Prof published by us in internal previous journals. However, the University of Hyderabad Hyderabad Hyderabad-500 046.

1%

Dept. of Plant Sciences

Publication

- James, G.O.. "Fatty acid profiling of Chlamydomonas reinhardtii under nitrogen deprivation", Bioresource Technology, 201102
- <1%

7 www.jbc.org
Internet Source

<1%

Michihiro Suga, Shin-Ichiro Ozawa, Kaori Yoshida-Motomura, Fusamichi Akita, Naoyuki Miyazaki, Yuichiro Takahashi. "Structure of the green algal photosystem I supercomplex with a decameric light-harvesting complex I", Nature Plants, 2019

<1%

Publication

Toth, S.Z.. "Photosynthetic electron transport activity in heat-treated barley leaves: The role of internal alternative electron donors to photosystem II", BBA - Bioenergetics, 200704

<1%

www.patentsencyclopedia.com

<1%

Ricarda Höhner, Johannes Barth, Leonardo Magneschi, Daniel Jaeger et al. "The Metabolic Status Drives Acclimation of Iron Deficiency Responses in as Revealed by Proteomics Based Hierarchical Clustering and Reverse

<1%

Genetics ", Molecular & Cellular Proteomics, 2013

Publication

12	Venkateswarlu Yadavalli, Satyabala Neelam, Akiri S.V.C. Rao, Attipalli R. Reddy, Rajagopal Subramanyam. "Differential degradation of photosystem I subunits under iron deficiency in rice", Journal of Plant Physiology, 2012 Publication	<1%
13	M. G. Esquível, A. R. Matos, J. Marques Silva. "Rubisco mutants of Chlamydomonas reinhardtii display divergent photosynthetic parameters and lipid allocation", Applied Microbiology and Biotechnology, 2017 Publication	<1%
14	pure.rug.nl Internet Source	<1%
15	www.jci.org Internet Source	<1%
16	preview-bmcneurosci.biomedcentral.com Internet Source	<1%
17	hdl.handle.net Internet Source	<1%
18	Venkateswarlu Yadavalli, Craig C. Jolley, Chandramouli Malleda, Balakumar Thangaraj,	<1%

Petra Fromme, Rajagopal Subramanyam.

"Alteration of Proteins and Pigments Influence the Function of Photosystem I under Iron Deficiency from Chlamydomonas reinhardtii", PLoS ONE, 2012

Publication

19

Xin Sheng, Akimasa Watanabe, Anjie Li, Eunchul Kim, Chihong Song, Kazuyoshi Murata, Danfeng Song, Jun Minagawa, Zhenfeng Liu. "Structural insight into light harvesting for photosystem II in green algae", Nature Plants, 2019 <1%

Publication

20

Jianhua Fan, Ivhong Zheng. "Acclimation to NaCl and light stress of heterotrophic Chlamydomonas reinhardtii for lipid accumulation", Journal of Bioscience and Bioengineering, 2017

<1%

Publication

21

Submitted to University of Reading
Student Paper

<1%

Exclude quotes On
Exclude bibliography On

Exclude matches

< 14 words